NUMBER-RESOLVED ANALYSIS OF MANY-BODY QUANTUM STATES

Von der Fakultät für Mathematik und Physik
der Gottfried Wilhelm Leibniz Universität Hannover

zur Erlangung des akademischen Grades

Doktorin der Naturwissenschaften
- Dr. rer. nat. -

genehmigte Dissertation von

M.Sc. Mareike Hetzel

2023

REFERENT:
apl. Prof. Dr. Carsten Klempt
Institut für Quantenoptik
Leibniz Universität Hannover

KORREFERENTIN:
Prof. Dr. Silke Ospelkaus-Schwarzer
Institut für Quantenoptik
Leibniz Universität Hannover

KORREFERENT:
Prof. Dr. Augusto Smerzi
QSTAR, INO-CNR und LENS
Universität von Florenz

TAG DER PROMOTION: 21. August 2023

Hannover

2023

ABSTRACT

Quantum sensors have emerged as a revolutionary technology that harnesses quantum phenomena to surpass the resolution of classical sensors. By leveraging the unique property of quantum particles to exist in superposition states, quantum sensors can be employed for interferometry, a highly precise measurement technique. Interferometers utilizing massive particles offer exceptional precision in measuring acceleration, rotation and time, making them highly relevant for navigation, geodesy and fundamental research. To enhance the sensitivity beyond classical limits and approach the fundamental Heisenberg limit, exploiting the quantum mechanical property of entanglement is crucial.

Achieving interferometry close to the Heisenberg limit requires carefully engineered entangled quantum states, low-noise interferometer components and a detection on the single-particle level. Since the sensitivity of an interferometer scales with the number of employed particles, a source capable of generating large entangled states is desirable. Due to their high phase-space density and well-defined spatial mode, Bose-Einstein condensates (BECs) present a promising source for atom interferometry. They offer great potential to create large entangled states, making them ideal candidates for quantum-enhanced atom interferometry.

However, a considerable challenge lies in pairing sources of entangled states with single-particle-resolving detection. This work addresses this challenge by presenting the creation and number-resolved analysis of many-body quantum states in an apparatus designed for atom interferometry close to the Heisenberg limit. Based on three publications, this thesis contributes to the development of tools for analyzing many-body quantum states.

By utilizing a hybrid evaporation approach that combines a magnetic quadrupole trap with a crossed-beam optical dipole trap, BECs containing 2×10^5 atoms are rapidly created within 3.3 s. A number-resolving detection based on a magneto-optical trap is presented, its noise sources are analyzed and its potential for preparing mesoscopic atomic ensembles is demonstrated. Building upon these findings, an enhanced version of the number-resolving detection is implemented in the experimental apparatus which maintains single-atom resolution for hundreds of atoms. The detection system is capable of accurately counting subsamples of the BEC prepared through microwave transitions and optical removals.

Furthermore, a coherent spin state consisting of 35 atoms is analyzed with number-resolution. The fidelity of the detector is characterized through quantum detector tomography and a state reconstruction is performed. The techniques developed in this work directly enable the number-resolved analysis of entangled states, such as a twin-Fock state, representing the next step towards atom interferometry at the Heisenberg limit.

Keywords: Bose-Einstein condensates, number-resolving detection, many-body quantum states, quantum-enhanced atom interferometry

CONTENTS

1 INTRODUCTION

1.1 QUANTUM MECHANICS AND ITS FUNDAMENTAL PRINCIPLES

In the early 20th century, a series of experiments and theoretical developments challenged our understanding of the behaviour of particles on a microscopic level. On the one hand, the interference patterns observed in the double-slit experiment, first performed by Thomas Young in 1802 [1], indicate the wave-like nature of light. On the other hand, Albert Einstein's explanation of the photoelectric effect, first observed 1887 by Heinrich Hertz [2], introduced the idea of light consisting of discrete particles, or photons, which seemed to contradict that notion [3]. In 1924, Louis de Broglie proposed that all particles, not just photons, had wave-like properties, as well [4]. This duality is a fundamental aspect of the theory developed at that time which is now known as quantum mechanics.

In the following years, several other key principles were proposed. Werner Heisenberg formulated the uncertainty principle, which states that two conjugate observables, such as position and momentum of a particle, cannot be precisely known at the same time [5]. The principle of superposition, proposed by Erwin Schrödinger, states that a quantum particle can have several possibilities in which state it is and the actual state is only defined when measured [6]. The concept of entanglement suggests that quantum particles in a superposition state can become correlated in a way that a measurement on one particle determines the state of the other particle as well. It attracted the attention of Albert Einstein, Boris Podolsky, and Nathan Rosen who proposed that quantum mechanics might be incomplete and the particles' states might be defined by elements of reality [7] or "hidden variables". To test this idea, John Stewart Bell developed an inequality that, if violated, excluded the existence of these "hidden variables" [8].

The experimental studies of entanglement were initiated in photonic systems where the creation of entanglement and its detection were first developed. In a groundbreaking experiment, Stuart Freedman and John Clauser created entangled pairs of photons emitted in a cascade in calcium atoms. By measuring coincidence rates, they observed the first violation of the Bell inequality [9]. Technical improvements, especially in the groups of Alain Aspect and Anton Zeilinger, allowed for the realization of Bell tests closing both the locality [10] and the detection loophole [11, 12]. Based on these findings, the development of various real-world applications followed, leading to the emergence of new fields ranging from quantum information science to quantum sensing. For their experimental work, Clauser, Aspect and Zeilinger were honoured with the Nobel Prize in physics in 2022 [13].

1.2 QUANTUM TECHNOLOGIES

The fascination in entanglement stems from its fundamentally counterintuitive implications and its impact on systems featuring many quantum particles. Even a single quantum particle can show surprising behaviour through effects like superposition. A system consisting of an increasing number of quantum particles becomes more complex with an exponentially growing number of possible quantum states. The understanding of these many-body quantum systems is fundamentally interesting and is an open challenge in a variety of physical realizations. Nowadays, the interest has turned towards the employment of their complex features to develop real-world applications. While the early experimental studies focused on photonic systems, the technological advances ever since facilitated the creation of entanglement in systems consisting of massive particles. Studying entanglement in several experimental platforms is of great interest for quantum technologies with different technical requirements, such as quantum simulation, computation and sensing. I shortly summarize these fields in the following.

Quantum simulation is a powerful approach in which one quantum system is built to study the behaviour of another quantum system that may be difficult to access experimentally. This technique can be used to investigate the properties of materials, chemical reactions and to test new theories about many-body quantum states [14–17]. The technical basis for such simulations is careful assembly, individual addressing and subsequent detection on the single-particle level.

In quantum computing, calculations are performed on quantum particles. The states of the quantum system are encoded as qubits, in analogy to classical bits. In contrast to classical computation, qubits can be prepared in a superposition state allowing quantum computers to solve certain problems much faster than classical computers [18, 19]. Gate operations for calculations performed on the qubits pose extremely high demands on the control and read-out of every qubit.

An important field in the scope of this work is quantum sensing in which quantum systems are utilized to measure physical quantities such as time, electromagnetic fields, acceleration, rotation or gravity. By employing fundamental properties of quantum mechanics, such as superposition, these quantum systems achieve sensitivities beyond those of conventional sensors for many metrological tasks [20].

Many quantum sensors are based on interferometry, one of today's most precise measurement techniques. Interferometers were invented for light beams and have achieved phenomenal results in an extremely broad range of applications, culminating in the detection of gravitational waves in 2015 [21]. They cannot only be operated with light, but also with massive particles such as atoms. While there are several interferometric schemes, generally each particle is prepared in a superposition of states. These superposition states experience a differential phase shift induced by the measurement observable. In a final projective measurement, the phase is mapped onto an occupational probability of the involved states. As this is a probabilistic measurement, many

realizations are necessary to correctly determine the occupation of states, and the measurement resolution is directly linked to the number of realizations. Performing the measurement with many particles in parallel therefore largely enhances the measurement resolution.

The uncertainty of the phase estimation $\Delta\theta$ for a measurement with N atoms independently passing the interferometer is limited by $\Delta\theta_{SQL} \geq 1/\sqrt{N}$, also known as the Standard Quantum Limit (SQL). If the interferometer uses entangled quantum states instead, a reduced uncertainty in the quantity of interest can enhance the interferometric resolution up to the ultimate Heisenberg limit $\Delta\theta_H \geq 1/N$ [22]. Therefore, the ability to create large, metrologically useful entangled states is of high interest for quantum sensing. However, maintaining the advantage of entangled states to achieve a sensitivity close to the Heisenberg limit demands a high-fidelity detection for correct counting of the particles in the involved states. Otherwise, detection noise covers up the sensitivity gain [23].

In the following, I focus on the creation and detection of entangled states for quantum sensing applications. I briefly review the common experimental platforms creating many-body quantum states, their mechanisms and results in entanglement generation and their detection fidelities. Next, I explain the advantages of the platform chosen for the experiments performed in this thesis and describe the experimental challenges in this system. Then I will shortly summarize the experimental results and the main findings of this thesis.

1.3 MANY-BODY QUANTUM SYSTEMS

In recent years, the applications of many-body quantum states gained broader interest and opened the challenge to create, control and detect quantum system with an increasing number of constituents. The operation of large quantum systems is interesting for quantum simulation as this allows to investigate increasingly complex problems where not even approximate solutions are known. For quantum computation, a large number of qubits is necessary to perform useful computations that cannot be solved on a classical computer. In most quantum sensing applications, only large system sizes reach sensitivities that outperform classical analogs. Thus, large quantum systems combined with the high-fidelity creation, control and detection of suited quantum states is crucial for all of these technologies. The simultaneous realization of these requirements remains an on-going challenge.

Various experimental platforms create many-body quantum systems, including ultracold neutral atoms [24], molecules [25] or trapped ions [17], quantum dots [26], superconducting circuits [27], nuclear magnetic resonance (NMR) systems [28] and photonic systems [29].

Fig. 1.1 illustrates the experimental progress in multi-particle entanglement generation in several of these experimental platforms over time. After the first analysis of entangled pairs of photons, it took decades to create the first 3-particle entangled state with photons [30]. In the following years, the size of entangled states has been increased one by one currently reaching 14 photons [39] or 6 photons entangled in 3 degrees of freedom [38].

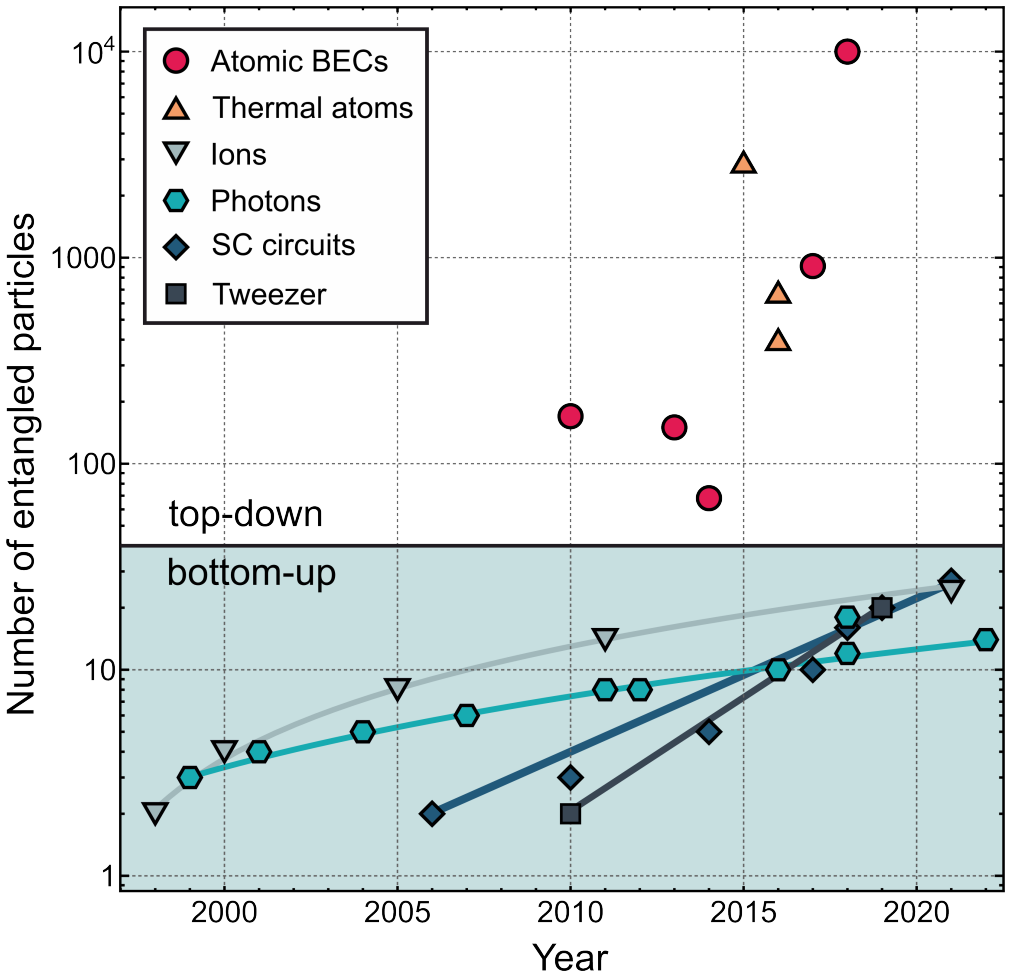

Figure 1.1: Achieved sizes of multi-particle entangled states in several experimental platforms over time. Systems are either built in a bottom-up approach such as in photons [30–39], ions [40–44], optical-tweezer atoms [45, 46] and superconducting circuits [47–53] or in a top-down approach as in thermal atoms [54–56] and atomic Bose-Einstein condensates (BECs) [23, 57–60]. The solid lines are guides to the eye.

The detection of photons on the single-particle level dates back to the 1930s [61]. Due to non-optimal efficiencies and dead times, accurately detecting them in large numbers is challenging. Although superconducting nanowire single-photon detectors (SNSPDs) have achieved system detection efficiencies of more than 98% [62], accurately detecting photonic many-body quantum states is a tremendous challenge [17].

The study of massive entangled particles started in ion experiments and the first pair of entangled ions was created in 1998 [40]. Entanglement in these systems is created by employing entangling gates, such as the controlled-NOT gate, enabling the engineering of various many-body quantum states. Currently, the number of entangled ions could be extended to 24 particles [44].

The creation of entanglement based on individually controlled neutral atoms is achieved in atomic optical tweezer experiments. An array of individually controlled, tightly focused laser beams holds single atoms in miniature laser

traps. Long-range interactions induced by the excitation or dressing to Rydberg states create entangled states. The first pair of neutral atoms entangled via the Rydberg blockade was created in 2010 [45]. After the development of techniques for the creation of defect-free arrays in 2016, this field gained a lot of momentum [63, 64] and the largest multi-particle entangled state created so far was a 20-particle Schrödinger-cat state [46].

Atomic quantum states are typically detected by illumination with near-resonant light. The corresponding counting resolution is limited by the shot noise of the scattered or absorbed photons. In trapped ion or optical tweezer experiments, trapping during detection allows for long illumination times and therefore large signals. For system sizes smaller than 100 particles, individual control can be maintained and detection efficiencies exceeding 99% have been achieved [65–68].

An alternative approach is the implementation of entangled states based on solid-state systems where qubits are realized by superconducting circuits. The states of the qubit are encoded in their discrete energy levels and entanglement can be created by a weak coupling between the individual circuits. This was experimentally realized in 2006 with two entangled circuits [47] and could be extended to 27 entangled qubits, by now [53]. These systems achieve control and readout with fidelities exceeding 98% [27].

The systems mentioned above operate in the bottom-up approach assembling the quantum state particle by particle. Due to their high-fidelity control and readout [27, 62, 67, 68], these systems are promising candidates for quantum simulation and computation. Systems designed for quantum computation attracted a lot of commercial interest and the involved companies do not publish all of their results. Therefore, better results than mentioned above might have been achieved by now. Note that these systems have excellent control over two-qubit entanglement generation. However, the transfer to multi-particle entanglement is challenging. In systems containing many qubits, not all qubits are necessarily entangled with each other or the multi-particle entanglement has not been analyzed in depth [69–71], depending on the application, this is also not necessary.

In contrast to quantum simulation and computation, quantum sensing usually relies on indistinguishable particles experiencing the same dynamics. In this case, a top-down approach is often advantageous. A large number of particles collectively addressed can be obtained in ultracold neutral atom experiments, either in thermal ensembles or in ensembles occupying a special quantum state called Bose-Einstein condensate (BEC). When bosons are cooled close to absolute zero temperature while maintaining a high density, they start to form a condensate in which the atoms collectively occupy the quantum mechanical ground state and can be described by a single macroscopic wave function [72]. This state, predicted by Albert Einstein and Satyendra Nath Bose in the 1920s [73, 74], was first experimentally realized in 1995 by Eric Cornell, Carl Wieman and Wolfgang Ketterle who were awarded the Nobel Prize for this achievement [75, 76]. In BECs, several interesting features, such as coherence and superfluidity, arise, which have led to a wide range of

experiments covering research questions from fundamental physics to many applications.

Both in thermal atoms and BECs, large entangled quantum states can be prepared and analyzed. In thermal ensembles, atom-light interactions have proven to successfully create large entangled states. In an early experiment, quantum correlations of photons were mapped onto thermal atoms [77]. Most commonly nowadays, entanglement in thermal atoms is created either by quantum non-demolition measurements or by interactions with single photons, typically inside an optical cavity. In quantum non-demolition measurements, a weak pre-measurement on an observable reduces its uncertainty before the final measurement is performed [78–82]. Alternatively, a system of an atomic ensemble placed inside an optical cavity can be engineered such that the absorption of single photons prepares large entangled states [54, 83]. These methods proved to be able to produce entangled states of up to 3000 atoms [54–56].

In BECs, the first experiments generating entanglement utilized non-linear interactions to implement one-axis twisting Hamiltonians that cause a sheering of the uncertainty distribution [57, 58, 84, 85]. Due to the indistinguishability of the atoms in a BEC, large entangled states can also be created by pairwise spin-changing collisions in which two atoms initially in $m_F = 0$ create a pair of entangled atoms in $m_F = \pm 1$ [59, 86–89]. The largest verified entangled state of up to 10000 particles employed this method [60].

In summary, there are many experimental techniques to create entanglement. BEC experiments with their high phase-space density and excellent options for manipulation are an ideal source of large entangled states suited for atom interferometry beyond the SQL. Maximizing the phase-space density is advantageous as this allows for longer interrogation times in an interferometric sequence and more precise control over the external degrees of freedom. BEC experiments offer the advantage of being nicely shielded from the environment and thereby suffering minimally from unwanted external influences. Due to their isolated setup, the internal and external states and interactions between the particles can be precisely controlled and manipulated via a variety of tools, such as magnetic fields, laser light, radio frequency (RF) and microwave (MW) fields. These tools allow for the engineering of states that are highly sensitive to the desired measurement variable such as electromagnetic or gravitational fields making them ideal sensors for such quantities. Therefore, BECs are the system of choice for this application.

1.4 CREATION AND DETECTION OF BECS

In quantum sensing, an experimental sequence consists of the generation of the quantum state and the actual measurement. As the system is not sensitive to the measurement observable during preparation time but only during measurement time, a fast BEC generation is beneficial for high measurement sensitivities. Traditional BEC experiments, however, suffer from low repetition rates that were often limited to one experimental realization per minute or less [90, 91]. Many technological advances in BEC creation have been

developed decreasing the preparation time. The realisation of two-dimensional magneto-optical traps (MOTs), have largely reduced the time necessary to load a large, laser-cooled ensemble [92, 93]. While laser-cooling techniques work comparatively quickly, they are usually not able to cool the atoms to quantum degeneracy. Therefore, forced evaporative cooling is commonly used as a final cooling step, typically performed in either optical or magnetic traps [94, 95].

Conventional magnetic traps offer a large trapping volume, but the rethermalization is slow and evaporation can easily take several seconds or tens of seconds [90, 91]. A dramatic increase in evaporation speed can be obtained by employing time-variable trapping potentials which maintain high rethermalization rates over the course of the evaporation. This approach has been implemented in the development of atom chips that create time-variable, tight magnetic confinement which has been proven to successfully create BECs in purely magnetic traps with repetition rates even above 1 Hz [96–98].

Magnetic traps, however, do not trap all atomic hyperfine levels which is a desirable degree of freedom for entanglement generation. Additionally, the implementation of an atom chip close to the atoms limits the optical access which is unfavourable for atom interferometry and detection.

A solution to both issues is the implementation of optical dipole traps (ODTs) which leave enough optical access and trap all hyperfine levels equally. However, ODTs either have a small initial trapping volume leading to high losses in the loading process or slow evaporation dynamics in larger trapping volumes. This challenge can be overcome by dynamically shaping the optical potential, either by sequentially employing several beams with decreasing waists [99], dynamically compressing the beam waists [100] or by quickly moving the ODT beam back and forth [101]. If the movement is faster than the trapping frequency, the atoms experience the time-average of the "painted" potential. Analog to the implementation of atom chips in magnetic traps, time-averaged potentials in optical dipole traps offer large trapping volumes and allow to maintain high rethermalization rates. Following this approach, BEC creation with less than 1 s of evaporation has been achieved [102]. Paired with a high-flux source, this method is on a par with the results achieved in atom chip experiments.

An alternative approach involving less engineering effort is a hybrid trap combining magnetic and optical trapping still resulting in a reasonable trade-off. The magnetic trap confines many atoms in its large volume and in a first evaporation step, the atomic density is increased such that the ensemble is efficiently transferred into a crossed-beam optical dipole trap. Due to the increased density, small beam waists can be chosen allowing for fast rethermalization. This way, evaporation durations of a few seconds can be achieved [103–106].

After BEC and entanglement generation, interferometry can be performed. For this, a high-fidelity characterization of the involved quantum states is desirable. Intense effort has been put in the development of techniques to prepare delicate quantum states and experiments have achieved impressive results. However, counting noise is one of the effects limiting the performance of experiments involving non-classical states and experiments would largely

profit from a detection on the single-particle level [23]. Additionally, a careful characterization of the unwanted processes during detection such as loss or atom number offset not only gives knowledge about these effects, but also allows for state reconstruction.

Experiments aiming at the creation of large entangled states of neutral atoms typically employ fluorescence or absorption detection with a short illumination. They report on detection noise ranging from 1.6 atoms at 3000 atoms [107], 10 atoms at 10^4 [23, 59, 108] to 50 atoms at 10^5 atoms [89]. Atom counting with single-particle resolution has not been achieved in these systems.

A method for detection of neutral atoms on the single-particle level is to collect the fluorescence light of atoms trapped in a MOT [109]. Trapping an atomic ensemble in a MOT for detection allows for illumination times on the order of tens to hundreds of milliseconds which is inaccessible for detection in free fall. In this configuration, number-resolved counting has been achieved for up to 1000 atoms [110] which could also be extended to the detection in two separate spatial modes [111]. An extension of this single-particle counting mechanism to BECs has not been demonstrated.

The accuracy of such a detection can still be compromised by loss and loading of atoms before or during the detection process. One method to carefully characterize these effects is quantum detector tomography (QDT), a method that allows for the detailed analysis of the characteristics of a detector's behaviour. It is based on the computation of a transfer matrix that links the ideal number distributions to the actual measurement outcomes. It requires a well-known initial state undergoing well-defined dynamics. A coherent spin state undergoing Rabi dynamics is an ideal candidate. QDT gives detailed information about particle loss or offset and allows for a state reconstruction.

This technique is well established in photonic experiments for single-photon counters and homodyne detection [112–114]. Recently, it has been applied to qubit readout in superconducting circuits and trapped ion systems as well [115, 116]. However, QDT has not been adapted for neutral atom experiments, so far.

1.5 STRUCTURE OF THE THESIS

In this thesis, I report on a high-flux source of BECs for atom interferometry. Within the BEC, entanglement has been generated via spin-changing collisions and the resulting entangled states are suited to enhance interferometric sensitivity. The experimental apparatus is paired with an accurate atom counting that has been applied to analyze a many-body quantum state with single-atom resolution. The experimental setup has been described in detail in Refs. [117] and [118]. This cumulative dissertation is based on three articles published or accepted in peer-reviewed journals that I review in the following.

NUMBER-RESOLVED PREPARATION OF MESOSCOPIC ATOMIC ENSEMBLES

The first publication describes our accurate atom counting setup, analyzes the contributing noise sources and demonstrates its use in preparing mesoscopic atomic ensembles with single-atom precision. The peer-reviewed and pub-

lished article "Number-resolved preparation of mesoscopic atomic ensembles" [119] and its author contributions are included in chapter 2.

The objective of this publication is to showcase the implementation of a number-resolving detection, similar to the one described in Ref. [110], within an apparatus designed for generating entangled states in BECs. The detection mainly consists of a set of MOT beams, a magnetic quadrupole field and a high-numerical aperture detection system. Due to limited optical access caused by additional components required for BEC creation, such as laser beams and coil pairs for cooling and trapping, the detection-MOT beams are spatially overlapped with the MOT beams with a large waist for state preparation on free space optics.

By utilizing small beam diameters for the detection-MOT, low laser powers can be employed, significantly reducing noise caused by light on the camera. This low-noise detection, combined with a large fluorescence signal, enables accurate counting of atomic ensembles. The publication includes a detailed analysis of the noise sources, identifying contributions from background signal, photoelectron shot noise, scattering rate noise, and atom loss during detection. The technique of accurate atom counting is then applied to actively prepare an atomic ensemble consisting of 7 atoms by repeatedly measuring and adjusting the atom number through brief periods of repumping light interruption. The target number is prepared with number fluctuations 18 dB below the shot noise level.

This publication demonstrates the successful implementation of accurate atom counting within an apparatus designed for creating entangled states in BECs. Clear quantization of the atomic peaks is observed up to 30 atoms and the noise model provides detailed information about the strengths and potential improvements of the detection system. The main noise source at larger atom numbers is identified as scattering rate noise, which arises from fluctuations in the frequency or intensity of the MOT beams leading to variations in the number of scattered photons. To address this issue, several enhancements have been made to the detection-MOT setup.

The homebuilt RF sources for the acousto-optic modulators (AOMs) have been replaced with Direct Digital Synthesis (DDS) sources featuring improved frequency stability characteristics. Additionally, the detection-MOT setup has been redesigned, replacing free-space optics with a fiber-based configuration. With these improvements, a more robust detection has been achieved.

RAPID GENERATION AND NUMBER-RESOLVED DETECTION OF SPINOR RUBIDIUM BOSE-EINSTEIN CONDENSATES Chapter 3 includes the preprint version [120] of the peer-reviewed and published article "Rapid generation and number-resolved detection of spinor rubidium Bose-Einstein condensates" [121] and the corresponding author contributions. The article focuses on the generation of a ^{87}Rb BEC with a high repetition rate and the subsequent selection and detection of a subensemble of the BEC with accurate atom counting. After briefly discussing the state-of-the-art in rapid BEC generation, the apparatus and the experimental sequence employed for BEC creation are presented.

The process begins with a high-flux two-dimensional MOT that captures atoms from the background gas and loads them into a three-dimensional MOT. A hybrid evaporation approach is then utilized, where the atoms are initially trapped in a magnetic quadrupole trap and undergo evaporative cooling through RF fields. Subsequently, the atoms are transferred to a crossed-beam ODT where further evaporative cooling takes place until Bose-Einstein condensation is achieved. This method enables the creation of BECs with 2×10^5 atoms in 3.3 s, comparable to the state-of-the-art hybrid evaporation schemes for rubidium BECs. By using MW transfers and resonant light for removal, a desired spin component is selected and detected using the detection-MOT. Subensembles of the BEC containing up to 16 atoms are analyzed, achieving a counting noise level of 0.2 atoms. This represents the first demonstration of the detection of spin states created in BECs with accurate atom counting.

The experiments conducted in this article greatly benefit from the insights gained in the previous analysis [119] and the subsequent redesign of the detection system. The upgraded detection system reveals broader counting peaks at small atom numbers, indicating increased noise caused by background light. This issue primarily arises from reflections of the MOT beams on the glass cell which enter the detection system. Reducing background noise would lead to improved single-atom resolution and enable accurate atom counting up to higher numbers.

Due to spatial constraints, completely preventing reflections from entering the detection system is not easily achievable. Alternatively, using beams with smaller waists would allow for reduced power while maintaining the same saturation parameter. However, the demonstrated resolution, potentially scaling up to hundreds of atoms, is already sufficient for analyzing many-body quantum states. Chapter 5 describes further improvements of the number-resolving detection as well as an enhanced BEC generation. By implementing an all-optical evaporation scheme, which prevents slowing of the evaporation dynamics over time and eliminates waiting time caused by coil heating, a faster BEC generation could be achieved.

TOMOGRAPHY OF A NUMBER-RESOLVING DETECTOR BY RECONSTRUCTION OF AN ATOMIC MANY-BODY QUANTUM STATE The third publication "Tomography of a number-resolving detector by reconstruction of an atomic many-body quantum state" presents the analysis of a coherent spin state using our number-resolving detection system [122]. The article has undergone peer review and has been accepted for publication at Physical Review Letters. The preprint version of the article, along with the corresponding author contributions, is included in chapter 4.

Building upon the techniques developed in our previous publication [121], a subensemble of a BEC containing 35 atoms, on average, is transferred to the level $|F = 2, m_F = 0\rangle$. A MW pulse of variable duration is applied on the clock transition $|F = 2, m_F = 0\rangle \rightarrow |F = 1, m_F = 0\rangle$. After removing atoms in the $F = 2$ manifold, the number of atoms in $|F = 1, m_F = 0\rangle$ is analyzed. Due to technical imperfections, an atom number offset is observed that can be attributed to non-perfect removal and loading of atoms from the background

during detection. The obtained histograms are compared to the expected Binomial distributions of atoms undergoing Rabi dynamics. Through the application of a quantum detector tomography, a transfer matrix is calculated that can be used to reconstruct the initial state. This is the first demonstration of QDT in a neutral-atom quantum system.

Our results demonstrate the detection of sensitive quantum states with single-atom precision. We explain experimental imperfections and reconstruct the initial quantum state using QDT. In the future, this method can be applied to entangled quantum states with characteristic atom number distributions.

OUTLOOK Chapter 5 provides a summary of the results described in publications [119, 121, 122] and outlines the technical improvements to the BEC generation and number-resolving detection implemented after publication of those articles. Additionally, it presents an ongoing experiment conducted in the laboratory which directly applies the techniques developed in this thesis. Furthermore, the chapter offers an outlook on future experiments.

2

NUMBER-RESOLVED PREPARATION OF MESOSCOPIC ATOMIC ENSEMBLES

AUTHORS

Andreas Hüper, Cebrail Pür, Mareike Hetzel, Jiao Geng, Jan Peise, Ilka Kruse, Mick Kristensen, Wolfgang Ertmer, Jan Arlt and Carsten Klempt

AUTHOR CONTRIBUTIONS

In this publication, I carried out measurements and reviewed and edited the manuscript. Andreas Hüper designed and built the apparatus, developed software, carried out measurements, analyzed and visualized the data and wrote the first manuscript. Cebrail Pür supported building the apparatus, carried out measurements and reviewed and edited the manuscript. Jiao Geng was involved in the methodology, building the apparatus, carrying out measurements, reviewing and editing the manuscript. Jan Peise was involved in the design of the project, provided technical assistance, reviewed and edited the manuscript. Ilka Kruse contributed to the project in its early stages, provided technical assistance, reviewed and edited the manuscript. Mick Kristensen developed software, reviewed and edited the manuscript. Jan Arlt and Wolfgang Ertmer were involved in the conceptualization and supervision of the project, reviewed and edited the manuscript. Carsten Klempt supervised the design and implementation of the experiments, provided funding and guidance to the authors throughout the research process, helped with data analysis and interpretation, edited and reviewed the manuscript.

New Journal of Physics
The open access journal at the forefront of physics

Deutsche Physikalische Gesellschaft DPG
IOP Institute of Physics

Published in partnership with: Deutsche Physikalische Gesellschaft and the Institute of Physics

OPEN ACCESS

RECEIVED
8 September 2020

ACCEPTED FOR PUBLICATION
3 December 2020

PUBLISHED
13 December 2021

PAPER

Number-resolved preparation of mesoscopic atomic ensembles

A Hüper[1], C Pür[1], M Hetzel[1], J Geng[1,3,4,*], J Peise[1], I Kruse[1], M Kristensen[2], W Ertmer[1,5], J Arlt[2] and C Klempt[1,5]

[1] Institut für Quantenoptik, Leibniz Universität Hannover, Welfengarten 1, 30167 Hannover, Germany
[2] Center for Complex Quantum Systems, Department of Physics and Astronomy, Aarhus University, Ny Munkegade 120, DK-8000 Aarhus C, Denmark
[3] Key Laboratory of 3D Micro/Nano Fabrication and Characterization of Zhejiang Province, School of Engineering, Westlake University, 18 Shilongshan Road, Hangzhou 310024, Zhejiang Province, China
[4] Institute of Advanced Technology, Westlake Institute for Advanced Study, 18 Shilongshan Road, Hangzhou 310024, Zhejiang Province, China
[5] DLR Institut für Satellitengeodäsie und Inertialsensorik, Callinstr. 36, 30167 Hannover
[*] Author to whom any correspondence should be addressed.

E-mail: geng.jiao@westlake.edu.cn

Keywords: single-atom resolution, accurate atom counting, sub-Poissonian number fluctuations

Abstract

The analysis of entangled atomic ensembles and their application for interferometry beyond the standard quantum limit requires an accurate determination of the number of atoms. We present an accurate fluorescence detection technique for atoms that is fully integrated into an experimental apparatus for the production of many-particle entangled quantum states. Number-resolved fluorescence measurements with single-atom accuracy for 1 up to 30 atoms are presented. According to our noise analysis, we extrapolate that the single-atom accuracy extends to a limiting atom number of 390(20) atoms. We utilize the accurate atom number detection for a number stabilization of the laser-cooled atomic ensemble. For a target ensemble size of 7 atoms prepared on demand, we achieve a 92(2)% preparation fidelity and reach number fluctuations 18(1) dB below the shot noise level using real-time feedback on the magneto-optical trap.

1. Introduction

Large systems of entangled particles can be built by successively adding more and more constituents and by engineering the entanglement between them [1, 2]. Alternatively, large numbers of up to 3000 mutually entangled ultracold atoms [3–6] can be generated by exploiting the indistinguishability of the atoms. To harness the full potential of such systems, the conceptual and technological challenge is to detect and control the number of indistinguishable atoms on the single-particle level.

A prime example is the application of entangled atomic ensembles for atom interferometry beyond the standard quantum limit (SQL) [7]. Atom interferometers allow measuring a quantity of interest (e.g. electromagnetic fields, time, acceleration, rotation, gravitational fields) by inferring the relative phase θ between two atomic states from their occupation number difference. The noise of this phase measurement is limited by the SQL to $\Delta\theta \geqslant N^{-1/2}$ for a given total number N of unentangled particles. The phase resolution can surpass the SQL by employing entangled particles, and may ultimately reach down to the ultimate Heisenberg limit $\Delta\theta \geqslant N^{-1}$. A phase resolution near the Heisenberg limit requires the counting of atoms with single-particle resolution. The need for an accurate detection of the particle number can be avoided by the application of echo protocols, which can only be implemented in very specific measurement tasks [8–11].

Large ensembles of 10^8 atoms have been detected using resonance fluorescence detection with a performance close to the quantum projection-noise [12]. A technique for measuring the number of neutral atoms in ultra-cold ensembles with single-particle resolution is realised by loading the atoms into a

magneto-optical trap (MOT) [13]. The method has been extended to two separate spatial modes [14] and thus became applicable for the operation of an atom interferometer. These experiments demonstrated single-particle resolving atom counting for up to 1200 atoms. In this sense, the atomic detection outperforms the capabilities in the analysis of indistinguishable photonic quantum states [15, 16]. However, a single-atom resolving detection still has to be combined with an apparatus for the generation of entanglement in BECs.

In this article, we present a single-particle resolving atom number detection in a MOT which is fully integrated into an apparatus for the generation of many-particle entangled quantum states. We demonstrate the counting of up to 30 atoms with single-particle resolution. According to our noise analysis, we extrapolate that the single-atom accuracy extends to a limiting atom number of 390(20) atoms.

Applying feedback mechanisms to quantum systems has proven useful in protecting the phase of a coherent spin state against noise [17] and stabilizing photon number states [18]. Similarly, accurate detection techniques aid the creation of desired atomic ensemble sizes with sub-Poissonian number fluctuations. The high-fidelity preparation of a few-fermion system in its ground state was verified using fluorescence detection in a MOT configuration [19], while a non-destructive Faraday imaging technique has been utilized to prepare ultracold atom clouds at the shot noise level [20, 21]. We apply the single-particle resolving atom counting to demonstrate a novel preparation of laser-cooled atomic samples. In a feedback loop, a dedicated loss process steadily reduces the number of atoms, while the atom number of the ensemble is regularly measured, until a target number is reached. We demonstrate the controlled preparation of 7 atoms with a fidelity of 92(2)%, which corresponds to a suppression of the number fluctuations by 18(1) dB below the shot noise level. These improved noise conditions in the initial ensemble can directly impact any following steps, for example the loading of optical dipole traps. Specifically, the preparation fidelity of single-atom microtraps [22] is strongly limited by two-body losses—a problem which could be bypassed by loading a deterministically prepared number of atoms into the trap with high efficiency [23]. We propose that the developed technique can also be employed to improve the counting capabilities under the influence of slow drifts. In the future, the developed number-resolving single-atom detection can be utilized for obtaining unprecedented fidelities in the analysis of many-particle quantum states.

2. Fluorescence imaging of individual atoms in a magneto-optical trap

The detection of ultracold atomic ensembles is typically realized by a short illumination of the freely falling cloud with resonant light. During the illumination of a few tens of microseconds, either the unabsorbed or the scattered photons are collected, until the atomic sample is accelerated and diluted too much due to the strong light pressure. The obtainable resolution in the counting of atoms is ultimately limited by the shot noise of the detected photons, or more precisely, by the shot noise of the photoelectrons that are counted in the detector. Much longer detection times can be reached, when the atoms are trapped during illumination. The additional trapping can be realized by far-detuned optical lattices [24–26], optical dipole traps [27–29] or MOTs [13, 23, 30–34]. In such traps, lifetimes above 1 s can be reached which allow for a greatly improved signal-to-noise ratio.

2.1. Emission and detection of photons

In our experiments, the detection system is integrated into an apparatus that allows for the fast creation of many-particle entangled states in a BEC. The setup includes a 3D-MOT with large beams with a $1/e^2$-width of 14 mm that is loaded by a $2D^+$–MOT [35] at a rate of $9.5(1) \times 10^9$ atoms per second, coils for a magnetic quadrupole trap with a gradient of 300 G cm^{-1}, and a crossed-beam dipole trap at a wavelength of 1064 nm. These components form a powerful source for the delivery of optically trapped Bose–Einstein condensates with a repetition time of only a few seconds. With an actively stabilized magnetic field, it will be possible to generate entangled ensembles by spin changing collisions. Spin changing collisions may be used to create high-fidelity twin-Fock states [5, 36, 37] or squeezed vacuum states [38–40]. In the described experimental system, the established techniques for the generation of entangled many-particle states will be combined with the number-resolving detection to achieve unprecedented fidelities and to perform atom interferometry at the ultimate Heisenberg limit.

For the detection, we trap ^{87}Rb atoms in an additional MOT with small beams with a $1/e^2$-width of 1.25 mm. The atoms are imaged onto a charge-coupled-device (CCD) camera with a photon detection efficiency of 97%. A large fraction (5%) of the scattered photons is captured by a custom designed objective with a high numerical aperture of NA = 0.45. Despite its high NA, the objective can be placed outside the vacuum cell, due to the combination of a large diameter of 50 mm and a large working distance of 48 mm of the first aspheric lens. A second plano-convex lens with a diameter of 75 mm and a focal length of

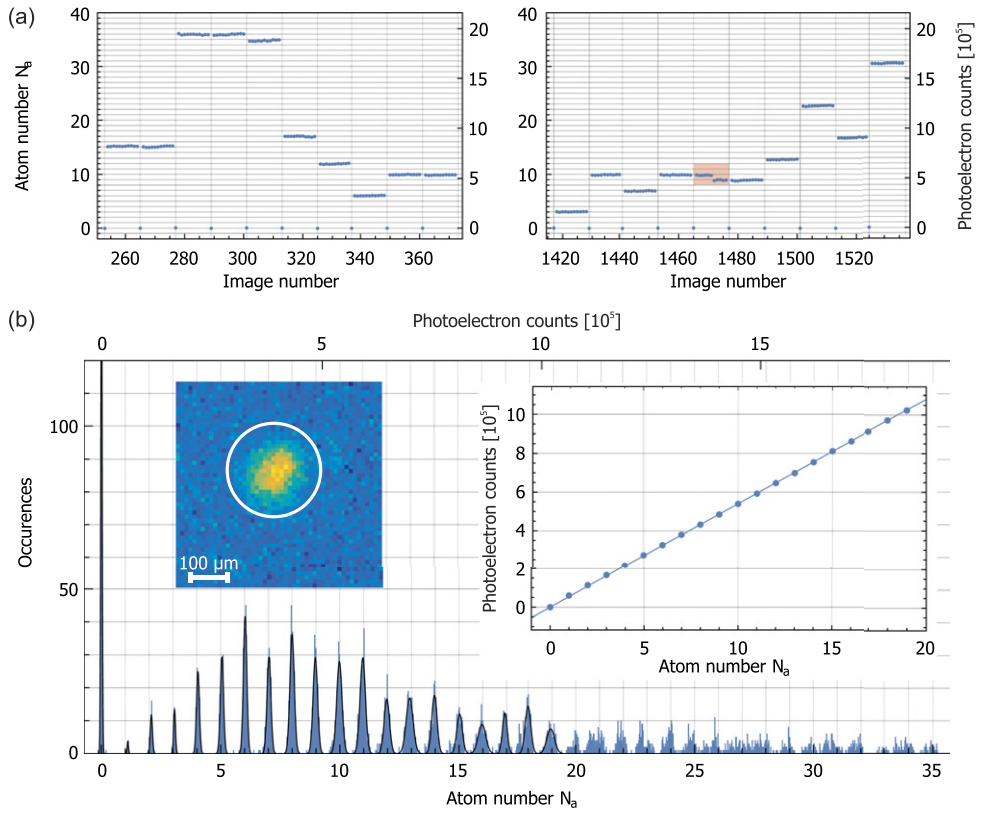

Figure 1. Number-resolving single-atom detection. (a) Two panels show example time traces of the recorded fluorescence signal in units of atom number (left axis) and photoelectrons (right axis). In rare cases the loss of a single atom is recorded (red highlight). (b) The histogram of all recorded fluorescence images is fit with a sum of Gaussian distributions. Inset left: fluorescence image of a single atom trapped in the detection MOT. The white circle exemplifies the region of interest over which counts are integrated. Inset right: the center positions of the Gaussian fits show a linear dependence on the atom number and are used to extract the calibration factor of $600(1) \times 10^3$ photoelectrons/atom/s.

142 mm completes the objective, which is housed inside an aluminum tube. The inside of the tube is painted with blackboard coating, reducing the transmission of unwanted background light. With a total magnification of $M = 2.62$ the resolution of the imaging system is limited by the pixel size of the CCD camera to about 5 μm. For an evaluation of the detection system, the recorded images of the trapped atomic cloud are processed as follows. The overall signal of a cloud of N_a atoms is determined by summing the counted photoelectrons over the area of the MOT image on the CCD camera (see figure 1(b)). Each atom within the MOT contributes a signal of $n_{ph} = R_{sc}\tau_{det}\eta$ photoelectrons, where R_{sc} is the photon scattering rate, τ_{det} the detection time and η the overall detection efficiency. The photon scattering rate is given by $R_{sc} = \Gamma/2 \times s_0/\left(1 + s_0 + 4\Delta^2/\Gamma^2\right)$, where $\Gamma = 2\pi \times 6.1$ MHz is the natural line width of the $^{87}RbD_2$ transition, Δ represents the detuning of the laser with respect to the resonance frequency of the transition and $s_0 = I/I_{sat}$ is the saturation parameter that describes the ratio of the collective intensity I of the laser beams and the isotropic saturation intensity $I_{sat} = 3.576(4)$ mW cm^{-2}. The photoelectron shot noise contributes a term of $\sigma^2_{psn} = N_a/n_{ph}$ to the total signal variance and can thus be reduced by extending the exposure time. The contrary holds true for the noise caused by atom loss. Due to the finite lifetime of the trap, atom loss contributes a term $\sigma^2_{loss} = N_a\tau_{det}/\tau_{life}$, where τ_{life} is the lifetime of the MOT. By employing small detection MOT beams, potential stray light sources causing unwanted background noise in the images are reduced. With a collective peak intensity of 24 mW cm^{-2}, the three beam pairs yield a combined saturation parameter of $s_0 = 6.65$. Together with the detuning of $\Delta = 2\pi \times 6$ MHz, the scattering rate is estimated to be $R_{sc} = 1.1 \times 10^7$photons/s. During an exposure of 90 ms, our detection system with its total efficiency of $\eta = 4.71\%$ is expected to collect 4.7×10^4 photoelectrons per atom.

2.2. Identification of single atoms

Our experimental procedure for the calibration of the atom number detection starts with the acquisition of a background image without atoms but with all relevant light sources. This is followed by the loading of atoms from the 2D$^+$–MOT into the 3D–MOT configuration for a duration of only 15 ms. Afterward the trapping light is switched off for a short duration of 10 ms before a small number of atoms is recaptured from the expanding cloud by activating our small detection MOT. Here, the atomic ensemble is held for 500 ms to ensure that the remaining untrapped atoms have left the detection region. Now, the fluorescence

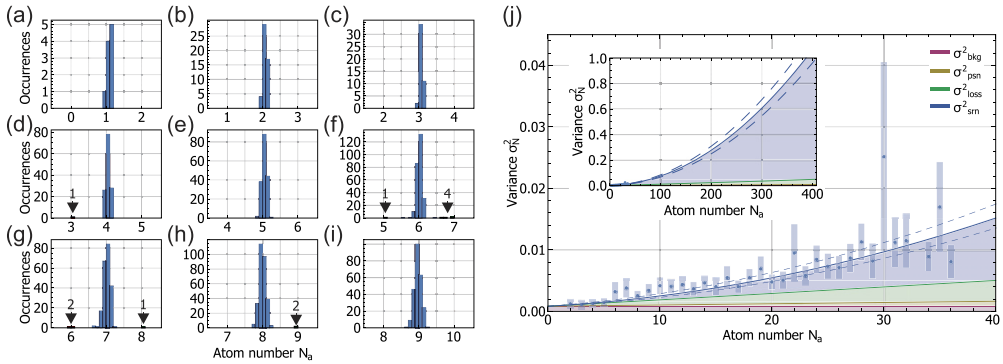

Figure 2. Analysis of consecutive fluorescence levels and noise model fit. (a–i) By comparing consecutively recorded fluorescence signals single atom loading and loss events are extracted. The histograms exemplify the event classification depending on the initial atom number from $N_a = 1$ to $N_a = 9$, respectively. The central peak in each histogram represents the survival of all atoms present in the MOT, while occurrences to its left and right correspond to loss and loading events, respectively. (j) The noise model is fit to the experimental data. The colors indicate the contributions from different noise sources. Inset: an extrapolation of the noise model fit suggests an upper limit of 390(20) atoms at which individual atoms become indistinguishable by our current detection setup.

signal of the atomic sample is acquired for a duration of $\tau_{det} = 90$ ms. During camera read-out, the atom cloud is held in the trap for 220 ms before another image is taken with the same exposure time. These two steps are repeated until a total set of 11 images is acquired. The time traces of the fluorescence signal (see figure 1(a)) exhibit clearly discernable levels. In rare cases, unwanted single-atom loss or loading events can be observed. A histogram based on more than 5200 recorded atom images shows well-resolved peaks for up to $N_a \approx 30$ atoms. The peaks reflect the integer number of atoms that are held in the trap. The clear visibility of these features proves that the resolution is well below the single-atom level. Fitting a sum of Gaussian functions to the first 20 peaks of the histogram reveals the center positions of the individual peaks. These center positions scale linearly with the detected camera counts, corresponding to single-atom count rate of $600(1) \times 10^3$ photoelectron counts per atom per second (see inset in figure 1(b)), which matches our expectation to within 10%. Quadratic contributions proved to be negligible in our case. This calibration yields an accurate absolute value for the number of atoms without the need of a precise specification of the experimental parameters such as laser powers, laser detunings and beam sizes.

3. Lifetime and loading rate analysis

For optimal performance of the detection setup, a long lifetime of the MOT is crucial as it limits the usable illumination time. Similarly, the detection benefits from a small loading rate, which could be caused by atoms being captured from the background gas or the residual flow from the $2D^+$–MOT cell. Both parameters, lifetime and loading rate, can be extracted from the recorded time traces. We evaluate each possible pair of successive measurements and classify them as loss, loading or survival event for atom numbers up to $N_a = 15$. For each atom number between $N_a = 1$ and 9, a histogram showcases the occurrences of those three events in figures 2(a)–(i). Importantly, across the full data set no two-body loss events were identified. This fact in conjunction with the occurrence of only 14 loss events across 24 482 observed individual atoms in the image pairs shows, that the total holding and detection time of $\tau_{hold} + \tau_{det} = 310$ ms is short compared to the lifetime of the trap. The loss process can be expected to follow Poissonian statistics, such that the lifetime is $\tau_{life} = (\tau_{hold} + \tau_{det}) / P_{loss}(\tau_{hold} + \tau_{det}) = 540(140)$s, where $P_{loss}(\Delta t)$ is the probability for a loss event to occur during the time span Δt. The loading rate $R_{load} = 0.014(4)\ s^{-1}$ is based on 12 observed events within a set of 2710 image pairs and is a result of the low capture velocity in combination with a low Rb background pressure. In total, these measurements show that the single-atom resolution of the atom number is not limited by a finite lifetime or residual loading, even for larger ensembles.

4. Noise model

The capability of our number detection is best analyzed based on the shot-to-shot number counting fluctuations, where long-term drifts of the scattering rate, which may be caused by intensity or frequency drifts in the laser light, are not considered. These shot-to-shot fluctuations can be described by the two-sample variance $\sigma_N^2 = \langle (N_{a,j+1} - N_{a,j})^2 \rangle_j / 2$, where j is an index running across successively captured images. The noise model [13, 21]

$$\sigma_N^2 = \sigma_{bkg}^2 + \sigma_{psn}^2 + \sigma_{srn}^2 + \sigma_{loss}^2 \quad (1)$$

includes contributions from background noise, photoelectron shot noise, scattering rate noise and noise from atom loss. From the acquired background images, the background contribution is calculated to be $\sigma^2_{\mathrm{bkg}} = 8.4 \times 10^{-4}$ and hence well below the single-atom level. The photoelectron shot noise $\sigma^2_{\mathrm{psn}} = N_{\mathrm{a}}/\left(\eta\tau_{\mathrm{det}} R_{\mathrm{sc}}\right)$ scales linearly with the atom number. The scattering rate noise $\sigma^2_{\mathrm{srn}} = N_{\mathrm{a}}^2\alpha^2/\tau_{\mathrm{det}}$ is caused by corresponding fluctuations in the intensity and frequency of the MOT light that are combined into the fluorescence noise parameter α. Finally, we consider the linear single-atom loss term $\sigma^2_{\mathrm{loss,lin}} = \tau_{\mathrm{det}} N_{\mathrm{a}}/\left(2\tau_{\mathrm{life}}\right)$, while we found contributions from mean atom-loss and two-body losses due to light-assisted collisions to be negligible for our data. The resulting noise model reads

$$\sigma_N^2 = \sigma^2_{\mathrm{bkg}} + N_{\mathrm{a}}\left(1/\left(\eta\tau_{\mathrm{det}} R_{\mathrm{sc}}\right) + \tau_{\mathrm{det}}/\left(2\tau_{\mathrm{life}}\right)\right) + N_{\mathrm{a}}^2\alpha^2/\tau_{\mathrm{det}}. \tag{2}$$

By fitting the noise model to our data for atom numbers up to $N_{\mathrm{a}} = 36$, with the fluorescence noise parameter as the only free parameter, we obtain a value of $\alpha = 7.6(4) \times 10^{-4}\ \mathrm{s}^{1/2}$. This corresponds to either 22 kHz in laser frequency noise or to a relative fluctuation of 0.039 in the saturation parameter s_0. Extrapolating the noise model to the critical single-atom detection threshold $\sigma_N^2 = 1$ yields a maximally discernable atom number of $N_{\mathrm{a}}^{\mathrm{max}} = 390(20)$ atoms.

5. Atom-number stabilization

We utilize our accurate atom counting to deliver precise atom numbers on demand, by interleaving the atom number measurement with a dedicated loss process, until a desired number is reached. We start out with an average cloud of $\langle N_{\mathrm{a}}\rangle = 15(4)$ atoms trapped in our detection MOT. Upon image acquisition, the atom number is estimated in real time. The image data is read out during a holding time of 180 ms and the field-programmable gate array (FPGA), that controls the experimental protocol stops the loss sequence once the detected number of atoms falls below a desired threshold of $N_{\mathrm{a}}^{\mathrm{thr}} = 7.5$ atoms. The prepared ensemble is stored in the MOT to check the final atom number with four additional number measurements. The loss is induced by turning off the repumping light for 3 ms during the 198 ms of holding time between the 90 ms detection windows (see figure 3(a)). Time traces in figure 3(b) show that the fluorescence level of the MOT detection halts at our desired atom number of $N_{\mathrm{a}} = 7$. All atoms have an independent and equal survival probability p_{s} with which they remain in the trap. Each loss step can be viewed as an independent series of Bernoulli trials, such that the atom number statistics will follow a binomial distribution. The histograms in figures 4(a) and (b) showcase the transitions from an input atom number $N_{\mathrm{a}}^{(\mathrm{i})}$ to an output atom number $N_{\mathrm{a}}^{(\mathrm{s})}$ for a single loss step. Collectively fitting the histogram data from $N_{\mathrm{a}}^{(\mathrm{i})} = 18$ to 8 with a binomial distribution

$$B\left(p_{\mathrm{s}}, N_{\mathrm{a}}^{(\mathrm{i})}, N_{\mathrm{a}}^{(\mathrm{s})}\right) = \binom{N_{\mathrm{a}}^{(\mathrm{i})}}{N_{\mathrm{a}}^{(\mathrm{s})}} p_{\mathrm{s}}^{N_{\mathrm{a}}^{(\mathrm{s})}}\left(1-p_{\mathrm{s}}\right)^{N_{\mathrm{a}}^{(\mathrm{i})}-N_{\mathrm{a}}^{(\mathrm{s})}} \tag{3}$$

reveals their common survival probability $p_{\mathrm{s}} = 96.66(4)\%$, that characterizes our loss process. For a given survival probability, it is possible to calculate a maximal obtainable preparation fidelity due to the unwanted accidental removal of two atoms in the final loss step. For our loss step, we expect a fidelity of 88% to obtain a state with exactly 7 atoms. This corresponds to a suppression of the number fluctuations of 17.3 dB below shot noise. Due to the high survival probability, single-step jumps from higher atom numbers (the dominant unwanted process would be a jump from 9 to 6 atoms) do not contribute to the obtained results. Figure 4(c) shows the final experimental result of the stabilization procedure. We obtain the target number of 7 atoms in 142 of the 155 cases, which corresponds to a state preparation with a 92(2)% fidelity. We obtain a too small result in 13 cases (6 atoms: 12 cases, 5 atoms: 1 case). From these data, we extract a suppression of 18(1) dB.

On average, 21(10) induced loss steps were needed to reach the desired threshold with an overall loss cycle time of 288 ms. This results in a total preparation time of 6 s. After the initial loading, about 63% of the preparation time are caused by the image readout, which can in principle be reduced by employing different hardware. The physical limit is set by the exposure time of 90 ms which is necessary to maintain the demonstrated number counting accuracy. For experimental configurations where the camera readout time is negligible, the fidelity of the ensemble preparation could be further improved by reducing the loss probability per step and increasing the number of steps to reach the threshold. Furthermore, the preparation speed could be increased by adjusting the loss probability dynamically depending on the current number of atoms in the trap. Additionally, the success rate of the procedure could be improved by enabling a reloading mechanism from our initial 2D–MOT in cases where the target number has been undercut.

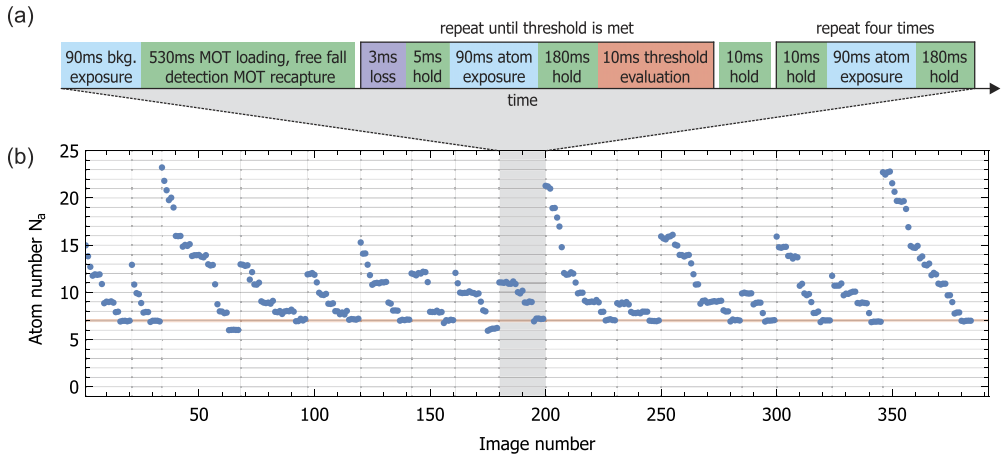

Figure 3. Stabilization experiment. (a) Experimental sequence for the atom number stabilization. (b) 15 example time traces ending in stabilized atom numbers with varying initial atom numbers in the MOT. A new measurement is started (vertical gray lines) once the target atom number of 7 (red horizontal line) has been hit or undercut for five successive images.

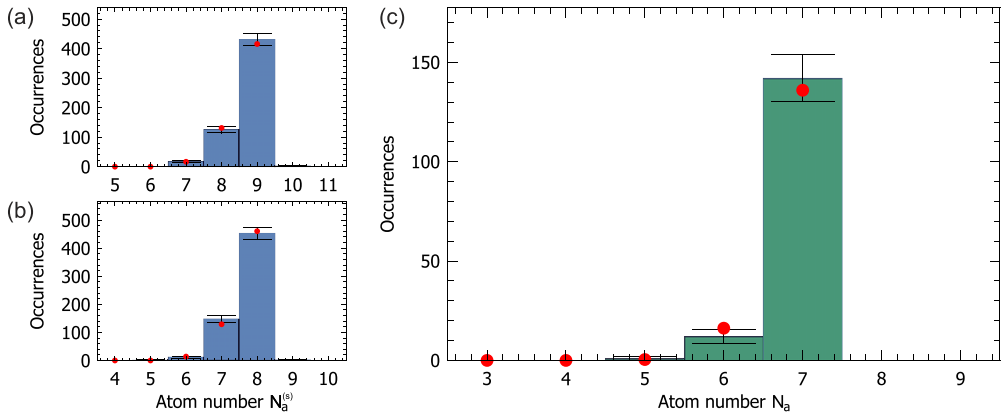

Figure 4. Loss characterization and stabilization result. (a, b) The exemplary histograms show the transition statistics of consecutive measurements for initial atom numbers $N_a^{(i)} = 9$ and 8 with the corresponding statistical errors. A collectively fit binomial model (red points) for the transitions statistics from initial atom numbers $N_a^{(i)} = 18$ to 8 results in a survival probability of $p_s = 96.66(4)\%$ for an individual atom over the course of a single loss step. (c) The histogram shows the atom number distribution for the successful stabilization with the corresponding statistical errors. It is derived from the atom number evaluation of the threshold image once the loss process is stopped. An ensemble of 7 atoms was prepared with a fidelity of 92(2)%, corresponding to an 18(1) dB suppression below shot noise. A truncated binomial distribution for our derived survival probability centered around 8 atoms describes the data accurately (red points).

6. Summary

In summary, we have demonstrated a number-resolving single-atom detection of up to 30 atoms in an experimental apparatus that is designed for the generation of entangled many-particle states. The shot-to-shot fluctuations suggest that the scattering rate noise limits the single-atom resolution to 390(20) atoms. In conjunction with our accurate atom number detection, we have employed a real-time feedback onto the repumping light of the MOT to stabilize the number of atoms in the laser-cooled ensemble. A preparation fidelity of 92(2)% was demonstrated for an ensemble of 7 atoms, corresponding to a suppression of 18(1) dB below the shot noise level. This technique allows to deliver number-stabilized atomic ensembles on demand.

Interestingly, the controlled and well characterized loss mechanism of the feed-back loop could also be employed to correct for the influence of long term drifts on the measurement of large atom numbers. Here, drifts become increasingly important, since the collective noise of all individual atoms should remain larger than the single-atom signal. To mitigate the effect of such drifts, the initial illumination can be followed by several iterations of engineered loss and detection. Thereby, one obtains a series of number measurements

that optimally spans the full range of atom numbers between the initial number and zero. This series of number measurements allows for an individual calibration of the current scattering rate, as each individual number measurement must correspond to an integer number. This procedure will enable a number-resolved detection signal even in the presence of parameter drifts.

In the future, we will apply the developed detection to analyze many-particle quantum states with single-particle resolution as well as advance our methods for metrology beyond the SQL [36, 40] toward the ultimate Heisenberg limit.

Acknowledgments

We acknowledge support from the Deutsche Forschungsgemeinschaft (DFG) under Germany's Excellence Strategy (EXC-2123 QuantumFrontiers 390837967), and through CRC 1227 (DQ-mat), project B01. JA and MK acknowledge support by the Danish National Research Foundation through the Center of Excellence "CCQ" (Grant Agreement No.: DNRF156), the VILLUM FONDEN research Grant No. 12398, and the Carlsberg foundation. The publication of this article was funded by the Open Access Fund of the Leibniz Universität Hannover.

ORCID iDs

A Hüper https://orcid.org/0000-0002-7161-4435
M Kristensen https://orcid.org/0000-0002-9667-2789
J Arlt https://orcid.org/0000-0002-5782-3927

References

[1] Bohnet J G, Sawyer B C, Britton J W, Wall M L, Rey A M, Foss-Feig M and Bollinger J J 2016 *Science* **352** 1297–301
[2] Zhong H S *et al* 2018 *Phys. Rev. Lett.* **121** 250505
[3] McConnell R, Zhang H, Hu J, Ćuk S and Vuletić V 2015 *Nature* **519** 439–42
[4] Haas F, Volz J, Gehr R, Reichel J and Estève J 2014 *Science* **344** 180–3
[5] Lücke B, Peise J, Vitagliano G, Arlt J, Santos L, Tóth G and Klempt C 2014 *Phys. Rev. Lett.* **112** 155304
[6] Hosten O, Engelsen N J, Krishnakumar R and Kasevich M A 2016 *Nature* **529** 505
[7] Pezzè L, Smerzi A, Oberthaler M K, Schmied R and Treutlein P 2018 *Rev. Mod. Phys.* **90** 035005
[8] Davis E, Bentsen G and Schleier-Smith M 2016 *Phys. Rev. Lett.* **116** 053601
[9] Hosten O, Krishnakumar R, Engelsen N J and Kasevich M A 2016 *Science* **352** 1552–5
[10] Anders F, Pezzè L, Smerzi A and Klempt C 2018 *Phys. Rev.* A **97** 043813
[11] Schulte M, Martínez-Lahuerta V J, Scharnagl M S and Hammerer K arXiv:1911.11801v1
[12] Biedermann G W, Wu X, Deslauriers L, Takase K and Kasevich M A 2009 *Opt. Lett.* **34** 347
[13] Hume D B, Stroescu I, Joos M, Muessel W, Strobel H and Oberthaler M K 2013 *Phys. Rev. Lett.* **111** 253001
[14] Stroescu I, Hume D B and Oberthaler M K 2015 *Phys. Rev.* A **91** 013412
[15] Calkins B *et al* 2013 *Opt. Express* **21** 22657
[16] Harder G, Bartley T J, Lita A E, Nam S W, Gerrits T and Silberhorn C 2016 *Phys. Rev. Lett.* **116** 143601
[17] Kohlhaas R, Bertoldi A, Cantin E, Aspect A, Landragin A and Bouyer P 2015 *Phys. Rev.* X **5** 021011
[18] Sayrin C *et al* 2011 *Nature* **477** 73–7
[19] Serwane F, Zürn G, Lompe T, Ottenstein T B, Wenz A N and Jochim S 2011 *Science* **332** 336–8
[20] Gajdacz M, Hilliard A J, Kristensen M A, Pedersen P L, Klempt C, Arlt J J and Sherson J F 2016 *Phys. Rev. Lett.* **117** 073604
[21] Kristensen M A, Gajdacz M, Pedersen P L, Klempt C, Sherson J F, Arlt J J and Hilliard A J 2017 *J. Phys. B: At. Mol. Opt. Phys.* **50** 034004
[22] Grünzweig T, Hilliard A, McGovern M and Anderse M F 2010 *Nat. Phys.* **6** 951–4
[23] Frese D, Ueberholz B, Kuhr S, Alt W, Schrader D, Gomer V and Meschede D 2000 *Phys. Rev. Lett.* **85** 3777–80
[24] Sherson J F, Weitenberg C, Endres M, Cheneau M, Bloch I and Kuhr S 2010 *Nature* **467** 68–72
[25] Bakr W S, Gillen J I, Peng A, Fölling S and Greiner M 2009 *Nature* **462** 74–7
[26] Elíasson O, Heck R, Laustsen J S, Müller R, Weidner C A, Arlt J J and Sherson J F 2019 arXiv:1912.03079
[27] Endres M *et al* 2016 *Science* **354** 1024–7
[28] Barredo D, de Léséleuc S, Lienhard V, Lahaye T and Browaeys A 2016 *Science* **354** 1021–3
[29] Ohl de Mello D, Schäffner D, Werkmann J, Preuschoff T, Kohfahl L, Schlosser M and Birkl G 2019 *Phys. Rev. Lett.* **122** 203601
[30] Raab E L, Prentiss M, Cable A, Chu S and Pritchard D E 1987 *Phys. Rev. Lett.* **59** 2631–4
[31] Hu Z and Kimble H J 1994 *Opt. Lett.* **19** 1888
[32] Haubrich D, Schadwinkel H, Strauch F, Ueberholz B, Wynands R and Meschede D 1996 *Europhys. Lett.* **34** 663–8
[33] Ruschewitz F, Bettermann D, Peng J L and Ertmer W 1996 *Europhys. Lett.* **34** 651–6
[34] Yoon S, Choi Y, Park S, Kim J, Lee J-H and An K 2006 *Appl. Phys. Lett.* **88** 211104
[35] Dieckmann K, Spreeuw R J C, Weidemüller M and Walraven J T M 1998 *Phys. Rev.* A **58** 3891–5
[36] Lücke B *et al* 2011 *Science* **334** 773–6
[37] Luo X-Y, Zou Y-Q, Wu L-N, Liu Q, Han M-F, Tey M K and You L 2017 *Science* **355** 620–3

[38] Hamley C D, Gerving C S, Hoang T M, Bookjans E M and Chapman M S 2012 *Nat. Phys.* **8** 305
[39] Peise J *et al* 2015 *Nat. Commun.* **6** 8984
[40] Kruse I *et al* 2016 *Phys. Rev. Lett.* **117** 143004

3

RAPID GENERATION AND NUMBER-RESOLVED DETECTION OF SPINOR RUBIDIUM BOSE-EINSTEIN CONDENSATES

AUTHORS

Cebrail Pür[1], Mareike Hetzel[1], Martin Quensen, Andreas Hüper, Jiao Geng, Jens Kruse, Wolfgang Ertmer and Carsten Klempt

AUTHOR CONTRIBUTIONS

For this publication, I set up the dipole trap laser system, developed the experimental sequence for BEC generation and detection, set up the updated detection system, carried out measurements, analyzed, interpreted and visualized data and wrote the initial draft of the manuscript. Cebrail Pür collected and analyzed experimental data, designed the updated detection system and wrote the initial draft of the manuscript. Martin Quensen set up the updated detection system, carried out measurements and reviewed and edited the manuscript. Andreas Hüper developed software, provided technical assistance, contributed to the conceptualization and reviewed and edited the manuscript. Jiao Geng contributed in early stages of the project and its methodology, set up parts of the dipole trap laser system, edited and reviewed the manuscript. Jens Kruse and Wolfgang Ertmer were involved in the conceptualization and supervision of the project, edited and reviewed the manuscript. Carsten Klempt supervised the design and implementation of the experiments, provided funding and guidance to the authors throughout the research process, helped with data analysis and interpretation, and wrote, edited and reviewed the manuscript.

1 equal contribution

Rapid generation and number-resolved detection of spinor Rubidium Bose-Einstein condensates

Cebrail Pür[1],[*] Mareike Hetzel[1],[*],[†] Martin Quensen[1], Andreas Hüper[1,2],
Jiao Geng[3,4], Jens Kruse[1,2], Wolfgang Ertmer[1,2], and Carsten Klempt[1,2]
[1]*Institut für Quantenoptik, Leibniz Universität Hannover, Welfengarten 1, D-30167 Hannover, Germany*
[2]*Deutsches Zentrum für Luft- und Raumfahrt e.V. (DLR),*
Institut für Satellitengeodäsie und Inertialsensorik (DLR-SI), Callinstraße 30b, D-30167 Hannover, Germany
[3]*Key Laboratory of 3D Micro/Nano Fabrication and Characterization of Zhejiang Province,*
School of Engineering, Westlake University, 18 Shilongshan Road, Hangzhou 310024, Zhejiang Province, China
[4]*Institute of Advanced Technology, Westlake Institute for Advanced Study,*
18 Shilongshan Road, Hangzhou 310024, Zhejiang Province, China
(Dated: February 2, 2023)

High data acquisition rates and low-noise detection of ultracold neutral atoms present important challenges for the state tomography and interferometric application of entangled quantum states in Bose-Einstein condensates. In this article, we present a high-flux source of ^{87}Rb Bose-Einstein condensates combined with a number-resolving detection. We create Bose-Einstein condensates of 2×10^5 atoms with no discernible thermal fraction within 3.3 s using a hybrid evaporation approach in a magnetic/optical trap. For the high-fidelity tomography of many-body quantum states in the spin degree of freedom [1], it is desirable to select a single mode for a number-resolving detection. We demonstrate the low-noise selection of subsamples of up to 16 atoms and their subsequent detection with a counting noise below 0.2 atoms. The presented techniques offer an exciting path towards the creation and analysis of mesoscopic quantum states with unprecedented fidelities, and their exploitation for fundamental and metrological applications.

I. HIGH-FLUX SOURCES OF BOSE-EINSTEIN CONDENSATES

Because of their well-controlled spatial mode and their phase coherence, Bose-Einstein condensates (BECs) of neutral atoms present a valuable resource for atom interferometry and quantum atom optics experiments in general. Many of the applications, however, require short preparation times. In atom interferometry, the preparation time defines the dead time of the sensor and therefore influences bandwidth and noise sensitivity. Short preparation times are also important as they often dominate the data acquisition rate. In our case, we wish to generate entangled many-body states, and perform a high-fidelity state tomography. The number of required measurements scales exponentially with the number of atoms. Therefore, an accurate characterization of quantum states with an increasing number of atoms requires the acquisition of large data sets, during which the environmental conditions have to remain stable. An improvement of the measurement rate not only improves the quality of the results, but in fact constitutes a requirement for scaling up the number of atoms in the generation of high-fidelity quantum states.

Besides few exemptions [2, 3], BECs are typically realized by forced evaporative cooling in conservative potentials resulting from inhomogeneous magnetic or optical fields. Figure 1 displays a selection of atom numbers and repetition rates obtained with atom-chip magnetic traps [4–8], macroscopic magnetic traps [9–15], all-optical traps [16–23], and combinations of magnetic and optical traps [24–27].

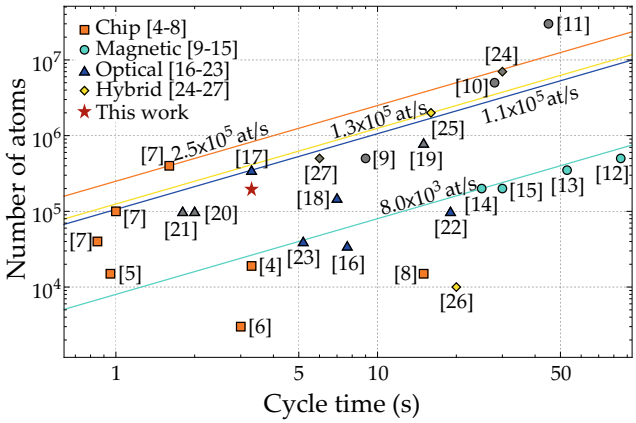

FIG. 1. Overview of the production time for different BEC sources with a given final atom number. Orange squares are atom-chip based experiments, teal circles correspond to magnetically trapped ensembles, blue triangles show all-optical evaporation and yellow diamonds represent hybrid magnetic and optical methods. Sources featuring other atomic species than rubidium are marked in grey. The red star marks the result of this work corresponding to an atomic flux of 6×10^4 atoms per second. Solid lines illustrate the atomic flux of the best performing experiments per category.

For our experiments, we aim at BECs with 10^5 rubidium atoms at a maximal repetition rate. At the same time, the set-up is supposed to enable the selection and

[*] These authors contributed equally.
[†] Author to whom correspondence should be addressed. hetzel@iqo.uni-hannover.de

detection of subensembles with single-particle counting resolution. The inclusion of such a high-performance detection excludes the implementation of an atom chip, which would promise short preparation times, but leads to detrimental light scattering on the chip surface.

In this article, we present our experimental set-up which enables the generation of 2×10^5 rubidium atoms with a cycle time of 3.3 s and the number-resolving detection of a subensemble in a specific spin state. The BEC generation relies on a macroscopic quadrupole trap combined with a crossed-beam optical dipole trap (cODT). The fluorescence detection is a fiber-based second generation from an earlier implementation [28]. This article describes the experimental set-up and the obtained results, also as a reference for the quantum detector tomography reported in the accompanying publication [1].

This paper is organized as follows. In Section II, we describe the details of our apparatus and our experimental sequence for fast BEC production. Section III presents the successive spin preparation of small ensembles by microwave transitions and subsequent optical removal of atoms. The number-resolving detection set-up is described in Section IV. Section V concludes with a summary and outlook.

II. RAPID CREATION OF BOSE-EINSTEIN CONDENSATES

The experimental set-up (Fig. 2) consists of two glass cells which are connected by two sequential differential pumping stages. The first, rectangular cell ($150 \times 60 \times 60$ mm) contains a two-dimensional magneto-optical trap ($2D^+$-MOT). The second, octagonal glass cell (seven 1" and two 3" viewports), contains a 3D-MOT. and further experiments are carried out. The experimental sequence is initiated by loading the MOT and continues with the BEC creation and the mode-selective detection (Fig. 3). The design of the $2D^+$-MOT is described in Ref. [29]. The 3D-MOT is operated with a coil pair of 20 windings each in the vertical direction, yielding 12 G/cm at 103 A. The cooling and detection laser light is generated by two external-cavity diode lasers [30], frequency-stabilized via modulation transfer spectroscopy [31], and 4 tapered amplifiers. Optical fibers deliver the light to the vacuum set-up where the light power is actively stabilized. Here six beams with a power of 35 mW and a waist of 7.5 mm are formed and enter the glass cell via the 3-inch windows at an angle of 45°. This beam configuration offers large optical access for detection with a numerical aperture $NA = 0.42$. The glass cell is anti-reflection-coated on both sides for 780nm-light to maximally suppress background light during the fluorescence detection. The initial loading rate of our 3D-MOT is 2.4×10^{10} atoms/s and within 200 ms 4×10^9 atoms are captured.

After MOT loading, an optical molasses cools the atoms to 18 μK. The atoms are optically pumped to the level $|F, m_F\rangle = |2, 2\rangle$ on the D2 $F = 2 \rightarrow F' = 2$ transition and loaded into a magnetic quadrupole trap (QPT). The magnetic field gradient, generated by a coil pair with 62 windings each, is linearly ramped up from 58 G/cm to 169 G/cm in 50 ms. The currents are measured by current transducers and actively stabilized to better than 10^{-4} relative stability. The $1/e$ lifetime cannot be measured during the maximally allowed continuous operation of 10 s and exceeds 150 s. We perform evaporation by two linear radiofrequency (rf) ramps from 20 MHz to 3.5 MHz within 1.6 s.

Afterwards, a crossed-beam optical dipole trapping potential is added with a trap center slightly below the magnetic trap center [25, 32]. The optical dipole potential is generated by a 55 W Coherent Mephisto MOPA laser with a wavelength of 1064 nm. Two beams, whose intensity is each stabilized via an acousto-optic deflector (AOD) enter the glass cell via free-space optics along x and y-direction with waists of 70μm and 35μm, respectively. The power is increased to 6.5 W and 600 mW within 200 ms, and the quadrupole field is ramped to zero within another 200 ms. Finally, the power of the dipole trap beams is decreased in six linear ramps to final values of 95 mW and 45 mW within 1.2 s resulting in simulated trap frequencies of $(\omega_x, \omega_y, \omega_z,) = 2\pi \times (60, 160, 150)$ Hz.

The evaporation is optimized for speed instead of atom number yielding an evaporation efficiency of $\gamma = 1.7$. After the final evaporation, we obtain BECs of 2×10^5 atoms with no discernible thermal fraction. The total BEC preparation takes 3.3 s. Due to an insufficient cooling of the quadrupole trap coils, this cycle rate can so far only be maintained for 200 repetitions. An operation for longer times requires an additional 2 s cool-down time, or an improvement of the water cooling which is planned for the future.

III. SELECTION OF A SUBENSEMBLE IN A SPECIFIC SPIN STATE

After the rapid creation of a BEC, we aim at the generation of many-body spin states and their analysis by selecting one spin mode for number-resolved detection. This spin-selective number detection is the prerequisite of the characterization of a coherent spin state in Ref. [1]. Here, we demonstrate that a particular spin component can be chosen for detection with a fluorescence-based number counting. The technique is demonstrated for up to 16 atoms, but can be extended to several hundred atoms in the near future. While this number seems to be small at the first glance, we would like to highlight that this spin-selective detection allows for a tomography of multi-particle states with much larger atom numbers, as long as they are sufficiently polarized (e.g. spin-squeezed states). As an example, we transfer a variable amount of atoms to the spin level $|1, 0\rangle$ while we remove all remaining components in the $F = 2$ manifold. The atoms in level $|1, 0\rangle$ are counted in a fiber-based miniature magneto-optical trap (mMOT). The same technique

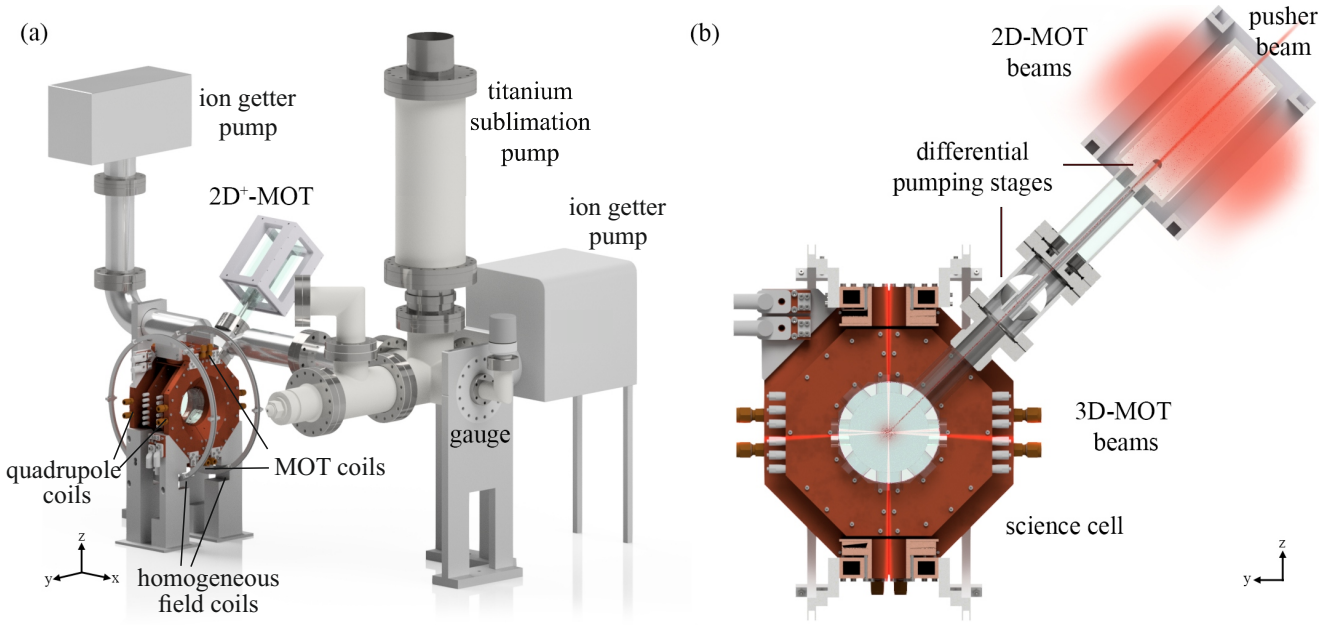

FIG. 2. (a) Computer-aided design of the ultra-high vacuum system with the two-chamber set-up and the coil system. The system contains two glass cells for the $2D^+$-MOT and the 3D-MOT/BEC-generation, which are connected via two differential pumping stages at a 45° angle. The connection tube and the science cell are individually pumped by two pump arrangements. The coil system surrounding the science cell is assembled by a pair of vertical 3D-MOT coils, a pair of horizontal quadrupole coils and a pair of orthogonally aligned Helmholtz coils. The science cell and the coil arrangement are optimized for a high-NA optical access along the x direction. (b) Cross-section of the two-chamber set-up and the coil system. Atoms are released from dispensers, building up the pressure inside the $2D^+$-MOT. A pusher beam guides the $2D^+$-MOT beam through the two differential pumping stages into the science chamber, where they are captured and cooled.

can be implemented for a large variety of many-particle spin states to select a specific spin level for counting. For the creation of many of these states, an ensemble in the spin level $|1,0\rangle$ serves as a starting point. Therefore, we characterize the necessary techniques by preparing and detecting a small fraction of the BEC in $|1,0\rangle$. We select a subensemble of the BEC that we transfer into the spin level $|1,1\rangle$ by choosing the length of the MW pulse as a fraction of its π-pulse length. We remove the remaining components in the $F=2$ manifold by a 100 μs resonant cooling light push. In the following, a MW π-pulse transfers the atoms to the spin level $|2,0\rangle$. To ensure there are no remaining fractions in F=1 caused by a non-perfect MW transfer, we employ a 100µs resonant repumping light push. A final MW pulse transfers the atoms into the spin level $|1,0\rangle$ and another removal of atoms in $F=2$ ensures the detection of the desired components in $F=1$. Between the optical removals short waiting times on the order of 10 ms have been implemented to guarantee that the mechanical shutters open and close reliably. The transfer of atoms to the level $|1,0\rangle$ from the initially prepared level $|2,2\rangle$ is carried out by a low-noise microwave source [33]. The quantization axis is given by a magnetic field of 0.78 G, which is actively stabilized to a magnetic field sensor, yielding a magnetic field noise of 170 μG.

A counting resolution on the single-atom level places strong requirements on the efficiency and selectivity of the final removal process. Two effects deteriorate the counting precision: (i) Atoms expelled from the trap may collide with atoms that are selected for detection and remove them unintentionally. (ii) The resonant light that is used to expel the $F=2$ atoms may pump atoms into the non-resonant $F=1$ levels before they leave the trap. To avoid unwanted loss due to collisions during the optical removal, we transfer the atoms into a single-beam optical dipole trap. Pumping the atoms into a closed cycling transition reduces the probability of populating non-resonant states. Therefore, we use a homogeneous magnetic field of 6.7 G and a σ^+-polarized light beam for optical removal of the $F=2$ manifold before we detect the atoms in $F=1$ in our number-resolving mMOT set-up. To avoid recapturing the previously removed atoms, we implement a waiting time of 150 ms after the final removal before detection.

IV. NUMBER-RESOLVING DETECTION

We detect the number of selected atoms in the $F=1$ manifold with an improved mMOT set-up that is based on the system described in Ref. [28]. The initial version of the detection set-up included beams distributed via free-space optics so that they could be superimposed

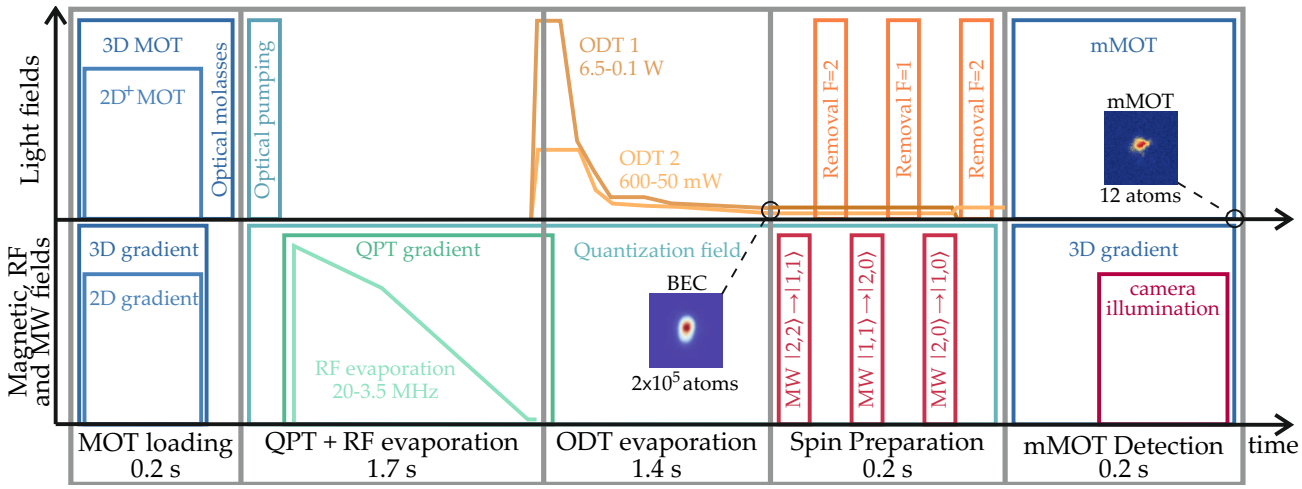

FIG. 3. Schematic of the experimental sequence. The upper and lower panels illustrate the light and magnetic fields, respectively. The field strengths and the time axis are not to scale. The BEC is created within 3.3 s in a hybrid evaporation approach in a magnetic/optical trap. Subsequently, the desired spin component is chosen and analyzed in the number-resolving mMOT set-up.

with the larger MOT beams creating our 3D-MOT for BEC generation. This set-up proved to be capable of accurate atom counting but it showed long-term instabilities due to the long beam paths. The updated version therefore features six fiber-based beams minimizing the optical path lengths. Each fiber is individually mounted and its output intensity is actively stabilized, enabling a precise balancing of the intensities of the counter-propagating beams. The exact position of the mMOT depends on several parameters as the magnetic field minimum, the precise beam alignment and their intensity balance. To precisely overlap the mMOT with the BEC position, the mMOT beams are aligned onto the BEC position. Homogeneous magnetic fields in both horizontal directions shift the magnetic field minimum to the BEC position. The beam intensities and thereby the exact mMOT position have been optimized by a differential evolution algorithm [34], because the nontrivial interference of the beams leads to jumps of the mMOT position. The mMOT is operated at a magnetic field gradient of 12 G/cm with a detuning of 10 MHz (1.7Γ) and an intensity of 6 times the saturation intensity. Due to spatial constraints, the new horizontal beams enter the science glass cell under an angle of 35°. This changed angle results in a higher background scattering in our detection objective and therefore in higher background noise $\sigma_{bg,new} = 0.15$ compared to 0.03 in the previous set-up [28]. Fig. 4 shows a histogram of the recorded fluorescence signal for 2433 repeated number measurements of atoms in the level $|1,0\rangle$. The histogram shows a clear quantization of the fluorescence signal, proving a counting resolution well below the single-atom limit. The counting noise depends on the total number of atoms and is well described by Gaussian functions with a width $\sigma_N = 0.169 + 0.0017N$. Assuming a linear scaling, this allows for single-particle detection of more than 400 atoms, in correspondence to our earlier quantification [28]. The data can now be binned at half-integer binning limits, with a number assignment fidelity ranging from 99.7% at 1 atom to 99.0% at 15 atoms.

The mMOT has a finite probability to capture unwanted atoms from the background gas. These atoms are mainly caused by the frequent use of the $2D^+$-MOT during the BEC creation, leading to a temporally increased background pressure. Atoms passing the small but still relevant trapping volume of the mMOT can be trapped and therefore counted in the detection process. This results in a detection offset of 0.27 atoms, which appears as a relevant signal in the quantum tomography of our number detection [1].

The effects contributing to the detection offset are characterized in Fig. 5. Panel (a) shows the unwanted background loading of the mMOT, once in the beginning (cyan rectangles) and once after 7.5 h of continuous operation (blue circles). The increase from 0.1 to 3.4 atoms per second extracted from linear fits is caused by the temporary increase of the background gas that builds up over time. We find that this build-up is generated by laser-cooled atoms in the $2D^+$-MOT beam and not by thermal atoms passing the two differential pumping stages.

To maintain accurate atom number counting, the loading of atoms from the background gas has to be minimized which poses a limit to the total mMOT operation time. At the same time, our single-particle counting resolution demands long illumination times. A total mMOT operation time of 115 ms including 65 ms for illumination yields a reasonable compromise. Fig. 5 (b) shows the linear dependence of the detection offset on the number of removed atoms N_{rem}. Non-perfect optical removals and increased recapturing of previously removed atoms

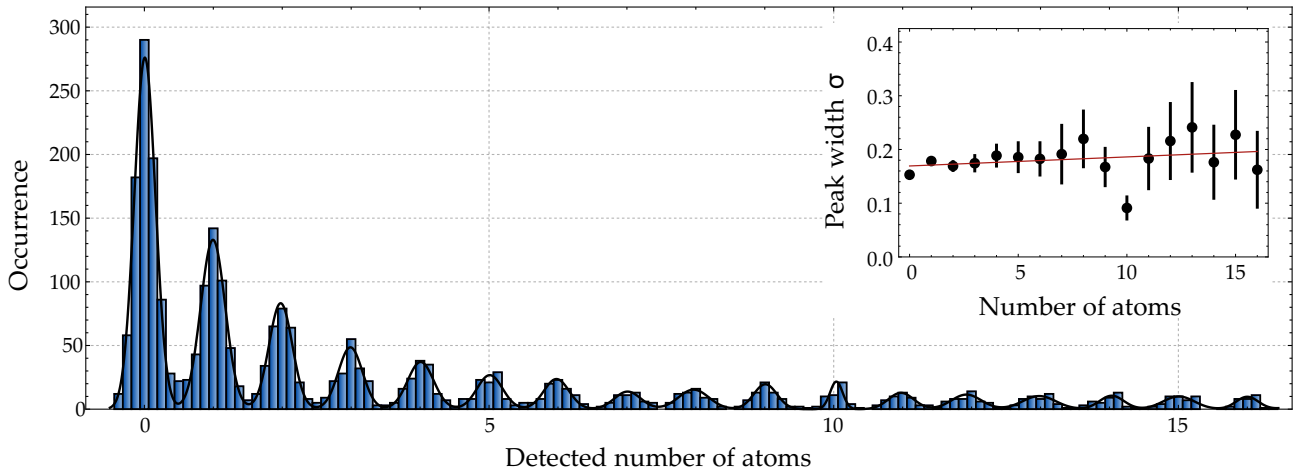

FIG. 4. Histogram of the fluorescence signal for up to 16 atoms. The signal (blue bars) shows a clear quantization for integer atom numbers. The individual peaks are fitted with Gaussian distributions (black line), whose widths are shown in the inset. The linear fit (solid red line) is compatible with a previously determined single-particle resolution limit of 400 atoms.

both contribute to this increasing detection offset N_{off} following $N_{off} = 0.26 + 0.001 N_{rem}$. The red star illustrates the detection offset obtained in Ref. [1]. Fig. 5 (c) illustrates the extinction ratio in dependence of the waiting time after the optical removal. The waiting time of 150 ms reduces the probability to recapture previously removed atoms in the mMOT by more than one order of magnitude. In summary, the described detection enables a number-resolving tomography of quantum many-body states up to a few hundred atoms.

V. CONCLUSION & OUTLOOK

In conclusion, we have presented a method for the generation and number-resolved detection of spinor BECs. We create BECs with 2×10^5 ^{87}Rb atoms within 3.3 s using a hybrid approach. The high-flux atom source consists of a 2D$^+$-MOT combined with a 3D-MOT. After transfer into a magnetic quadrupole trap, a first rf-evaporation step is applied to increase the phase space density and to efficiently transfer the atoms into the optical dipole potential, in which fast efficient evaporation is performed. Our experiment shows a high flux BEC creation of 6×10^4 atoms/s, which is close to the published record for Rb [25], disregarding the atom chip experiments which do not provide sufficient optical access. The cycle time can be further improved by decreasing the evaporation time in the crossed optical dipole trap. We can readily implement dynamically shaped potentials using our acousto-optical deflector set-up, which will give us independent control of the trap depth and trapping frequencies, leading to accelerated evaporation dynamics.

We select a single spin level for detection and optically remove residual atoms with an extinction ratio of 0.001. We resolve the created output states with a detection offset of 0.27 atoms and a number assignment fidelity of 99% at 15 atoms. The presented techniques pave the way for the high-fidelity tomography of polarized many-particle entangled states, such as single- and two-mode spin-squeezed states.

ACKNOWLEDGMENTS

This work is supported by the QuantERA grants SQUEIS and MENTA. We acknowledge financial support from the Deutsche Forschungsgemeinschaft (DFG, German Research Foundation) - Project-ID 274200144 - SFB 1227 DQ-mat within the project B01 and Germany's Excellence Strategy - EXC-2123 QuantumFrontiers-Project-ID 390837967. M.Q. acknowledges support from the Hannover School for Nanotechnology (HSN).

[1] M. Hetzel, L. Pezzè, C. Pür, M. Quensen, A. Hüper, J. Geng, J. Kruse, L. Santos, W. Ertmer, A. Smerzi, and C. Klempt, Tomography of a number-resolving detector by reconstruction of an atomic many-body quantum state, arXiv:2207.01270 (2022).

[2] A. Urvoy, Z. Vendeiro, J. Ramette, A. Adiyatullin, and V. Vuletić, Direct laser cooling to Bose-Einstein condensation in a dipole trap, Phys. Rev. Lett. **122**, 203202 (2019).

[3] S. Stellmer, B. Pasquiou, R. Grimm, and F. Schreck, Laser cooling to quantum degeneracy, Phys. Rev. Lett. **110**, 263003 (2013).

[4] D. M. Farkas, K. M. Hudek, E. A. Salim, S. R. Segal, M. B. Squires, and D. Z. Anderson, A compact, trans-

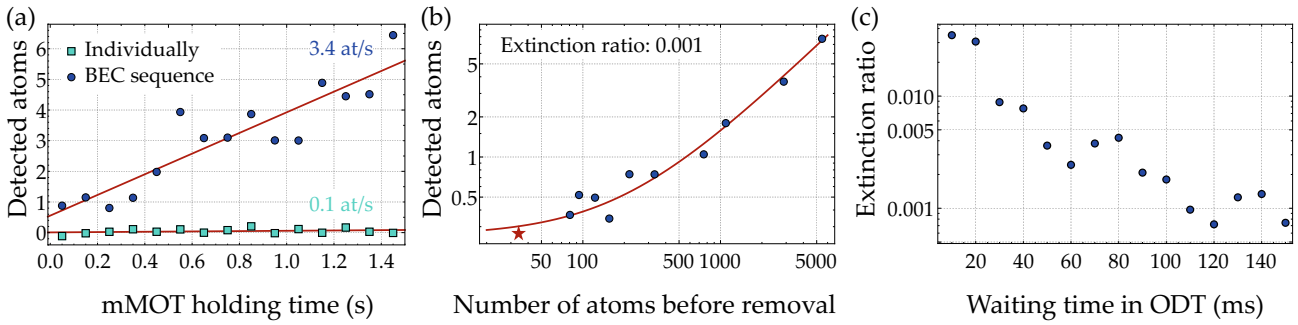

FIG. 5. Characterization of the detection offset. (a) The frequent use of the 2D$^+$-MOT temporarily increases the background gas and therefore the mMOT loading rate from initially 0.1 (cyan rectangles) to 3.4 atoms/s (blue circles) after 7.5 hours of operation. (b) The detection offset linearly depends on the number of atoms before removal.The red line shows a linear fit with an initial offset that is caused by a non-perfect optical removal of atoms. The red star marks the detection offset in Ref. [1]. (c) The extinction ratio of the optical removal improves with an increasing subsequent waiting time before detection.

portable, microchip-based system for high repetition rate production of Bose–Einstein condensates, Appl. Phys. Lett. **96**, 093102 (2010).

[5] D. M. Farkas, E. A. Salim, and J. Ramirez-Serrano, Production of Rubidium Bose-Einstein Condensates at a 1 Hz Rate, arXiv:1403.4641 (2014).

[6] M. Horikoshi and K. Nakagawa, Atom chip based fast production of Bose-Einstein condensate, Applied Physics B **82**, 363 (2006).

[7] J. Rudolph, W. Herr, C. Grzeschik, T. Sternke, A. Grote, M. Popp, D. Becker, H. Müntinga, H. Ahlers, A. Peters, C. Lämmerzahl, K. Sengstock, N. Gaaloul, W. Ertmer, and E. M. Rasel, A high-flux BEC source for mobile atom interferometers, New J. Phys. **17**, 065001 (2015).

[8] S. Abend, M. Gebbe, M. Gersemann, H. Ahlers, H. Müntinga, E. Giese, N. Gaaloul, C. Schubert, C. Lämmerzahl, W. Ertmer, W. P. Schleich, and E. M. Rasel, Atom-chip fountain gravimeter, Phys. Rev. Lett. **117**, 203003 (2016).

[9] K. B. Davis, M. O. Mewes, M. R. Andrews, N. J. van Druten, D. S. Durfee, D. M. Kurn, and W. Ketterle, Bose-Einstein condensation in a gas of sodium atoms, Phys. Rev. Lett. **75**, 3969 (1995).

[10] M.-O. Mewes, M. R. Andrews, N. J. van Druten, D. M. Kurn, D. S. Durfee, and W. Ketterle, Bose-Einstein condensation in a tightly confining dc magnetic trap, Phys. Rev. Lett. **77**, 416 (1996).

[11] D. S. Naik and C. Raman, Optically plugged quadrupole trap for Bose-Einstein condensates, Phys. Rev. A **71**, 033617 (2005).

[12] T. Esslinger, I. Bloch, and T. W. Hänsch, Bose-Einstein condensation in a quadrupole-ioffe-configuration trap, Phys. Rev. A **58**, R2664 (1998).

[13] S. Kumar, S. Sarkar, G. Verma, C. Vishwakarma, M. Noaman, and U. Rapol, Bose-einstein condensation in an electro-pneumatically transformed quadrupole-Ioffe magnetic trap, New Journal of Physics **17**, 023062 (2015).

[14] R. Dubessy, K. Merloti, L. Longchambon, P.-E. Pottie, T. Liennard, A. Perrin, V. Lorent, and H. Perrin, Rubidium-87 Bose-Einstein condensate in an optically plugged quadrupole trap, Phys. Rev. A **85**, 10.1103/PhysRevA.85.013643 (2012).

[15] S. Peil, J. V. Porto, B. L. Tolra, J. M. Obrecht, B. E. King, M. Subbotin, S. L. Rolston, and W. D. Phillips, Patterned loading of a Bose-Einstein condensate into an optical lattice, Phys. Rev. A **67**, 051603 (2003).

[16] M. D. Barrett, J. A. Sauer, and M. S. Chapman, All-Optical Formation of an Atomic Bose-Einstein Condensate, Phys. Rev. Lett. **87**, 010404 (2001).

[17] T. Kinoshita, T. Wenger, and D. S. Weiss, All-optical Bose-Einstein condensation using a compressible crossed dipole trap, Phys. Rev. A **71**, 011602 (2005).

[18] J.-F. Clément, J.-P. Brantut, M. Robert-de Saint-Vincent, R. A. Nyman, A. Aspect, T. Bourdel, and P. Bouyer, All-optical runaway evaporation to Bose-Einstein condensation, Phys. Rev. A **79**, 061406 (2009).

[19] M. Landini, S. Roy, G. Roati, A. Simoni, M. Inguscio, G. Modugno, and M. Fattori, Direct evaporative cooling of ^{39}K atoms to Bose-Einstein condensation, Physical Review A **86**, 033421 (2012).

[20] S. Stellmer, R. Grimm, and F. Schreck, Production of quantum-degenerate strontium gases, Physical Review A **87**, 013611 (2013).

[21] R. Roy, A. Green, R. Bowler, and S. Gupta, Rapid cooling to quantum degeneracy in dynamically shaped atom traps, Phys. Rev. A **93**, 043403 (2016).

[22] D. Xie, D. Wang, W. Gou, W. Bu, and B. Yan, Fast production of rubidium Bose-Einstein condensate in a dimple trap, JOSA B **35**, 500 (2018).

[23] G. Condon, M. Rabault, B. Barrett, L. Chichet, R. Arguel, H. Eneriz-Imaz, D. Naik, A. Bertoldi, B. Battelier, P. Bouyer, and A. Landragin, All-Optical Bose-Einstein Condensates in Microgravity, Physical Review Letters **123**, 240402 (2019).

[24] G. Colzi, E. Fava, M. Barbiero, C. Mordini, G. Lamporesi, and G. Ferrari, Production of large Bose-Einstein condensates in a magnetic-shield-compatible hybrid trap, Physical Review A **97**, 053625 (2018).

[25] Y.-J. Lin, A. R. Perry, R. L. Compton, I. B. Spielman, and J. V. Porto, Rapid production of ^{87}Rb Bose-Einstein condensates in a combined magnetic and optical potential, Phys. Rev. A **79**, 063631 (2009).

[26] M. Zaiser, J. Hartwig, D. Schlippert, U. Velte, N. Winter, V. Lebedev, W. Ertmer, and E. M. Rasel, Simple method for generating Bose-Einstein condensates in a weak hybrid trap, Phys. Rev. A **83**, 035601 (2011).

[27] Q. Bouton, R. Chang, A. L. Hoendervanger, F. Nogrette, A. Aspect, C. I. Westbrook, and D. Clément, Fast production of Bose-Einstein condensates of metastable helium, Physical Review A **91**, 061402 (2015).

[28] A. Hüper, C. Pür, M. Hetzel, J. Geng, J. Peise, I. Kruse, M. Kristensen, W. Ertmer, J. Arlt, and C. Klempt, Number-resolved preparation of mesoscopic atomic ensembles, New J. Phys. **23**, 113046 (2021).

[29] S. Jöllenbeck, J. Mahnke, R. Randoll, W. Ertmer, J. Arlt, and C. Klempt, Hexapole-compensated magneto-optical trap on a mesoscopic atom chip, Phys. Rev. A **83**, 043406 (2011).

[30] X. Baillard, A. Gauguet, S. Bize, P. Lemonde, P. Laurent, A. Clairon, and P. Rosenbusch, Interference-filter-stabilized external-cavity diode lasers, Opt. Comm. **266**, 609 (2006).

[31] D. J. McCarron, S. A. King, and S. L. Cornish, Modulation transfer spectroscopy in atomic rubidium, Measurement Science and Technology **19**, 105601 (2008).

[32] G. Kleine Büning, J. Will, W. Ertmer, C. Klempt, and J. Arlt, A slow gravity compensated atom laser, Appl. Phys. B **100**, 117 (2010).

[33] B. Meyer, A. Idel, F. Anders, J. Peise, and C. Klempt, Dynamical low-noise microwave source for cold atom experiments, arXiv:2003.10989 (2020).

[34] I. Geisel, K. Cordes, J. Mahnke, S. Jöllenbeck, J. Ostermann, J. Arlt, W. Ertmer, and C. Klempt, Evolutionary optimization of an experimental apparatus, Appl. Phys. Lett. **102**, (2013).

4

TOMOGRAPHY OF A NUMBER-RESOLVING DETECTOR BY RECONSTRUCTION OF AN ATOMIC MANY-BODY QUANTUM STATE

AUTHORS

Mareike Hetzel, Luca Pezzè, Cebrail Pür, Martin Quensen, Andreas Hüper, Jiao Geng, Jens Kruse, Luis Santos, Wolfgang Ertmer, Augusto Smerzi, and Carsten Klempt

AUTHOR CONTRIBUTIONS

In this publication, I developed the experimental sequence, carried out measurements, analyzed and visualized experimental data and wrote the initial draft of the manuscript. Luca Pezzè developed the theoretical methods and description, analyzed and interpreted the data and wrote the initial draft of the manuscript. Cebrail Pür contributed in early stages of the project, built the microwave source, reviewed and edited the manuscript. Martin Quensen carried out measurements, reviewed and edited the manuscript. Andreas Hüper contributed in early stages of the project, provided technical assistance, reviewed and edited the manuscript. Jiao Geng contributed in early stages of the project and reviewed the manuscript. Jens Kruse and Wolfgang Ertmer were involved in the conceptualization and supervision of the project and reviewed the manuscript. Luis Santos and Augusto Smerzi developed the theoretical description, analysis and interpretation of the data, reviewed and edited the manuscript. Carsten Klempt supervised the design and implementation of the experiments, provided funding and guidance to the authors throughout the research process, helped with data analysis and interpretation, wrote, edited and reviewed the manuscript.

Tomography of a number-resolving detector by reconstruction of an atomic many-body quantum state

Mareike Hetzel[1],* Luca Pezzè[2], Cebrail Pür[1], Martin Quensen[1], Andreas Hüper[1,5], Jiao Geng[3,4], Jens Kruse[1,5], Luis Santos[6], Wolfgang Ertmer[1,5], Augusto Smerzi[2], and Carsten Klempt[1,5]

[1]*Institut für Quantenoptik, Leibniz Universität Hannover, Welfengarten 1, D-30167 Hannover, Germany*

[2]*QSTAR and INO-CNR and LENS, Largo Enrico Fermi 2, 50125 Firenze, Italy*

[3]*Key Laboratory of 3D Micro/Nano Fabrication and Characterization of Zhejiang Province, School of Engineering, Westlake University, 18 Shilongshan Road, Hangzhou 310024, Zhejiang Province, China*

[4]*Institute of Advanced Technology, Westlake Institute for Advanced Study, 18 Shilongshan Road, Hangzhou 310024, Zhejiang Province, China*

[5]*Deutsches Zentrum für Luft- und Raumfahrt e.V. (DLR), Institut für Satellitengeodäsie und Inertialsensorik (DLR-SI), Callinstraße 30b, D-30167 Hannover, Germany*

[6]*Institut für Theoretische Physik, Leibniz Universität Hannover, Appelstraße 2, D-30167 Hannover, Germany*

(Dated: July 5, 2022)

The high-fidelity analysis of many-body quantum states of indistinguishable atoms requires the accurate counting of atoms. Here we report the tomographic reconstruction of an atom-number-resolving detector. The tomography is performed with an ultracold rubidium ensemble that is prepared in a coherent spin state by driving a Rabi coupling between the two hyperfine clock levels. The coupling is followed by counting the occupation number in one level. We characterize the fidelity of our detector and show that a negative-valued Wigner function is associated with it. Our results offer an exciting perspective for the high-fidelity reconstruction of entangled states and can be applied for a future demonstration of Heisenberg-limited atom interferometry.

High-fidelity preparation, manipulation, and detection of quantum states of many indistinguishable atoms have been greatly improved during the last decades. These improvements facilitate exciting developments ranging from fundamental quantum atom optics experiments [1, 2] to entanglement-enhanced metrology applications [3]. In metrology, entangled states of neutral atoms serve as highly sensitive input states of atom interferometers, reducing the resolution limit from the Standard Quantum Limit to the ultimate Heisenberg limit [4]. Possible applications range from quantum interferometry [5–14] and magnetometry [15–18] to atomic clocks [19–22] and inertial sensing [23, 24]. To date, the atom counting noise represents one of the most crucial limitations in current experiments, affecting both fundamental studies and metrological applications.

Recent experiments creating entangled atomic quantum states in ensembles of indistinguishable atoms have reported counting noise that ranges from 3 atoms at a total number of a 600 atoms [25], to 1.6 atoms at 3000 atoms [26], to 10 atoms at 10^4 [27, 28], to better than 17 atoms at 10^5 [14], and to 50 atoms at 5×10^5 [11]. An improvement of the counting noise below the value of the single atom, where the quantization of the atomic signal becomes apparent, promises a quantitative and qualitative improvement. For example, such a counting resolution would allow for the direct detection of Bell correlations between two separated atomic ensembles [29] and the observation of parity signals in Hong-Ou-Mandel-like interference experiments with many-particle states [30, 31]. In metrology, a number-resolving counting can be applied to demonstrate a Heisenberg-limited resolution in atom interferometry [32, 33]. A number-resolving counting has been obtained in a cavity-based detection [34], but is so far restricted to a discrimination between 0 and 1, and the scaling to larger numbers is an open challenge. Single-atom resolved detection has also been obtained in free-falling clouds with

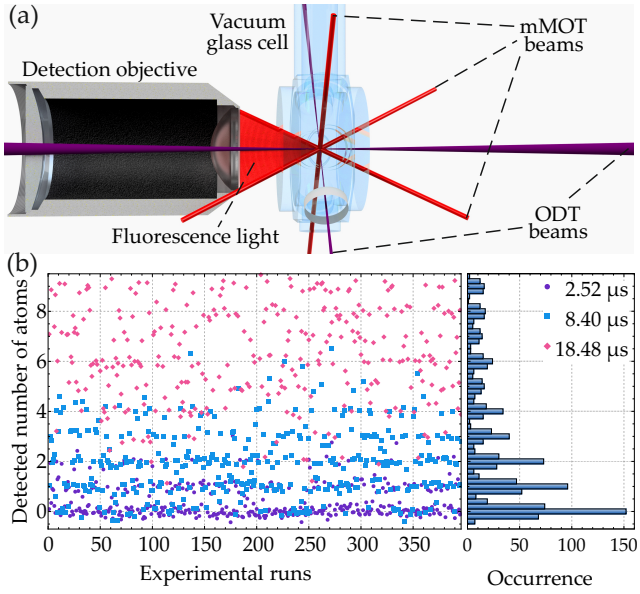

FIG. 1. (a) Sketch of the experimental setup. A coherent spin state is created in a crossed-beam optical dipole trap and analyzed in a number-resolving mMOT detection scheme. (b) Time trace of the sequentially measured number of atoms in dependence of the MW pulse length. The number of atoms in $|1,0\rangle$ after 2.52 μs (purple circles), 8.4 μs (blue rectangles) and 18.48 μs (pink diamonds) is shown for up to 9 atoms for 1106 successive measurements. The accumulation of data points at integer numbers is indicating our number-resolving counting. The histogram of the fluorescence signal on the right further illustrates this effect. Negative values are caused by background substraction.

a sheet of resonant light [35], and was applied to extract local correlations. A number-resolved counting for up to 1000 atoms has been demonstrated in a millimeter-sized magneto-optical trap (mMOT) [36, 37], but was so far not applied to the detection of many-body quantum states.

The fine calibration of quantum measurement devices generally requires quantum detection tomography (QDT) techniques [38, 39]. The goal of QDT is to provide a set of positive-operator-valued measures (POVM) that fully characterize the detector, beyond the assumption of projective measurements. So far, QDT has been mainly investigated for optical photocounting and homodyne detection [40–44] and very recently also applied to characterize qubit readout for pairs of trapped ions [45] and quantum computing machines [46]. Although QDT is necessary for quantum state preparation, control, reconstruction, and error mitigation, its potential has not yet been leveraged for the characterization of neutral-atom quantum systems. In this case, the technique is specifically promising, because of the small inherent detection loss compared to optical systems and the large achievable atom numbers compared to ion systems.

In this Letter, we apply a MOT-based number counting [47] to analyze the dynamics of a many-body spin state. We generate an atomic Bose-Einstein condensate (BEC) in one atomic clock level, apply a microwave (MW) coupling pulse of variable duration on the atomic clock transition, and count the number of atoms in the other, initially empty level. We are able to follow the time evolution of the coherent spin state with a clear resolution of the number quantization. By applying a stochastic matrix approach to the recorded histograms, we obtain a set of nonclassical POVM operators that fully characterize the detection process. The expected Poissonian distributions can be reproduced with a statistics-limited fidelity of up to 99%. We predict that the single-level detection is capable of operating an interferometric measurement with up to 7.8 dB squeezing-enhanced phase sensitivity gain, if the same total number can be provided with smaller fluctuations. This sensitivity gain can be further enhanced by increasing the mean atom number. Our detection capability promises a novel quality for the analysis of entangled quantum states and demonstration of Heisenberg-limited interferometry.

In our experiments, we generate a BEC of 10^5 ^{87}Rb atoms in a crossed-beam optical dipole trap with a preparation time of 3.3 s. The details of the BEC production can be found in Ref. [48]. We prepare the BEC in the hyperfine level $|F, m_F\rangle = |2, 2\rangle$ and reduce the number of atoms to enter the regime of our number-resolved counting. The reduction is realized by transferring 34 atoms to the level $|1, 1\rangle$, on average, and a subsequent optical removal of the residual atoms in the $F = 2$ manifold. A further MW pulse transfers the remaining atoms to the level $|2, 0\rangle$. A final resonant light push on the $F = 1$ manifold terminates our state preparation with 34 and 0 atoms in the clock states $|2, 0\rangle$ and $|1, 0\rangle$, respectively. The total number of particles fluctuates by 6.4 atoms, which is dominated by projection noise (5.8 atoms).

We apply a resonant MW pulse on the clock transition with a variable duration ranging from $t = 2.5\,\mu$s to $56\,\mu$s. The many-body state in the pseudo-spin-1/2 system can thus be represented by a coherent spin state (CSS), with maximal total spin, but variable rotation angle θ. The analysis of the CSS is based on counting the number of atoms in the level $|1, 0\rangle$. To this end, the atoms in the level $|2, 0\rangle$ are removed and the remaining atoms are counted by fluorescence detection in the mMOT. The quality of the state analysis thus depends on the efficiency of the removal procedure. Therefore, the detection process starts with a strong reduction of the atomic density by switching off one of the two dipole trap laser beams. A σ^+-polarized light push at a magnetic field of 6.7 G quickly pumps all $F = 2$ atoms into a closed cycling transition reducing the probability to fall into a non-resonant state. The resonant atoms are accelerated and leave the trap, while the probability of unwanted collisions is reduced by the low density. The removal of atoms in the level $|2, 0\rangle$ has a finite extinction ratio of 42.4 dB, resulting in an unwanted, Poisson-distributed remainder of 0.27 atoms maximally. These atoms are produced by two processes: (i) They escape the removal process to the level $F = 1$ because of imperfect optical pumping. (ii) They are captured from the background gas, which is temporally increased after the operation of the two-dimensional magneto-optical trap. We detect the remaining atoms in the mMOT setup, consisting of a magneto-optical trap with millimeter-sized illumination beams [47, 48]. The optical dipole trap is switched off to start an equilibration phase in the mMOT of 50 ms, during which the magnetic fields settle and the atoms are compressed and cooled. Subsequently, the main atom counting signal is obtained by collecting fluorescence light for 65 ms with a charge-coupled-device (CCD) camera. Finally, a second image without atoms is recorded for background subtraction. The spin preparation and detection processes require a total of 1.8 s. After nine measurement runs, the system is halted for 60 s to avoid a slow increase of the mMOT capture rate from the background gas.

Fig. 1 (a) shows a sketch of the experimental setup including the mMOT and ODT beams and the high-numerical-aperture detection objective. Fig. 1 (b) shows a time trace of 100 consecutive number measurements in $|1, 0\rangle$ shown for three different MW pulse lengths. The measured number of atoms accumulate at integer numbers, enabling a number assignment fidelity ranging from 99.7% at 1 atoms to 99.0% at 15 atoms [48].

Fig. 2 (a) shows the mean number of the transferred atoms as a function of the microwave pulse duration. The mean atom number follows a sinusoidal Rabi oscillation with a Rabi frequency $\Omega = 2\pi \times 8.2$ kHz (see below). Figs. 2 (b)-(f) present the exemplary histograms, which can be associated to rotation angles $\theta = \Omega t$. Without rotation (b), the distribution shows the detection of recaptured atoms, which can be treated as statistical dark counts in the detection system. For finite rotations (c)-(f), the distributions shift to higher atom number and increased width.

Under the assumptions that the microwave generates a ho-

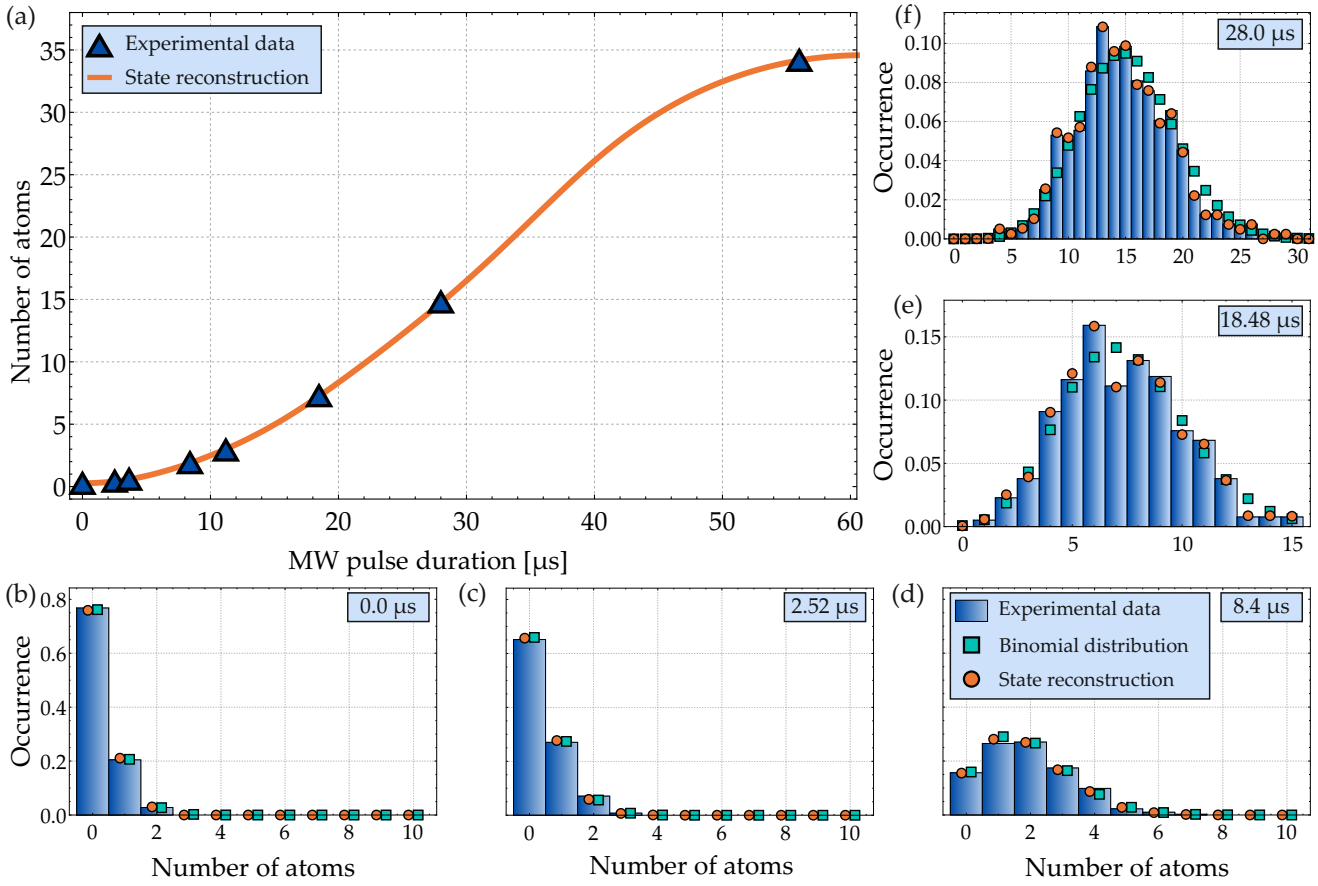

FIG. 2. (a) Mean number of atoms detected in $|1,0\rangle$ in dependence of the MW pulse duration. Each data point (blue triangle) corresponds to an individual atom number distribution. Those are exemplarily shown in the histograms in (b)-(f) for MW pulses ranging from $t = 0\,\mu$s to $28\,\mu$s. The ideal binomial distributions accounting for the detection offset and the atom number fluctuations are illustrated in the cyan rectangles. The solid orange line and the orange circles show the results obtained from the QDT algorithm (see text).

mogeneous coupling to the cloud and that the level $|1,0\rangle$ is initially completely empty – that are both very well fulfilled in our case – we can employ the recorded data for QDT. We associate the two clock levels $|1,0\rangle$ and $|2,0\rangle$ with the letters a and b, respectively, to simplify the notation. We model the detection by expressing the probability of a measurement result n (the number of atoms in clock level a) as

$$P_V(n|t) = \sum_{m=0}^{+\infty} V_{n,m} P_{\mathrm{id}}(m|t), \tag{1}$$

in terms of a stochastic matrix (Markov mapping) V with non-negative elements $V_{n,m} \geq 0$, which satisfies the normalization property $\sum_n V_{n,m} = 1$ for all m. Physically, the quantity $V_{n,m}$ can be interpreted as the probability to measure n atoms if m atoms reach the detector. We use the ideal probability $P_{\mathrm{id}}(m|t) = \mathrm{Tr}[|m\rangle\langle m|\hat{\rho}(t)]$, where $\hat{\rho} = \sum_{N=0}^{+\infty} \rho_N |N\rangle_b |0\rangle_a \langle 0|_a \langle N|_b$ is the generic atomic state before starting the dynamics, $\hat{U}(t) = \exp[-i\Omega_R t(\hat{a}^\dagger \hat{b} + \hat{a}\hat{b}^\dagger)/2]$ describes the Rabi coupling and $\hat{\rho}(t) = \hat{U}(t)\hat{\rho}\hat{U}(t)^\dagger$. The assumption that the initial state is diagonal is well justified experimentally. The matrix V provides a full characterization of the detection process, including finite resolutions and biases. It should be noticed that Eq. (1) can be rewritten as $P_V(n|t) = \mathrm{Tr}[\hat{\rho}(t)\hat{\Pi}_n]$, in terms of a POVM set $\{\hat{\Pi}_n\}$, where

$$\hat{\Pi}_n = \sum_{m=0}^{+\infty} V_{n,m} |m\rangle\langle m|. \tag{2}$$

V being positive semi-definite guarantees that $\hat{\Pi}_n \geq 0$, while the condition $\sum_n V_{n,m} = 1$ for all m guarantees the completeness relation $\sum_n \hat{\Pi}_n = \mathbb{1}$.

Our QDT protocol consists of finding the coefficients ρ_N, $V_{n,m}$ and Ω_R that minimize a cost function $C = \sum_j d_H^2(t_j)$. This is given by the sum over all times t_j of the squared statistical distance $d_H^2(t_j)$ [49] between the probability distribution $P_V(n|t_j)$ and the experimental histogram $P_{\mathrm{exp}}(n|t_j)$ [e.g. Fig. 2(b)-(f)],

$$d_H^2(t_j) = \sum_n \left(\sqrt{P_V(n|t_j)} - \sqrt{P_{\mathrm{exp}}(n|t_j)} \right)^2. \tag{3}$$

The constrained minimization of Eq. (3) is performed with a gradient descent algorithm [50]. We emphasize that a reliable

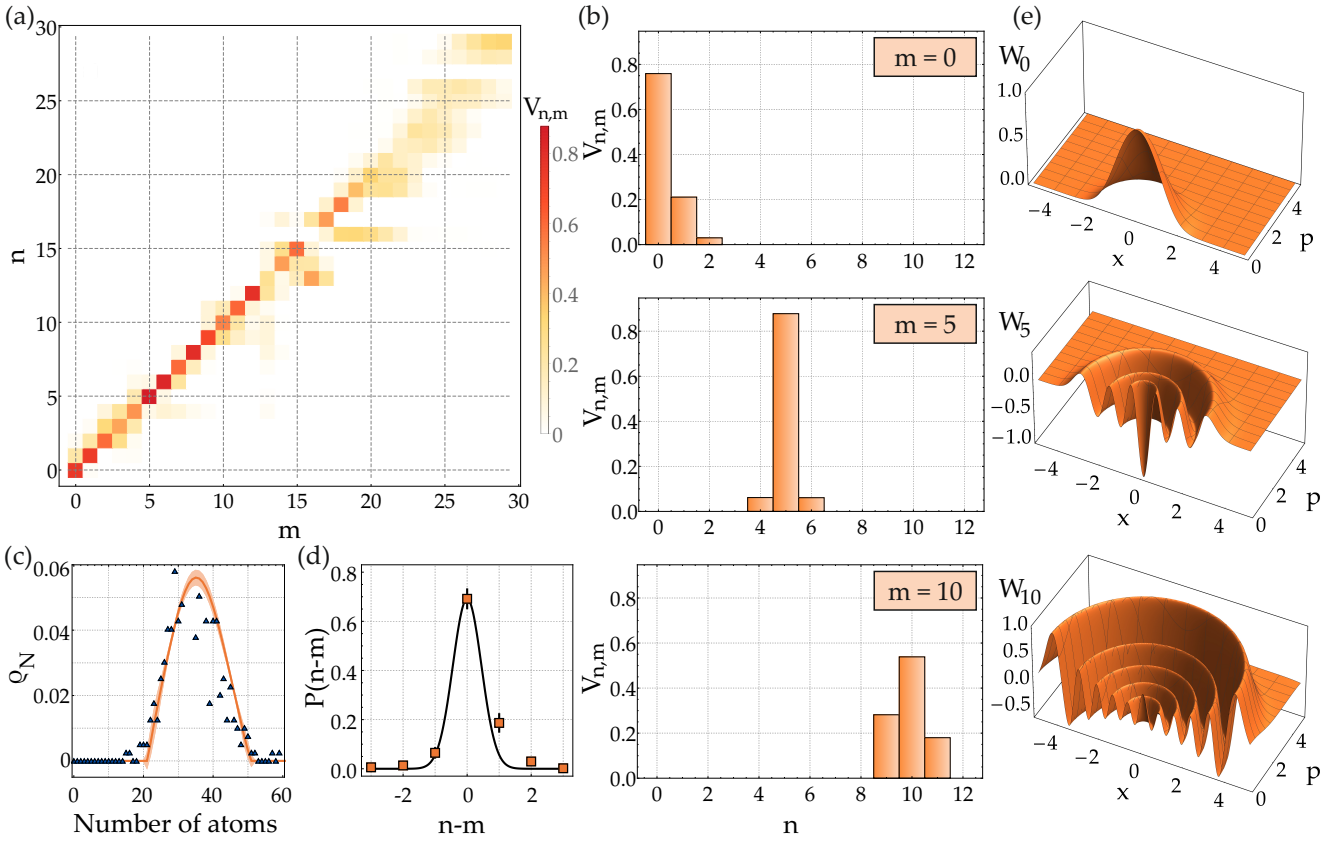

FIG. 3. Panel (a): reconstructed stochastic map $V_{n,m}$ (linear color scale) as a function of n and m. The highest weight is concentrated along the diagonal $n = m$. Panel (b): $V_{n,m}$ as a function of n and for $m = 0$, $m = 5$ and $m = 10$. Panel (c): coefficients ρ_N of the reconstructed state (orange line with uncertainty shade, see text). The blue triangles show the experimentally obtained state in $|1, 0\rangle$ after a 56 μs MW pulse. Panel (d) shows $P(n - m)$ as a function of $n - m$ (squares). The black line is a Gaussian fit to the data for $n \leq m$ Panel (e): the Wigner function of the POVM operator $\hat{\Pi}_0$, $\hat{\Pi}_5$ and $\hat{\Pi}_{10}$, in the (x, p) phase space. Negative Wigner values are observed for $\hat{\Pi}_{n\geq 1}$.

characterization of the POVM set requires a substantial overlap between probability distributions at different times in order to avoid overfitting [50]. For our experimental parameters, see Fig. 2, this is guaranteed for $0 \leq n \lesssim 20$.

In Fig. 2 we compare the experimental histograms (bars) with the probabilities derived from the QDT (orange circles), namely Eq. (1) with V, ρ_N and Ω_R calculated using the minimization algorithm. The agreement is excellent, as the obtained probability distribution $P_V(n|t_j)$ achieves a very high fidelity with $P_{\rm exp}(n|t_j)$, for all t_j (notice that the iterative optimization algorithm is stopped when $C = 0.01$, which is a value close to saturation [50]). The histograms are consistent with that calculated with a binomial distribution (green squares). The latter assume a Gaussian distribution of the total number of atoms with measured mean and standard deviation, ideal Rabi transfer and the convolution with a binomial distribution with a mean number of 0.27 atoms to account for the unwanted detection of background atoms. The mean number of atoms as a function of time, $\sum_n P_V(n, t)n$ for the reconstructed V, ρ_N and Ω_R interpolates well the detection events as shown in Fig. 2(a). It should be noticed that the Rabi frequency extracted from the tomographic reconstruction $\Omega_R = 8.2 \pm 0.2$ kHz agrees precisely with the result of a sinusoidal fit to the data.

In Fig. 3 we show the results of our joint detection and state reconstruction. Figure 3(a) shows the elements $V_{n,m}$. For most values of m, the weights $V_{n,m}$ concentrate around the diagonal $n = m$, where they reach their maximal value. In other words, if m atoms reach the detector, the most probable event is to detect $n = m$. The probability of such detection events is quantified below. For instance, in panel (b) we show $V_{n,m}$ as a function of n and for the specific values $m = 0$, 5 and 10: the histograms are cuts of the plot of panel (a). For $m \gtrsim 20$, the reconstructed $V_{n,m}$ spreads away from the diagonal. Here, the QDT becomes uncertain because the recorded probability distributions do not overlap sufficiently and the optimization method is affected by overfitting of the data [51]. To recognize the overfitting effect, we have performed a 'learning test', see Ref. [50], in which the experimental histogram at time t_j is compared with the reconstructed $P_V(n|t_j)$, where the coef-

ficients Ω_R, $\hat{\rho}$, and V are calculated from the minimization algorithm using all the experimental data except those at time t_j. In this case, we observe a fidelity between $P_V(n|t_j)$ and $P_{\text{exp}}(n|t_j)$ above 99% for times t_j up to 18.48 μs [50]. In the future, a QDT at larger atom numbers can be obtained by taking more histograms with larger statistics. In panel (c) we show the reconstructed elements ρ_N as a function of the number of particles. As we see, the reconstructed diagonal state has approximately a Gaussian shape with mean $\overline{N} = 35.4$ and root mean square error $\Delta N = 6.4 \approx \overline{N}^{1/2}$.

For $m \lesssim 20$, as $V_{n,m}$ is strongly peaked around $n = m$. It is thus convenient to calculate $P(n-m) = \sum_m V_{n-m,m} P_m$, giving the reconstructed probability that $n - m$ particles are detected if m particles hit the detector. Here, $P_m = \sum_j P_{\text{id}}(m|t_j)$ is the overall probability that m particles hit the detector, for the considered measurement times t_j and takes into account the most likely detection events and it is almost negligible for $m \gtrsim 20$. For a noiseless detector $P(n-m)$ is a delta peak at $n = m$, regardless the P_m distribution. In the case of our noisy detector, $P(n-m)$ is still strongly peaked at $n = m$, with an overall probability of about 70%, see Fig. 3 (d). The slight asymmetry of the distribution V_{n-m} reflects the unwanted recapture of atoms described above, which biases V_{n-m} to positive values of $n - m$. By calculating the variance of the $P(n-m)$ distribution for $n \leq m$ (thus not affected by the atom recapture) we can extract a detection sensitivity $\sigma = 0.4 \pm 0.02$. This counting uncertainty is larger than the uncertainty obtained from Fig. 1, because the finite number of measurements additionally deteriorates the QDT.

As shown in Eq. (2), accessing the matrix V allows us to characterize the POVM elements $\hat{\Pi}_n$. For instance, in Fig. 3(d), we plot the Wigner distribution of the reconstructed POVM operators $\hat{\Pi}_n$, $W_n(x,p) = \sum_m V_{n,m} W(x,p;m)$, where $W(x,p;m)$ is the Wigner function of the Fock state $|m\rangle$ [52]. For $n = 0$ the Wigner function is positive, as expected, corresponding to the detection of vacuum. On the contrary, for $n \geq 1$, the Wigner functions $W_n(q,p)$ have negative values, indicating the absence of a classical analogue of these operators. To emphasise the fundamental quantum nature of our detection we notice that a POVM with negative Wigner function is necessary to prove Bell's non-locality with Gaussian states (which have positive Wigner distributions) [40, 53].

Measuring the atom number in a single level, as done in our experiment, still allows to surpass the standard quantum limit of phase sensitivity, for instance provided that (i) each fixed-N state is spin squeezed and (ii) the distribution of the total atom number ρ_N has sufficiently low fluctuations. Using the results of our QDT and the atom number distribution, we can predict an optimal gain of about 1.3 over the standard quantum limit, when squeezing the relative atom number distribution [50]. A higher gain, up to 7.8 dB is possible when also reducing ΔN, for our detection and $\bar{N} \approx 36$. The gain further increases when increasing $\bar{N}$.

In summary, we have employed a number-resolving detector to analyze the dynamics of a coherent spin state derived from an atomic BEC. We have characterized the detection process by the simultaneous reconstruction of the diagonal quantum state and the detector's POVM operators. The latter are characterized by negative Wigner functions, thus unveiling the inherent quantum nature of the detector. In the future, the presented detector and the developed QDT techniques will be directly extended to entangled many-body states, promising the detection of entanglement with unprecedented fidelity in the regime of up to 100 atoms.

Acknowledgements. This work is supported by the QuantERA grants SQUEIS and MENTA. We acknowledge financial support from the Deutsche Forschungsgemeinschaft (DFG, German Research Foundation)-Project-ID 274200144-SFB 1227 DQ-mat within the project B01 and Germany's Excellence Strategy—EXC-2123 QuantumFrontiers—Project-ID 390837967. M.Q. acknowledges support from the Hannover School for Nanotechnology (HSN).

* hetzel@iqo.uni-hannover.de

[1] A. D. Cronin, J. Schmiedmayer, and D. E. Pritchard, Optics and interferometry with atoms and molecules, Rev. Mod. Phys. **81**, 1051 (2009).
[2] T. Byrnes and E. Ilo-Okeke, *Quantum Atom Optics, Theory and Applications to Quantum Technology* (Cambridge University Press, Cambridge, 2021).
[3] L. Pezzè, A. Smerzi, M. K. Oberthaler, R. Schmied, and P. Treutlein, Quantum metrology with nonclassical states of atomic ensembles, Rev. Mod. Phys. **90**, 10.1103/revmodphys.90.035005 (2018).
[4] L. Pezzé and A. Smerzi, Entanglement, nonlinear dynamics, and the heisenberg limit, Phys. Rev. Lett. **102**, 100401 (2009).
[5] J. Appel, P. J. Windpassinger, D. Oblak, U. B. Hoff, N. Kærgaard, and E. S. Polzik, Mesoscopic atomic entanglement for precision measurements beyond the standard quantum limit, Proc. Natl. Acad. Sci. U. S. A. **106**, 10960 (2009).
[6] M. H. Schleier-Smith, I. D. Leroux, and V. Vuletić, States of an ensemble of two-level atoms with reduced quantum uncertainty, Phys. Rev. Lett. **104**, 073604 (2010).
[7] C. Gross, T. Zibold, E. Nicklas, J. Estève, and M. K. Oberthaler, Nonlinear atom interferometer surpasses classical precision limit, Nature **464**, 1165 (2010).
[8] M. Riedel, P. Böhi, Y. Li, T. Hänsch, A. Sinatra, and P. Treutlein, Atom-chip-based generation of entanglement for quantum metrology, Nature **464**, 1170 (2010).
[9] B. Lücke, M. Scherer, J. Kruse, L. Pezzé, F. Deuretzbacher, P. Hyllus, O. Topic, J. Peise, W. Ertmer, J. Arlt, L. Santos, A. Smerzi, and C. Klempt, Twin matter waves for interferometry beyond the classical limit, Science **334**, 773 (2011).
[10] Z. Chen, J. Bohnet, S. Sankar, J. Dai, and J. Thompson, Conditional spin squeezing of a large ensemble via the vacuum Rabi splitting, Phys. Rev. Lett. **106**, 133601 (2011).
[11] C. D. Hamley, C. S. Gerving, T. M. Hoang, E. M. Bookjans, and M. S. Chapman, Spin-nematic squeezed vacuum in a quantum gas, Nature Phys. **8**, 305 (2012).
[12] T. Berrada, S. van Frank, R. Bücker, T. Schumm, J.-F. Schaff, and J. Schmiedmayer, Integrated mach-zehnder interferometer for bose-einstein condensates, Nat. Commun. **4**, (2013).
[13] H. Strobel, W. Muessel, D. Linnemann, T. Zibold, D. B. Hume,

L. Pezzè, A. Smerzi, and M. K. Oberthaler, Fisher information and entanglement of non-gaussian spin states, Science **345**, 424 (2014).
[14] O. Hosten, N. J. Engelsen, R. Krishnakumar, and M. A. Kasevich, Measurement noise 100 times lower than the quantum-projection limit using entangled atoms, Nature **529**, 505 (2016).
[15] W. Wasilewski, K. Jensen, H. Krauter, J. J. Renema, M. V. Balabas, and E. S. Polzik, Quantum noise limited and entanglement-assisted magnetometry, Phys. Rev. Lett. **104**, 133601 (2010).
[16] R. J. Sewell, M. Koschorreck, M. Napolitano, B. Dubost, N. Behbood, and M. W. Mitchell, Magnetic sensitivity beyond the projection noise limit by spin squeezing, Phys. Rev. Lett. **109**, 253605 (2012).
[17] W. Muessel, H. Strobel, D. Linnemann, D. B. Hume, and M. K. Oberthaler, Scalable spin squeezing for quantum-enhanced magnetometry with Bose-Einstein condensates, Phys. Rev. Lett. **113**, 103004 (2014).
[18] C. F. Ockeloen, R. Schmied, M. F. Riedel, and P. Treutlein, Quantum metrology with a scanning probe atom interferometer, Phys. Rev. Lett. **111**, 143001 (2013).
[19] A. Louchet-Chauvet, J. Appel, J. J. Renema, D. Oblak, N. Kjaergaard, and E. S. Polzik, Entanglement-assisted atomic clock beyond the projection noise limit, New J. Phys. **12**, 065032 (2010).
[20] I. D. Leroux, M. H. Schleier-Smith, and V. Vuletić, Orientation-Dependent Entanglement Lifetime in a Squeezed Atomic Clock, Phys. Rev. Lett. **104**, 250801 (2010).
[21] I. Kruse, K. Lange, J. Peise, B. Lücke, L. Pezzè, J. Arlt, W. Ertmer, C. Lisdat, L. Santos, A. Smerzi, and C. Klempt, Improvement of an atomic clock using squeezed vacuum, Phys. Rev. Lett. **117**, 143004 (2016).
[22] E. Pedrozo-Peñafiel, S. Colombo, C. Shu, A. F. Adiyatullin, Z. Li, E. Mendez, B. Braverman, A. Kawasaki, D. Akamatsu, Y. Xiao, and V. Vuletić, Entanglement on an optical atomic-clock transition, Nature **588**, 414 (2020).
[23] F. Anders, A. Idel, P. Feldmann, D. Bondarenko, S. Loriani, K. Lange, J. Peise, M. Gersemann, B. Meyer-Hoppe, S. Abend, N. Gaaloul, C. Schubert, D. Schlippert, L. Santos, E. Rasel, and C. Klempt, Momentum entanglement for atom interferometry, Phys. Rev. Lett. **127**, 140402 (2021).
[24] G. P. Greve, C. Luo, B. Wu, and J. K. Thompson, Entanglement-enhanced matter-wave interferometry in a high-finesse cavity, arXiv:2110.14027 (2021).
[25] M. Fadel, T. Zibold, B. Décamps, and P. Treutlein, Spatial entanglement patterns and Einstein-Podolsky-Rosen steering in Bose-Einstein condensates, Science **360**, 409 (2018), http://science.sciencemag.org/content/360/6387/409.full.pdf.
[26] A. Qu, B. Evrard, J. Dalibard, and F. Gerbier, Probing spin correlations in a bose-einstein condensate near the single-atom level, Phys. Rev. Lett. **125**, 033401 (2020).
[27] B. Lücke, J. Peise, G. Vitagliano, J. Arlt, L. Santos, G. Tóth, and C. Klempt, Detecting multiparticle entanglement of Dicke states, Phys. Rev. Lett. **112**, 155304 (2014).
[28] X.-Y. Luo, Y.-Q. Zou, L.-N. Wu, Q. Liu, M.-F. Han, M. K. Tey, and L. You, Deterministic entanglement generation from driving through quantum phase transitions, Science **355**, 620 (2017), http://science.sciencemag.org/content/355/6325/620.full.pdf.
[29] F. Laloë and W. J. Mullin, Interferometry with independent Bose-Einstein condensates: parity as an epr/bell quantum variable, Eur. Phys. J. B **70**, 377 (2009).
[30] R. A. Campos, B. E. A. Saleh, and M. C. Teich, Quantum-mechanical lossless beam splitter: Su(2) symmetry and photon statistics, Phys. Rev. A **40**, 1371 (1989).
[31] Z. Y. Ou, J.-K. Rhee, and L. J. Wang, Observation of four-photon interference with a beam splitter by pulsed parametric down-conversion, Phys. Rev. Lett. **83**, 959 (1999).
[32] M. J. Holland and K. Burnett, Interferometric detection of optical phase shifts at the Heisenberg limit, Phys. Rev. Lett. **71**, 1355 (1993).
[33] P. Bouyer and M. A. Kasevich, Heisenberg-limited spectroscopy with degenerate Bose-Einstein gases, Phys. Rev. A **56**, R1083 (1997).
[34] F. Haas, J. Volz, R. Gehr, J. Reichel, and J. Estève, Entangled states of more than 40 atoms in an optical fiber cavity, Science **344**, 180 (2014), http://www.sciencemag.org/content/344/6180/180.full.pdf.
[35] R. Bücker, A. Perrin, S. Manz, T. Betz, C. Koller, T. Plisson, J. Rottmann, T. Schumm, and J. Schmiedmayer, Single-particle-sensitive imaging of freely propagating ultracold atoms, New J. Phys. **11**, 103039 (2009).
[36] D. B. Hume, I. Stroescu, M. Joos, W. Muessel, H. Strobel, and M. K. Oberthaler, Accurate atom counting in mesoscopic ensembles, Phys. Rev. Lett. **111**, 253001 (2013).
[37] I. Stroescu, D. B. Hume, and M. K. Oberthaler, Double-well atom trap for fluorescence detection at the Heisenberg limit, Phys. Rev. A **91**, 013412 (2015).
[38] A. Luis and L. L. Sánchez-Soto, Complete characterization of arbitrary quantum measurement processes, Phys. Rev. Lett. **83**, 3573 (1999).
[39] J. Fiurášek, Maximum-likelihood estimation of quantum measurement, Phys. Rev. A **64**, 024102 (2001).
[40] J. Lundeen, A. Feito, H. Coldenstrodt-Ronge, C. Silberhorn, T. C. Ralph, J. Eisert, M. B. Plenio, and I. A. Walmsley, Tomography of quantum detectors, Nat. Phys. **5**, 27 (2009).
[41] L. Zhang, H. Coldenstrodt-Ronge, A. Datta, G. Puentes, J. S. Lundeen, X.-M. Jin, B. J. Smith, M. B. Plenio, and I. A. Walmsley, Mapping coherence in measurement via full quantum tomography of a hybrid optical detector, Nat. Phot. **6**, 364 (2012).
[42] S. Grandi, A. Zavatta, M. Bellini, and M. G. A. Paris, Experimental quantum tomography of a homodyne detector, New J. of Phys. **19**, 053015 (2017).
[43] A. Zhang, J. Xie, H. Xu, K. Zheng, H. Zhang, Y.-T. Poon, V. Vedral, and L. Zhang, Experimental self-characterization of quantum measurements, Phys. Rev. Lett. **124**, 040402 (2020).
[44] G. Brida, L. Ciavarella, I. P. Degiovanni, M. Genovese, L. Lolli, M. G. Mingolla, F. Piacentini, M. Rajteri, E. Taralli, and M. G. A. Paris, Quantum characterization of superconducting photon counters, New J. of Phys. **14**, 085001 (2012).
[45] A. C. Keith, C. H. Baldwin, S. Glancy, and E. Knill, Joint quantum-state and measurement tomography with incomplete measurements, Phys. Rev. A **98**, 042318 (2018).
[46] Y. Chen, M. Farahzad, S. Yoo, and T.-C. Wei, Detector tomography on ibm quantum computers and mitigation of an imperfect measurement, Phys. Rev. A **100**, 052315 (2019).
[47] A. Hüper, C. Pür, M. Hetzel, J. Geng, J. Peise, I. Kruse, M. Kristensen, W. Ertmer, J. Arlt, and C. Klempt, Number-resolved preparation of mesoscopic atomic ensembles, New J. Phys. **23**, 113046 (2021).
[48] C. Pür, M. Hetzel, M. Quensen, A. Hüper, J. Geng, J. Kruse, W. Ertmer, and C. Klempt, Rapid generation and number-resolved detection of spinor rubidium Bose-Einstein condensates, In Preparation.
[49] I. Bengtsson and K. Zyczkowski, *Geometry of Quantum States: An Introduction to Quantum Entanglement* (Cambridge University Press, Cambridge, 2006).
[50] See supplemental material for more details about the optimiza-

tion algorithm and a detailed analysis about the possibility to reach sub-shot noise sensitivities, .

[51] See for instance M. A. Nielsen, *Neural Networks and Deep Learning* (Determination Press, 2015), available online at http://neuralnetworksanddeeplearning.com.

[52] Explicitly, $W_n(x,p) = \sum_m V_{n,m} \frac{(-1)^m}{\pi} e^{-(x^2+p^2)} L_m[2(p^2+x^2)]$, where $L_m(x)$ denotes the m-th Laguerre polynomial.

[53] K. Banaszek and K. Wódkiewicz, Nonlocality of the einstein-podolsky-rosen state in the wigner representation, Phys. Rev. A **58**, 4345 (1998).

5 OUTLOOK

This thesis describes the generation and number-resolved analysis of a many-body quantum state. The subsequent sections outline the technical updates that have already been implemented for the generation of BECs and their number-resolving detection after submission of the publications within this thesis. Additionally, an extension of the techniques established in this thesis for detecting entangled many-body quantum states is introduced, along with an experiment that employs these states. Lastly, the long-term objective of Heisenberg-limited atom interferometry is outlined.

5.1 ALL-OPTICAL BEC GENERATION

In publication [121], we discuss our hybrid evaporation approach which involves two steps: the initial evaporation in a magnetic quadrupole trap and subsequent cooling in a crossed-beam optical dipole trap. The cycle time of this approach is limited by the rethermalization rates in both static cooling schemes, as well as an additional waiting time due to heating of the coils.

To overcome this limitation and improve evaporation dynamics, we have implemented time-averaged potentials in our ODT setup. Time-averaged potentials are created by rapidly and periodically moving the ODT beams. If the beams are moved faster than the trapping frequency, the atoms experience the time-average of the potential generated by the moving beams, hence referred to as time-averaged or "painted" potentials. This approach allows us to create harmonic potentials that initially have a large spatial amplitude for high-efficiency transfer into the ODT. We then smoothly decrease the painting stroke, which is the spatial amplitude of the beam's movement. By dynamically shaping the trapping potential throughout the evaporation process, we can maintain high evaporation dynamics and achieve rapid creation of an all-optical BEC.

As the implementation of time-averaged potentials has been included in the design from beginning on, both optical dipole trap beams pass acousto-optical deflectors (AODs) that are ideal for this application. In the past, the AODs were primarily used for switching and intensity stabilization of the light and not for dynamic modulation. By applying sophisticated RF signals which are modulated in the $10 - 100\,\mathrm{kHz}$-regime, we can move the beams faster than the typical trap frequencies in an ODT, which are below $10\,\mathrm{kHz}$.

For generating the RF signals, we employ a software-defined radio as a source. This device allows us to arbitrarily shape the input signal of the AODs [123, 124]. The analog RF signal is converted into a digital signal that can then be processed using software. Instead of manipulating the analog RF signal using analog tools, the conversion to a digital signal allows for easier programming of complex signal shapes suitable for versatile applications.

The initial dipole trap setup included two beams with waists of 35 and 70 µm, respectively. To create more delicate potential shapes, we replaced the focusing lens of the 70 µm beam with an objective that narrows the beam down to 5 µm [125]. During evaporation, harmonic potentials in horizontal direction are painted with both beams. The 35 µm beam creates a large trapping volume for capturing atoms from the molasses phase. In the course of the evaporation, the painting stroke is reduced from 1 mm to zero. Depending on the following experiment, the painting stroke of the 5 µm beam is reduced from 200 µm to about 15 µm or less.

To optimize the evaporation sequence, we employed a machine-learning algorithm called Differential Evolution [126]. This approach enabled us to find optimal parameters and avoid getting trapped in local optima. As a result, Bose-Einstein condensation in the all-optical evaporation approach can be reached after 250 ms of evaporation. The total cycle time of 1.3 s is primarily limited by 1 s of MOT loading. Increasing the 2D-MOT flux by a more frequent use of the dispenser could reduce the cycle time to 500 ms, competing with the fastest rubidium BEC known to us [127]. The new results are illustrated in Fig. 5.1 which gives an updated overview of the state-of-the-art in BEC generation with respect to the achieved atomic flux.

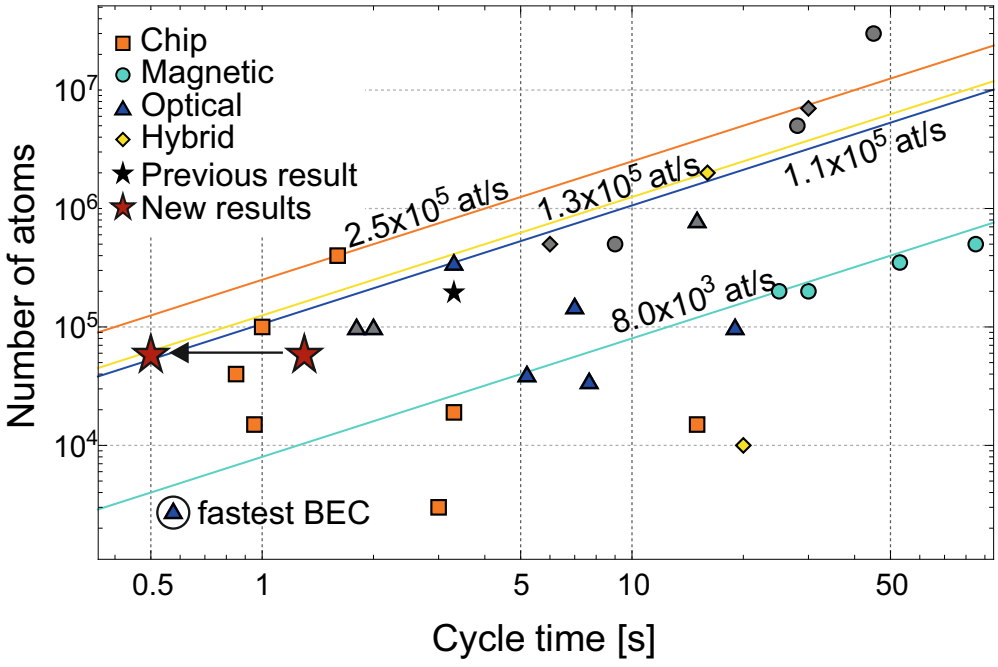

Figure 5.1: Updated overview of the BEC production time and atom number in different sources, adapted from Ref. [121]. Experiments based on atom chips (orange rectangles), magnetic traps (teal circles), all-optical schemes (blue triangles) and hybrid setups (yellow diamonds) are compared to our previous (black star) and new results (red stars). Atomic species other than rubidium are marked in grey. The black arrow illustrates the expected improvement of our new results by a more frequent use of the dispenser.

5.2 IMPROVED ATOM NUMBER COUNTING CAPABILITIES

In the initial implementation of the detection-MOT presented in Ref. [119], good noise characteristics were observed for small atom numbers. However, the system suffered from instabilities caused by long beam paths. To address this issue, a redesigned version was developed at the cost of a higher noise contribution caused by background light.

In the updated setup, the incident angle of the beams with respect to the detection system was reduced. This led to a small amount of light being scattered into the detection system from reflections at the glass cell surface, causing additional noise. Due to spatial constraints, avoiding reflections to enter the detection system is difficult. Alternatively, reducing the laser power decreases the background signal and therefore the noise contribution. By decreasing the beam diameter from 3 mm to 1 mm, the laser power can be reduced by a factor of 9 while maintaining the saturation parameter. Fig. 5.2 shows the results obtained by this upgrade. The single-atom counting capabilities significantly improved and an extrapolation suggests a single-atom resolution of up to 700 atoms.

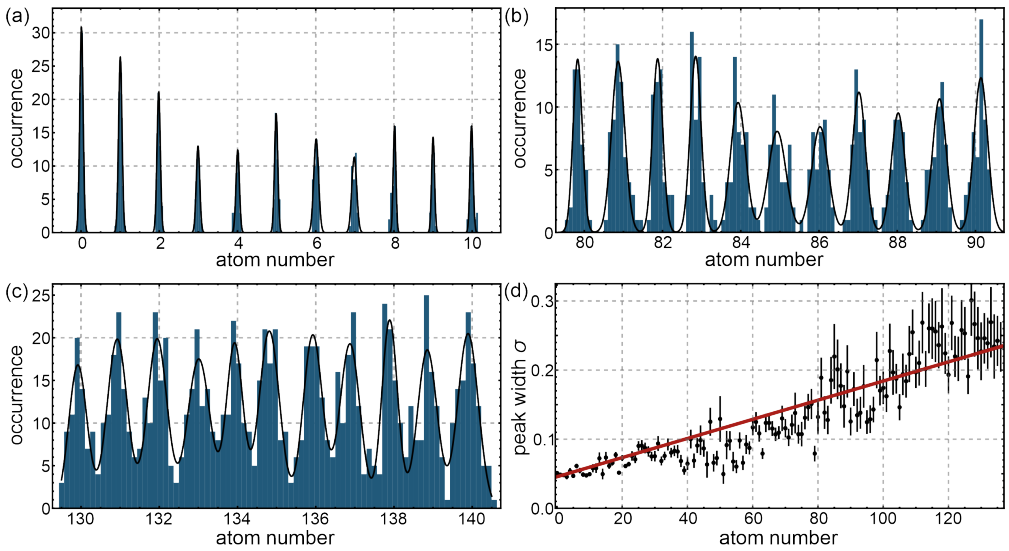

Figure 5.2: Accurate atom counting capabilities in the newest version of the detection-MOT setup. (a)-(c) The histograms of repeated number measurements display distinct peaks at integer numbers. The peaks' widths σ are fitted with Gaussian distributions (solid black line). The black data points in (d) show the result of the fitted widths and the error bars give the standard error of the fit. The red solid line is a linear fit to the widths. Extrapolating the linear fit to $\sigma = 1$ gives a number resolution threshold of 700 atoms.

For certain measurements, it is desirable to have a detection system that can resolve multiple spatial modes, such as several hyperfine levels split by a Stern-Gerlach pulse. However, maintaining the single-atom counting capabilities in this case is very challenging. In a detection-MOT configuration, atoms initially spatially separated, are confined in a single trap center and become indistinguishable. There are options to split a MOT into multiple spatially separated parts, i.e. by shining in a blue-detuned laser beam while

maintaining single-atom resolution [128]. Alternatively, spatially resolved detection by illumination with red-detuned light in molasses configuration is possible. Without the magnetic quadrupole field, the confining force of the MOT is avoided and the atomic clouds expand only slowly. The cooling effect of the molasses still allows for long illumination times on the order of milliseconds. This configuration has been previously implemented in other setups and counting resolution close the the single-atom level has been achieved [107]. Implementing this detection configuration in our apparatus is feasible without major modifications. We tested this method and achieved accurate atom counting in three spatially separated modes.

5.3 NUMBER-RESOLVED TWO-MODE SQUEEZED VACUUM STATE

As a next step towards Heisenberg-limited atom interferometry, the number-resolved analysis of an entangled state is of high interest. One excellent candidate is the two-mode squeezed vacuum. By initiating spin changing collisions of atoms in $|F = 1, m_F = 0\rangle$, pairs of atoms in $m_F = \pm 1$ are created. The resulting state $|\Psi\rangle$ is called two-mode squeezed vacuum and can be described as

$$|\Psi\rangle = \sum_{n=0}^{\infty} c_n |n\rangle_1 \otimes |n\rangle_{-1} \tag{5.1}$$

where $|n\rangle_{\pm 1}$ are number or Fock states in the levels $m_F = \pm 1$. The coefficients c_n depend on the strength and duration of the spin dynamics and describe the relative quantity of created pairs [129].

Experimentally, a two-mode squeezed vacuum is created by the preparation of a BEC in $|F = 1, m_F = 0\rangle$ and a MW dressing that enables spin changing collisions. For its number-resolved detection, remaining atoms in $|F = 1, m_F = 0\rangle$ are removed and the state is detected in MOT-configuration. The joint detection of atoms in $m_F = \pm 1$ results in a characteristic atom number distribution in which only even and no odd numbers occur. This distribution is also referred to as odd-even oscillations and it is a strong signature of a non-classical state. Our preliminary results are displayed in Fig. 5.3.

One effect deteriorating the detection of clear odd-even oscillations is an atom number offset. Imperfect removal of atoms in $|F = 1, m_F = 0\rangle$ before detection and loading atoms during detection both increase the number of counted atoms. This effect, already described in Refs. [121, 122], is well understood and characterized by the QDT. This atom number offset in the case of a two-mode squeezed vacuum state will lead to the detection of odd numbers. Another experimental challenge is the removal of all atoms in $|F = 1, m_F = 0\rangle$ without loss of atoms in $m_F = \pm 1$. Spin-changing collisions demand high atomic densities as found in BECs. For the number-resolved detection of a two-mode squeezed vacuum state, however, small populations are favourable. As a result, a few hundreds of atoms occupying the same spatial mode as the two-mode squeezed vacuum state have to be removed. Due to high densities in the BEC and heating by the removal process, this results in a loss effect which further increases the number of odd numbers. With the independently

measured atom number offset of 0.3 atoms, a loss of 10% can be fitted to the data shown in Fig. 5.3. Optimizing the experimental techniques for the detection of clear odd-even oscillations is ongoing work in the laboratory.

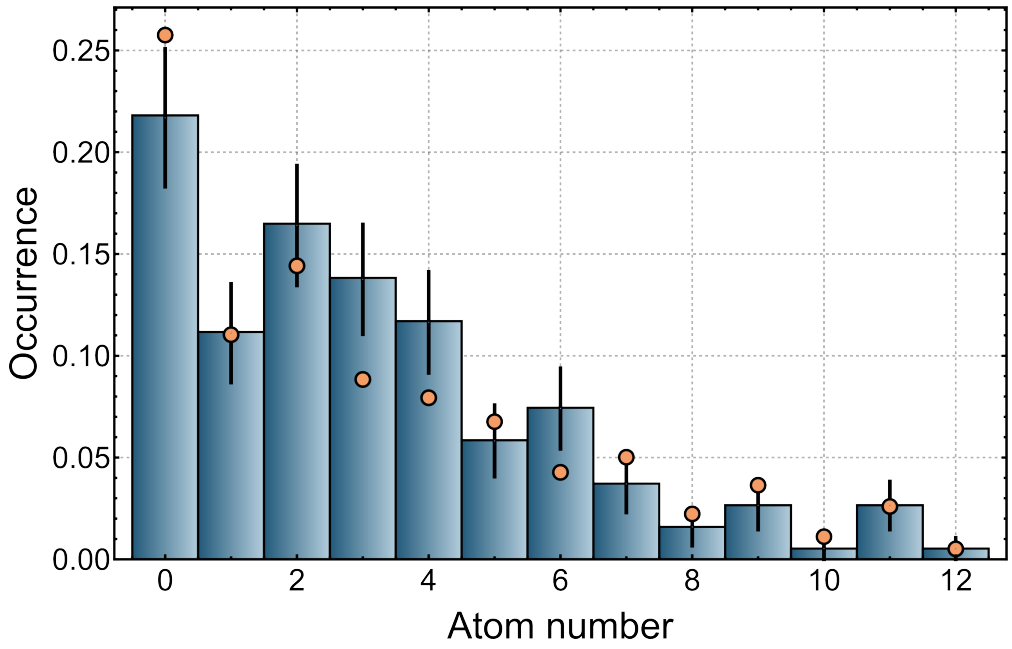

Figure 5.3: Preliminary data of a number-resolved two-mode squeezed vacuum state. The blue histograms show the experimental data with error bars giving the statistical error. The orange points show a simulation of a two-mode squeezed vacuum state taking an atom number offset of 0.3 atoms and an atom loss of 10% into account. The atom number offset has been obtained from an independent measurement. The number of atoms in the two-mode squeezed vacuum has been matched to the measured number of atoms. The loss has been fitted to the data points.

5.4 ATOMIC HONG-OU-MANDEL EXPERIMENT

The preparation of a two-mode squeezed vacuum state combined with a number-resolving detection enables the realization of an atomic Hong-Ou-Mandel experiment. In its first realization [130], Hong, Ou and Mandel prepared entangled pairs of photons by parametric down-conversion, superposed the beams on a beam splitter and measured the number of coincident photons at the output ports of the beam splitter. When the beam splitter was positioned such that the photon pairs arrived at the same time, the coincidences at the output ports decreased. This means that photons arriving simultaneously at the beam splitter, leave the beam splitter together at the same output port. This behaviour is characteristic for bosons and therefore can be observed with bosonic atoms, as well. The first atomic Hong-Ou-Mandel experiment has been performed in the group of Christopher Westbrook [131].

In our experiment, pairs of atoms are created by the generation of a two-mode squeezed vacuum state. A beam splitter between the two modes can be realized by MW pulses in the following way. A first MW π-pulse transfers all

atoms of one mode to $|F = 2, m_F = 0\rangle$ and a second MW $\pi/2$-pulse couples the two modes acting as a beam splitter. As a result, two atoms combined at the beam splitter will occupy the same mode afterwards. If the two-mode squeezed vacuum state contains more than two atoms, pairs of atoms leave the beam splitter together leading to the detection of only even numbers in each mode. This could be observed by removing one of the modes and detecting the remaining atoms in the detection-MOT or by keeping both modes and applying the detection in molasses-configuration, allowing for the detection of both modes simultaneously. As soon as the number-resolved detection of the two-mode squeezed vacuum state has succeeded, all of the necessary tools have been developed and implemented and the sequence could be easily adapted for this experiment.

5.5 LONG-TERM GOAL

In the long term, the experiment aims to transition from the number-resolved analysis of many-body quantum states to quantum-enhanced atom interferometry. This shift is particularly interesting for experiments that are not limited by technical noise sources but rather by shot noise. Typical atom interferometric gravimeters, for instance, face limitations due to technical noise such as vibrations. However, for differential measurements, these noise sources can be strongly suppressed by common noise rejection, making quantum-enhanced atom interferometry highly appealing. Applications in fundamental research, such as gravitational wave detection, can be built upon differential atom interferometric measurements, offering significant advantages through quantum enhancement. Proposals like the European Laboratory for Gravitation and Atominterferometric Research (ELGAR) pursue this approach [132].

Previous experiments have achieved impressive results by surpassing the SQL with both small and large numbers of particles. The ultimate experimental goal is to achieve a measurement sensitivity as close to the Heisenberg limit as possible. While experiments with small particle numbers, as trapped ion experiments, have shown metrological gain at the Heisenberg limit with up to 10 particles, this poses a significant challenge in experiments with large atom numbers [117]. First of all, a quantum state suitable for interferometric sequences has to be created. While certain entangled states, such as the Greenberger-Horne-Zeilinger state, exhibit high sensitivity but are vulnerable to technical noise, the twin-Fock state offers greater robustness while still providing metrological gain close to the Heisenberg limit. Experimentally, the twin-Fock state has been shown to surpass the SQL, but a phase sensitivity close to the Heisenberg limit could not be achieved. One experiment has specifically identified detection noise as the main limitation [87]. Our experimental setup was especially designed to overcome this issue. With our number-resolving detection, potentially scaling to 700 atoms, we have the opportunity to extend interferometric sensitivity close to the Heisenberg limit from 10 particles to hundreds of atoms.

BIBLIOGRAPHY

[1] T. Young. "On the Theory of Light and Colours." In: *Proc. Roy. Soc. Lond. A* 92 (1802), pp. 12–48.

[2] H. Hertz. "Ueber einen Einfluss des ultravioletten Lichtes auf die electrische Entladung." In: *Annalen der Physik* 267.8 (1887), pp. 983–1000. DOI: https://doi.org/10.1002/andp.18872670827. eprint: https://onlinelibrary.wiley.com/doi/pdf/10.1002/andp.18872670827. URL: https://onlinelibrary.wiley.com/doi/abs/10.1002/andp.18872670827.

[3] A. Einstein. "Über einen die Erzeugung und Verwandlung des Lichtes betreffenden heuristischen Gesichtspunkt." In: *Annalen der Physik* 322.6 (1905), pp. 132–148. DOI: https://doi.org/10.1002/andp.19053220607. eprint: https://onlinelibrary.wiley.com/doi/pdf/10.1002/andp.19053220607. URL: https://onlinelibrary.wiley.com/doi/abs/10.1002/andp.19053220607.

[4] L. V. P. R. de Broglie. "Recherches sur la théorie des quanta." PhD thesis. 1924.

[5] W. Heisenberg. "Über den anschaulichen Inhalt der quantentheoretischen Kinematik und Mechanik." In: *Zeitschrift für Physik A Hadrons and Nuclei* 43.3 (1927), pp. 172–198. ISSN: 0939-7922. DOI: 10.1007/BF01397280.

[6] E. Schrödinger. "Quantisierung als Eigenwertproblem." In: *Annalen der Physik* 384.4 (1926), pp. 361–376. DOI: https://doi.org/10.1002/andp.19263840404. eprint: https://onlinelibrary.wiley.com/doi/pdf/10.1002/andp.19263840404. URL: https://onlinelibrary.wiley.com/doi/abs/10.1002/andp.19263840404.

[7] A. Einstein, B. Podolsky, and N. Rosen. "Can quantum-mechanical description of physical reality be considered complete?" In: *Phys. Rev.* 47.10 (1935), pp. 777–780. DOI: 10.1103/PhysRev.47.777.

[8] J. S. Bell. "On the Einstein-Podolsky-Rosen paradox." In: *Physics* 1.3 (1964), pp. 195–200.

[9] S. J. Freedman and J. F. Clauser. "Experimental Test of Local Hidden-Variable Theories." In: *Phys. Rev. Lett.* 28 (1972), pp. 938–941. DOI: 10.1103/PhysRevLett.28.938. URL: http://link.aps.org/doi/10.1103/PhysRevLett.28.938.

[10] A. Aspect, P. Grangier, and G. Roger. "Experimental Realization of Einstein-Podolsky-Rosen-Bohm *Gedankenexperiment*: A New Violation of Bell's Inequalities." In: *Phys. Rev. Lett.* 49.2 (1982), pp. 91–94. ISSN: 0031-9007. DOI: 10.1103/PhysRevLett.49.91.

[11] M. A. Rowe, D. Kielpinski, V. Meyer, C. A. Sackett, W. M. Itano, C. Monroe, and D. J. Wineland. "Experimental violation of a Bell's inequality with efficient detection." In: *Nature* 409.6822 (2001), pp. 791–794. ISSN: 0028-0836. DOI: 10.1038/35057215.

[12] M. Giustina et al. "Significant-Loophole-Free Test of Bell's Theorem with Entangled Photons." In: *Phys. Rev. Lett.* 115 (2015), p. 250401. DOI: 10.1103/PhysRevLett.115.250401. URL: http://link.aps.org/doi/10.1103/PhysRevLett.115.250401.

[13] The Nobel Committee for Physics. "Scientific Background on the Nobel Prize in Physics 2022." In: (2022). URL: https://www.nobelprize.org/prizes/physics/2022/advanced-information/.

[14] E. Altman et al. "Quantum Simulators: Architectures and Opportunities." In: *PRX Quantum* 2 (2021), p. 017003. DOI: 10.1103/PRXQuantum.2.017003. URL: https://link.aps.org/doi/10.1103/PRXQuantum.2.017003.

[15] I. Georgescu, S. Ashhab, and F. Nori. "Quantum simulation." In: *RMP* 86.1 (2014), pp. 153–185. DOI: 10.1103/RevModPhys.86.153.

[16] C. Gross and I. Bloch. "Quantum simulations with ultracold atoms in optical lattices." In: *Science* 357.6355 (2017), pp. 995–1001. DOI: 10.1126/science.aal3837. eprint: https://www.science.org/doi/pdf/10.1126/science.aal3837. URL: https://www.science.org/doi/abs/10.1126/science.aal3837.

[17] R. Blatt and C. F. Roos. "Quantum simulations with trapped ions." In: *Nature Phys.* 8.4 (2012), pp. 277–284. ISSN: 1745-2473. DOI: 10.1038/nphys2252.

[18] H. Häffner, C. Roos, and R. Blatt. "Quantum computing with trapped ions." In: *Phys. Rep.* 469.4 (2008), pp. 155–203. ISSN: 0370-1573. DOI: 10.1016/j.physrep.2008.09.003.

[19] T. D. Ladd, F. Jelezko, R. Laflamme, Y. Nakamura, C. Monroe, and J. L. O'Brien. "Quantum computers." In: *Nature* 464.7285 (2010), pp. 45–53. ISSN: 1476-4687. DOI: 10.1038/nature08812. URL: https://doi.org/10.1038/nature08812.

[20] K. Bongs, M. Holynski, J. Vovrosh, P. Bouyer, G. Condon, E. Rasel, C. Schubert, W. P. Schleich, and A. Roura. "Taking atom interferometric quantum sensors from the laboratory to real-world applications." In: *Nature Reviews Physics* 1.12 (2019), pp. 731–739. ISSN: 2522-5820. DOI: 10.1038/s42254-019-0117-4. URL: https://doi.org/10.1038/s42254-019-0117-4.

[21] LIGO Scientific Collaboration and Virgo Collaboration. "Observation of Gravitational Waves from a Binary Black Hole Merger." In: *Phys. Rev. Lett.* 116 (2016), p. 061102. DOI: 10.1103/PhysRevLett.116.061102. URL: http://link.aps.org/doi/10.1103/PhysRevLett.116.061102.

[22] L. Pezzè, A. Smerzi, M. K. Oberthaler, R. Schmied, and P. Treutlein. "Quantum metrology with nonclassical states of atomic ensembles." In: *Rev. Mod. Phys.* 90.3 (2018). DOI: 10.1103/revmodphys.90.035005.

[23] B. Lücke. "Multi-particle entanglement in a spinor Bose-Einstein condensate for quantum-enhanced interferometry." PhD thesis. 2014.

[24] I. Bloch, J. Dalibard, and W. Zwerger. "Many-body physics with ultracold gases." In: *Rev. Mod. Phys.* 80 (2008), pp. 885–964. DOI: 10.1103/RevModPhys.80.885.

[25] L. Carr, D. DeMille, R. Krems, and J. Ye. "Cold and ultracold molecules: science, technology and applications." In: *New J. Phys.* 11 (2009). DOI: 10.1088/1367-2630/11/5/055049.

[26] R. Hanson, L. P. Kouwenhoven, J. R. Petta, S. Tarucha, and L. M. K. Vandersypen. "Spins in few-electron quantum dots." In: *Rev. Mod. Phys.* 79 (2007), pp. 1217–1265. DOI: 10.1103/RevModPhys.79.1217. URL: https://link.aps.org/doi/10.1103/RevModPhys.79.1217.

[27] M. H. Devoret and R. J. Schoelkopf. "Superconducting Circuits for Quantum Information: An Outlook." In: *Science* 339.6124 (2013). DOI: 10.1126/science.1231930. eprint: https://www.science.org/doi/pdf/10.1126/science.1231930. URL: https://www.science.org/doi/abs/10.1126/science.1231930.

[28] D. G. Cory, M. D. Price, and T. F. Havel. "Nuclear magnetic resonance spectroscopy: An experimentally accessible paradigm for quantum computing." In: *Physica D: Nonlinear Phenomena* 120.1-2 (1998), pp. 82–101. DOI: 10.1016/s0167-2789(98)00046-3. URL: https://doi.org/10.1016%2Fs0167-2789%2898%2900046-3.

[29] A. Aspuru-Guzik and P. Walther. "Photonic Quantum Simulators." In: *Nature Physics* 8 (2012). DOI: 10.1038/nphys2253.

[30] D. Bouwmeester, J.-W. Pan, M. Daniell, H. Weinfurter, and A. Zeilinger. "Observation of Three-Photon Greenberger-Horne-Zeilinger Entanglement." In: *Phys. Rev. Lett.* 82 (1999), pp. 1345–1349. DOI: 10.1103/PhysRevLett.82.1345. URL: http://link.aps.org/doi/10.1103/PhysRevLett.82.1345.

[31] J.-W. Pan, M. Daniell, S. Gasparoni, G. Weihs, and A. Zeilinger. "Experimental Demonstration of Four-Photon Entanglement and High-Fidelity Teleportation." In: *Phys. Rev. Lett.* 86.20 (2001), pp. 4435–4438. DOI: 10.1103/PhysRevLett.86.4435.

[32] Z. Zhao, Y.-A. Chen, A.-N. Zhang, T. Yang, H. J. Briegel, and J.-W. Pan. "Experimental demonstration of five-photon entanglement and open-destination teleportation." In: *Nature* 430.6995 (2004), pp. 54–58. ISSN: 1476-4687. DOI: 10.1038/nature02643. URL: https://doi.org/10.1038/nature02643.

[33] C.-Y. Lu, X.-Q. Zhou, O. Gühne, W.-B. Gao, J. Zhang, Z.-S. Yuan, A. Goebel, T. Yang, and J.-W. Pan. "Experimental entanglement of six photons in graph states." In: *Nature Physics* 3.2 (2007), pp. 91–95. ISSN: 1745-2481. DOI: 10.1038/nphys507. URL: https://doi.org/10.1038/nphys507.

[34] Y.-F. Huang, B.-H. Liu, L. Peng, Y.-H. Li, L. Li, C.-F. Li, and G.-C. Guo. "Experimental generation of an eight-photon Greenberger–Horne–Zeilinger state." In: *Nature Communications* 2.1 (2011), p. 546. ISSN: 2041-1723. DOI: 10.1038/ncomms1556. URL: https://doi.org/10.1038/ncomms1556.

[35] X.-C. Yao, T.-X. Wang, P. Xu, H. Lu, G.-S. Pan, X.-H. Bao, C.-Z. Peng, C.-Y. Lu, Y.-A. Chen, and J.-W. Pan. "Observation of eight-photon entanglement." In: *Nature Photon.* 6.4 (2012), pp. 225–228. ISSN: 1749-4885. DOI: 10.1038/nphoton.2011.354.

[36] X.-L. Wang et al. "Experimental Ten-Photon Entanglement." In: *Phys. Rev. Lett.* 117 (2016), p. 210502. DOI: 10.1103/PhysRevLett.117.210502. URL: http://link.aps.org/doi/10.1103/PhysRevLett.117.210502.

[37] H.-S. Zhong et al. "12-Photon Entanglement and Scalable Scattershot Boson Sampling with Optimal Entangled-Photon Pairs from Parametric Down-Conversion." In: *Phys. Rev. Lett.* 121 (2018), p. 250505. DOI: 10.1103/PhysRevLett.121.250505. URL: https://link.aps.org/doi/10.1103/PhysRevLett.121.250505.

[38] X.-L. Wang et al. "18-Qubit Entanglement with Six Photons' Three Degrees of Freedom." In: *Phys. Rev. Lett.* 120 (2018), p. 260502. DOI: 10.1103/PhysRevLett.120.260502. URL: https://link.aps.org/doi/10.1103/PhysRevLett.120.260502.

[39] P. Thomas, L. Ruscio, O. Morin, and G. Rempe. "Efficient generation of entangled multiphoton graph states from a single atom." In: *Nature* 608.7924 (2022), pp. 677–681. ISSN: 1476-4687. DOI: 10.1038/s41586-022-04987-5. URL: https://doi.org/10.1038/s41586-022-04987-5.

[40] Q. A. Turchette, C. S. Wood, B. E. King, C. J. Myatt, D. Leibfried, W. M. Itano, C. Monroe, and D. J. Wineland. "Deterministic Entanglement of Two Trapped Ions." In: *Phys. Rev. Lett.* 81 (1998), pp. 3631–3634. DOI: 10.1103/PhysRevLett.81.3631. URL: https://link.aps.org/doi/10.1103/PhysRevLett.81.3631.

[41] C. A. Sackett et al. "Experimental entanglement of four particles." In: *Nature* 404.6775 (2000), p. 256. ISSN: 0028-0836. DOI: 10.1038/35005011.

[42] H. Häffner et al. "Scalable multiparticle entanglement of trapped ions." In: *Nature* 438.7068 (2005), p. 643. ISSN: 0028-0836. DOI: 10.1038/nature04279.

[43] T. Monz, P. Schindler, J. T. Barreiro, M. Chwalla, D. Nigg, W. A. Coish, M. Harlander, W. Hänsel, M. Hennrich, and R. Blatt. "14-Qubit Entanglement: Creation and Coherence." In: *Phys. Rev. Lett.* 106 (2011), p. 130506. DOI: 10.1103/PhysRevLett.106.130506. URL: http://link.aps.org/doi/10.1103/PhysRevLett.106.130506.

[44] I. Pogorelov et al. "Compact Ion-Trap Quantum Computing Demonstrator." In: *PRX Quantum* 2 (2021), p. 020343. DOI: 10.1103/PRXQuantum.2.020343. URL: https://link.aps.org/doi/10.1103/PRXQuantum.2.020343.

[45] T. Wilk, A. Gaëtan, C. Evellin, J. Wolters, Y. Miroshnychenko, P. Grangier, and A. Browaeys. "Entanglement of Two Individual Neutral Atoms Using Rydberg Blockade." In: *Phys. Rev. Lett.* 104 (2010), p. 010502. DOI: 10.1103/PhysRevLett.104.010502. URL: https://link.aps.org/doi/10.1103/PhysRevLett.104.010502.

[46] A. Omran et al. "Generation and manipulation of Schrödinger cat states in Rydberg atom arrays." In: *Science* 365.6453 (2019), pp. 570–574. DOI: 10.1126/science.aax9743.

[47] M. Steffen, M. Ansmann, R. C. Bialczak, N. Katz, E. Lucero, R. McDermott, M. Neeley, E. M. Weig, A. N. Cleland, and J. M. Martinis. "Measurement of the Entanglement of Two Superconducting Qubits via State Tomography." In: *Science* 313.5792 (2006), pp. 1423–1425. DOI: 10.1126/science.1130886. eprint: https://www.science.org/doi/pdf/10.1126/science.1130886. URL: https://www.science.org/doi/abs/10.1126/science.1130886.

[48] L. DiCarlo, M. D. Reed, L. Sun, B. R. Johnson, J. M. Chow, J. M. Gambetta, L. Frunzio, S. M. Girvin, M. H. Devoret, and R. J. Schoelkopf. "Preparation and measurement of three-qubit entanglement in a superconducting circuit." In: *Nature* 467.7315 (2010), pp. 574–578. ISSN: 0028-0836. DOI: 10.1038/nature09416.

[49] R. Barends et al. "Superconducting quantum circuits at the surface code threshold for fault tolerance." In: *Nature* 508.7497 (2014), pp. 500–503. ISSN: 1476-4687. DOI: 10.1038/nature13171. URL: https://doi.org/10.1038/nature13171.

[50] C. Song et al. "10-Qubit Entanglement and Parallel Logic Operations with a Superconducting Circuit." In: *Phys. Rev. Lett.* 119 (2017), p. 180511. DOI: 10.1103/PhysRevLett.119.180511. URL: https://link.aps.org/doi/10.1103/PhysRevLett.119.180511.

[51] Y. Wang, Y. Li, Z.-Q. Yin, and B. Zeng. "16-qubit IBM universal quantum computer can be fully entangled." In: *npj Quantum Information* 4.1 (2018), p. 46. ISSN: 2056-6387. DOI: 10.1038/s41534-018-0095-x. URL: https://doi.org/10.1038/s41534-018-0095-x.

[52] C. Song et al. "Generation of multicomponent atomic Schrödinger cat states of up to 20 qubits." In: *Science* 365.6453 (2019), pp. 574–577. DOI: 10.1126/science.aay0600. eprint: https://www.science.org/doi/pdf/10.1126/science.aay0600. URL: https://www.science.org/doi/abs/10.1126/science.aay0600.

[53] G. J. Mooney, G. A. L. White, C. D. Hill, and L. C. L. Hollenberg. "Generation and verification of 27-qubit Greenberger-Horne-Zeilinger states in a superconducting quantum computer." In: *Journal of Physics Communications* 5.9 (2021), p. 095004. DOI: 10.1088/2399-6528/ac1df7. URL: https://dx.doi.org/10.1088/2399-6528/ac1df7.

[54] R. McConnell, H. Zhang, J. Hu, S. Ćuk, and V. Vuletić. "Entanglement with negative Wigner function of almost 3,000 atoms heralded by one photon." In: *Nature* 519.7544 (2015), pp. 439–442. ISSN: 0028-0836. DOI: 10.1038/nature14293.

[55] O. Hosten, N. J. Engelsen, R. Krishnakumar, and M. A. Kasevich. "Measurement noise 100 times lower than the quantum-projection limit using entangled atoms." In: *Nature* 529 (2016), p. 505. DOI: 10.1038/nature16176.

[56] K. C. Cox, G. P. Greve, J. M. Weiner, and J. K. Thompson. "Deterministic Squeezed States with Collective Measurements and Feedback." In: *Phys. Rev. Lett.* 116 (2016), p. 093602. DOI: 10.1103/PhysRevLett.116.093602. URL: https://link.aps.org/doi/10.1103/PhysRevLett.116.093602.

[57] C. Gross, T. Zibold, E. Nicklas, J. Estève, and M. K. Oberthaler. "Nonlinear atom interferometer surpasses classical precision limit." In: *Nature* 464.7292 (2010), p. 1165. ISSN: 0028-0836. DOI: 10.1038/nature08919.

[58] T. Berrada, S. van Frank, R. Bücker, T. Schumm, J.-F. Schaff, and J. Schmiedmayer. "Integrated Mach-Zehnder interferometer for Bose-Einstein condensates." In: *Nat. Commun.* 4 (2013). DOI: 10.1038/ncomms3077.

[59] X.-Y. Luo, Y.-Q. Zou, L.-N. Wu, Q. Liu, M.-F. Han, M. K. Tey, and L. You. "Deterministic entanglement generation from driving through quantum phase transitions." In: *Science* 355.6325 (2017), pp. 620–623. ISSN: 0036-8075. DOI: 10.1126/science.aag1106. URL: http://science.sciencemag.org/content/355/6325/620.

[60] Y.-Q. Zou, L.-N. Wu, Q. Liu, X.-Y. Luo, S.-F. Guo, J.-H. Cao, M. K. Tey, and L. You. "Beating the Classical Precision Limit with Spin-1 Dicke States of More than 10,000 Atoms." In: *Proc. Natl. Acad. Sci. U.S.A.* 115.25 (2018), pp. 6381–6385. ISSN: 0027-8424, 1091-6490. DOI: 10.1073/pnas.1715105115.

[61] H. Iams and B. Salzberg. "The secondary emission phototube." In: *Proceedings of the Institute of Radio Engineers* 23.1 (1935), pp. 55–64.

[62] I. Esmaeil Zadeh, J. Chang, J. W. N. Los, S. Gyger, A. W. Elshaari, S. Steinhauer, S. N. Dorenbos, and V. Zwiller. "Superconducting nanowire single-photon detectors: A perspective on evolution, state-of-the-art, future developments, and applications." In: *Applied Physics Letters* 118.19 (2021), p. 190502. DOI: 10.1063/5.0045990. eprint: https://doi.org/10.1063/5.0045990. URL: https://doi.org/10.1063/5.0045990.

[63] M. Endres, H. Bernien, A. Keesling, H. Levine, E. R. Anschuetz, A. Krajenbrink, C. Senko, V. Vuletic, M. Greiner, and M. D. Lukin. "Atom-by-atom assembly of defect-free one-dimensional cold atom arrays." In: *Science* 354.6315 (2016), pp. 1024–1027. ISSN: 0036-8075. DOI: 10.1126/science.aah3752. URL: http://science.sciencemag.org/content/354/6315/1024.

[64] D. Barredo, S. de Léséleuc, V. Lienhard, T. Lahaye, and A. Browaeys. "An atom-by-atom assembler of defect-free arbitrary two-dimensional atomic arrays." In: *Science* 354.6315 (2016), pp. 1021–1023. ISSN: 0036-8075. DOI: 10.1126/science.aah3778. URL: http://science.sciencemag.org/content/354/6315/1021.

[65] F. Kranzl, M. K. Joshi, C. Maier, T. Brydges, J. Franke, R. Blatt, and C. F. Roos. "Controlling long ion strings for quantum simulation and precision measurements." In: *Phys. Rev. A* 105 (2022), p. 052426. DOI: 10.1103/PhysRevA.105.052426. URL: https://link.aps.org/doi/10.1103/PhysRevA.105.052426.

[66] T. Xia, M. Lichtman, K. Maller, A. W. Carr, M. J. Piotrowicz, L. Isenhower, and M. Saffman. "Randomized Benchmarking of Single-Qubit Gates in a 2D Array of Neutral-Atom Qubits." In: *Phys. Rev. Lett.* 114 (2015), p. 100503. DOI: 10.1103/PhysRevLett.114.100503. URL: https://link.aps.org/doi/10.1103/PhysRevLett.114.100503.

[67] R. Blatt and D. Wineland. "Entangled states of trapped atomic ions." In: *Nature* 453.7198 (2008), pp. 1008–1015. ISSN: 0028-0836. DOI: 10.1038/nature07125.

[68] A. M. Kaufman and K.-K. Ni. "Quantum science with optical tweezer arrays of ultracold atoms and molecules." In: *Nature Physics* 17.12 (2021), pp. 1324–1333. ISSN: 1745-2481. DOI: 10.1038/s41567-021-01357-2. URL: https://doi.org/10.1038/s41567-021-01357-2.

[69] H. Bernien et al. "Probing Many-Body Dynamics on a 51-Atom Quantum Simulator." In: *Nature* 551.7682 (2017), pp. 579–584. ISSN: 0028-0836, 1476-4687. DOI: 10.1038/nature24622.

[70] F. Arute et al. "Quantum supremacy using a programmable superconducting processor." In: *Nature* 574.7779 (2019), pp. 505–510. ISSN: 1476-4687. DOI: 10.1038/s41586-019-1666-5. URL: https://doi.org/10.1038/s41586-019-1666-5.

[71] J. G. Bohnet, B. C. Sawyer, J. W. Britton, M. L. Wall, A. M. Rey, M. Foss-Feig, and J. J. Bollinger. "Quantum spin dynamics and entanglement generation with hundreds of trapped ions." In: *Science* 352.6291 (2016), pp. 1297–1301. ISSN: 0036-8075. DOI: 10.1126/science.aad9958. URL: http://science.sciencemag.org/content/352/6291/1297.

[72] H. Metcalf and P. Van der Straten. *Laser cooling and trapping of atoms*. Springer, New York, 1999.

[73] S. Bose. "Plancks Gesetz und Lichtquantenhypothese." In: *Z. Phys.* 26.1 (1924), pp. 178–181. DOI: 10.1007/BF01327326.

[74] A. Einstein. "Quantentheorie des idealen einatomigen Gases II." In: *Sitzber. Kgl. Preuss. Akad. Wiss., Phys. Math. Kl. Bericht* 3 (1925), p. 18.

[75] E. A. Cornell and C. E. Wieman. "Nobel Lecture: Bose-Einstein condensation in a dilute gas, the first 70 years and some recent experiments." In: *Rev. Mod. Phys.* 74.3 (2002), pp. 875–893. DOI: 10.1103/RevModPhys.74.875.

[76] W. Ketterle. "Nobel lecture: When atoms behave as waves: Bose-Einstein condensation and the atom laser." In: *Rev. Mod. Phys.* 74.4 (2002), pp. 1131–1151. DOI: 10.1103/RevModPhys.74.1131.

[77] J. Hald, J. L. Sørensen, C. Schori, and E. S. Polzik. "Spin squeezed atoms: A macroscopic entangled ensemble created by light." In: *Phys. Rev. Lett.* 83.7 (1999), p. 1319. DOI: 10.1103/PhysRevLett.83.1319.

[78] A. Kuzmich, L. Mandel, and N. P. Bigelow. "Generation of Spin Squeezing via Continuous Quantum Nondemolition Measurement." In: *Phys. Rev. Lett.* 85 (2000), pp. 1594–1597. DOI: 10.1103/PhysRevLett.85.1594. URL: http://link.aps.org/doi/10.1103/PhysRevLett.85.1594.

[79] J. Appel, P. J. Windpassinger, D. Oblak, U. B. Hoff, N. Kærgaard, and E. S. Polzik. "Mesoscopic atomic entanglement for precision measurements beyond the standard quantum limit." In: *Proc. Natl. Acad. Sci. U. S. A.* 106.27 (2009), p. 10960. DOI: 10.1073/pnas.0901550106.

[80] R. J. Sewell, M. Koschorreck, M. Napolitano, B. Dubost, N. Behbood, and M. W. Mitchell. "Magnetic Sensitivity Beyond the Projection Noise Limit by Spin Squeezing." In: *Phys. Rev. Lett.* 109 (2012), p. 253605. DOI: 10.1103/PhysRevLett.109.253605.

[81] Z. Chen, J. Bohnet, S. Sankar, J. Dai, and J. Thompson. "Conditional spin squeezing of a large ensemble via the vacuum Rabi splitting." In: *Phys. Rev. Lett.* 106.13 (2011), p. 133601. DOI: 10.1103/PhysRevLett.106.133601.

[82] M. H. Schleier-Smith, I. D. Leroux, and V. Vuletić. "States of an ensemble of two-level atoms with reduced quantum uncertainty." In: *Phys. Rev. Lett.* 104 (2010), p. 073604. DOI: 10.1103/PhysRevLett.104.073604. URL: http://link.aps.org/doi/10.1103/PhysRevLett.104.073604.

[83] F. Haas, J. Volz, R. Gehr, J. Reichel, and J. Estève. "Entangled States of More Than 40 Atoms in an Optical Fiber Cavity." In: *Science* 344.6180 (2014), pp. 180–183. DOI: 10.1126/science.1248905. URL: http://www.sciencemag.org/content/344/6180/180.abstract.

[84] J. Estève, C. Gross, A. Weller, S. Giovanazzi, and M. K. Oberthaler. "Squeezing and entanglement in a Bose-Einstein condensate." In: *Nature* 455.7217 (2008), pp. 1216–1219. ISSN: 0028-0836. DOI: 10.1038/nature07332.

[85] M. Riedel, P. Böhi, Y. Li, T. Hänsch, A. Sinatra, and P. Treutlein. "Atom-chip-based generation of entanglement for quantum metrology." In: *Nature* 464.7292 (2010), p. 1170. ISSN: 0028-0836. DOI: 10.1038/nature08988.

[86] M.-S. Chang, Q. Qin, W. Zhang, L. You, and M. S. Chapman. "Coherent spinor dynamics in a spin-1 Bose condensate." In: *Nature Phys.* 1.2 (2005), pp. 111–116. ISSN: 1745-2473. DOI: 10.1038/nphys153.

[87] B. Lücke et al. "Twin matter waves for interferometry beyond the classical Limit." In: *Science* 334.6057 (2011), pp. 773–776. ISSN: 0036-8075, 1095-9203. DOI: 10.1126/science.1208798. URL: http://www.sciencemag.org/content/334/6057/773.

[88] C. Gross, H. Strobel, E. Nicklas, T. Zibold, N. Bar-Gill, G. Kurizki, and M. K. Oberthaler. "Atomic homodyne detection of continuous-variable entangled twin-atom states." In: *Nature* 480 (2011), p. 219. ISSN: 1476-4687. DOI: 10.1038/nature10654.

[89] C. D. Hamley, C. S. Gerving, T. M. Hoang, E. M. Bookjans, and M. S. Chapman. "Spin-nematic squeezed vacuum in a quantum gas." In: *Nature Phys.* 8 (2012), p. 305. ISSN: 1745-2481. DOI: 10.1038/nphys2245.

[90] T. Esslinger, I. Bloch, and T. W. Hänsch. "Bose-Einstein condensation in a quadrupole-Ioffe-configuration trap." In: *Phys. Rev. A* 58.4 (1998), R2664–R2667. DOI: 10.1103/PhysRevA.58.R2664.

[91] U. Ernst, A. Marte, F. Schreck, J. Schuster, and G. Rempe. "Bose-Einstein condensation in a pure Ioffe-Pritchard field configuration." In: *EPL (Europhysics Letters)* 41.1 (1998), p. 1. ISSN: 0295-5075. DOI: 10.1209/epl/i1998-00107-2. URL: https://iopscience.iop.org/article/10.1209/epl/i1998-00107-2/meta.

[92] E. Riis, D. S. Weiss, K. A. Moler, and S. Chu. "Atom funnel for the production of a slow, high-density atomic beam." In: *Phys. Rev. Lett.* 64.14 (1990), pp. 1658–1661. DOI: 10.1103/PhysRevLett.64.1658.

[93] K. Dieckmann, R. J. C. Spreeuw, M. Weidemüller, and J. T. M. Walraven. "Two-dimensional magneto-optical trap as a source of slow atoms." In: *Phys. Rev. A* 58.5 (1998), pp. 3891–3895. DOI: 10.1103/PhysRevA.58.3891.

[94] W. Ketterle, D. Durfee, and D. Stamper-Kurn. "Making, probing and understanding Bose-Einstein condensates." In: *In Bose-Einstein condensation in atomic gases, Proceedings of the International School of Physics "Enrico Fermi", Course CXL*. 1999.

[95] R. Grimm, M. Weidemüller, and Y. B. Ovchinnikov. "Optical dipole traps for neutral atoms." In: *Adv. At. Mol. Opt. Phys.* 42 (2000), p. 95.

[96] M. Horikoshi and K. Nakagawa. "Atom chip based fast production of Bose-Einstein condensate." In: *Applied Physics B* 82.3 (2006), pp. 363–366. ISSN: 1432-0649. DOI: 10.1007/s00340-005-2083-z. URL: https://doi.org/10.1007/s00340-005-2083-z.

[97] D. M. Farkas, E. A. Salim, and J. Ramirez-Serrano. "Production of Rubidium Bose-Einstein Condensates at a 1 Hz Rate." In: *arXiv:1403.4641* (2014). URL: http://arxiv.org/abs/1403.4641.

[98] J. Rudolph et al. "A high-flux BEC source for mobile atom interferometers." In: *New J. Phys.* 17.6 (2015), p. 065001. DOI: 10.1088/1367-2630/17/6/065001. URL: http://stacks.iop.org/1367-2630/17/i=6/a=065001.

[99] T. Kinoshita, T. Wenger, and D. S. Weiss. "All-optical Bose-Einstein condensation using a compressible crossed dipole trap." In: *Phys. Rev. A* 71 (2005), p. 011602. DOI: 10.1103/PhysRevA.71.011602. URL: https://link.aps.org/doi/10.1103/PhysRevA.71.011602.

[100] S. Stellmer, R. Grimm, and F. Schreck. "Production of quantum-degenerate strontium gases." In: *Physical Review A* 87.1 (2013), p. 013611. URL: https://link.aps.org/doi/10.1103/PhysRevA.87.013611.

[101] R. Roy, A. Green, R. Bowler, and S. Gupta. "Rapid cooling to quantum degeneracy in dynamically shaped atom traps." In: *Phys. Rev. A* 93 (2016), p. 043403. DOI: 10.1103/PhysRevA.93.043403. URL: https://link.aps.org/doi/10.1103/PhysRevA.93.043403.

[102] A. Herbst, H. Albers, K. Stolzenberg, S. Bode, and D. Schlippert. "Rapid generation of all-optical ^{39}K Bose-Einstein condensates using a low-field Feshbach resonance." In: *Phys. Rev. A* 106 (2022), p. 043320. DOI: 10.1103/PhysRevA.106.043320. URL: https://link.aps.org/doi/10.1103/PhysRevA.106.043320.

[103] Y.-J. Lin, A. R. Perry, R. L. Compton, I. B. Spielman, and J. V. Porto. "Rapid production of ^{87}Rb Bose-Einstein condensates in a combined magnetic and optical potential." In: *Phys. Rev. A* 79.6 (2009), p. 063631. DOI: 10.1103/PhysRevA.79.063631.

[104] M. Zaiser, J. Hartwig, D. Schlippert, U. Velte, N. Winter, V. Lebedev, W. Ertmer, and E. M. Rasel. "Simple method for generating Bose-Einstein condensates in a weak hybrid trap." In: *Phys. Rev. A* 83.3 (2011), p. 035601. ISSN: 1050-2947, 1094-1622. DOI: 10.1103/PhysRevA.83.035601.

[105] Q. Bouton, R. Chang, A. L. Hoendervanger, F. Nogrette, A. Aspect, C. I. Westbrook, and D. Clément. "Fast production of Bose-Einstein condensates of metastable helium." In: *Physical Review A* 91.6 (2015), p. 061402. DOI: 10.1103/PhysRevA.91.061402. URL: https://link.aps.org/doi/10.1103/PhysRevA.91.061402 (visited on 01/27/2021).

[106] G. Colzi, E. Fava, M. Barbiero, C. Mordini, G. Lamporesi, and G. Ferrari. "Production of large Bose-Einstein condensates in a magnetic-shield-compatible hybrid trap." In: *Physical Review A* 97.5 (2018), p. 053625. DOI: 10.1103/physreva.97.053625.

[107] A. Qu, B. Evrard, J. Dalibard, and F. Gerbier. "Probing Spin Correlations in a Bose-Einstein Condensate Near the Single-Atom Level." In: *Phys. Rev. Lett.* 125 (2020), p. 033401. DOI: 10.1103/PhysRevLett.125.033401. URL: https://link.aps.org/doi/10.1103/PhysRevLett.125.033401.

[108] A. Periwal, E. S. Cooper, P. Kunkel, J. F. Wienand, E. J. Davis, and M. Schleier-Smith. "Programmable interactions and emergent geometry in an array of atom clouds." In: *Nature* 600.7890 (2021), pp. 630–635. ISSN: 1476-4687. DOI: 10.1038/s41586-021-04156-0. URL: https://doi.org/10.1038/s41586-021-04156-0.

[109] F. Serwane, G. Zürn, T. Lompe, T. B. Ottenstein, A. N. Wenz, and S. Jochim. "Deterministic Preparation of a Tunable Few-Fermion System." In: *Science* 332.6027 (2011), pp. 336–338. ISSN: 0036-8075. DOI: 10.1126/science.1201351. URL: http://science.sciencemag.org/content/332/6027/336.

[110] D. B. Hume, I. Stroescu, M. Joos, W. Muessel, H. Strobel, and M. K. Oberthaler. "Accurate Atom Counting in Mesoscopic Ensembles." In: *Phys. Rev. Lett.* 111 (2013), p. 253001. DOI: 10.1103/PhysRevLett.111.253001. URL: http://link.aps.org/doi/10.1103/PhysRevLett.111.253001.

[111] I. Stroescu, D. B. Hume, and M. K. Oberthaler. "Double-well atom trap for fluorescence detection at the Heisenberg limit." In: *Phys. Rev. A* 91.1 (2015), p. 013412. DOI: 10.1103/PhysRevA.91.013412. URL: http://link.aps.org/doi/10.1103/PhysRevA.91.013412.

[112] J. S. Lundeen, A. Feito, H. Coldenstrodt-Ronge, K. L. Pregnell, C. Silberhorn, T. C. Ralph, J. Eisert, M. B. Plenio, and I. A. Walmsley. "Tomography of quantum detectors." In: *Nature Physics* 5.1 (2009), pp. 27–30. ISSN: 1745-2481. DOI: 10.1038/nphys1133. URL: https://doi.org/10.1038/nphys1133.

[113] L. Zhang, H. B. Coldenstrodt-Ronge, A. Datta, G. Puentes, J. S. Lundeen, X.-M. Jin, B. J. Smith, M. B. Plenio, and I. A. Walmsley. "Mapping coherence in measurement via full quantum tomography of a hybrid optical detector." In: *Nature Photonics* 6.6 (2012), pp. 364–368. ISSN: 1749-4893. DOI: 10.1038/nphoton.2012.107. URL: https://doi.org/10.1038/nphoton.2012.107.

[114] S. Grandi, A. Zavatta, M. Bellini, and M. G. A. Paris. "Experimental quantum tomography of a homodyne detector." In: *New J. of Phys.* 19.5 (2017), p. 053015. DOI: 10.1088/1367-2630/aa6f2c. URL: https://doi.org/10.1088/1367-2630/aa6f2c.

[115] A. C. Keith, C. H. Baldwin, S. Glancy, and E. Knill. "Joint quantum-state and measurement tomography with incomplete measurements." In: *Phys. Rev. A* 98 (2018), p. 042318. DOI: 10.1103/PhysRevA.98.042318. URL: https://link.aps.org/doi/10.1103/PhysRevA.98.042318.

[116] Y. Chen, M. Farahzad, S. Yoo, and T.-C. Wei. "Detector tomography on IBM quantum computers and mitigation of an imperfect measurement." In: *Phys. Rev. A* 100 (2019), p. 052315. DOI: 10.1103/PhysRevA.100.052315. URL: https://link.aps.org/doi/10.1103/PhysRevA.100.052315.

[117] A. Hüper. "Accurate atom counting for entanglement-enhanced atom interferometry." PhD thesis. 2019.

[118] C. Pür. "Experimental setup for fast BEC generation and number-stabilized atomic ensembles." PhD thesis. 2022.

[119] A Hüper, C Pür, M Hetzel, J Geng, J Peise, I Kruse, M Kristensen, W Ertmer, J Arlt, and C Klempt. "Number-resolved preparation of mesoscopic atomic ensembles." In: *New J. Phys.* 23.11 (2021), p. 113046. DOI: 10.1088/1367-2630/abd058.

[120] C. Pür, M. Hetzel, M. Quensen, A. Hüper, J. Geng, J. Kruse, W. Ertmer, and C. Klempt. "Rapid generation and number-resolved detection of spinor rubidium Bose-Einstein condensates." In: *arXiv* (2023). arXiv: 2301.08172 [cond-mat.quant-gas].

[121] C. Pür, M. Hetzel, M. Quensen, A. Hüper, J. Geng, J. Kruse, W. Ertmer, and C. Klempt. "Rapid generation and number-resolved detection of spinor rubidium Bose-Einstein condensates." In: *Phys. Rev. A* 107 (2023), p. 033303. DOI: 10.1103/PhysRevA.107.033303. URL: https://link.aps.org/doi/10.1103/PhysRevA.107.033303.

[122] M. Hetzel et al. "Tomography of a number-resolving detector by reconstruction of an atomic many-body quantum state." In: *arXiv* (2022). arXiv: 2207.01270 [quant-ph].

[123] M. Hetzel. "Dynamical two-dimensional potentials for ultracold atoms." MA thesis. 2018.

[124] V. Vollenkemper. "Arbitrary Waveforms for Time-Averaged Optical Potentials Using Software Defined Radio." MA thesis. 2022.

[125] J. Lemburg. "Micrometer-scale Dynamical Optical Potentials for Ultracold Atoms." MA thesis. 2021.

[126] I. Geisel, K. Cordes, J. Mahnke, S. Jöllenbeck, J. Ostermann, J. Arlt, W. Ertmer, and C. Klempt. "Evolutionary optimization of an experimental apparatus." In: *Appl. Phys. Lett.* 102.21 (2013). DOI: http://dx.doi.org/10.1063/1.4808213. URL: http://scitation.aip.org/content/aip/journal/apl/102/21/10.1063/1.4808213.

[127] Z. Vendeiro, J. Ramette, A. Rudelis, M. Chong, J. Sinclair, L. Stewart, A. Urvoy, and V. Vuletić. "Machine-learning-accelerated Bose-Einstein condensation." In: *Phys. Rev. Res.* 4 (2022), p. 043216. DOI: 10.1103/PhysRevResearch.4.043216. URL: https://link.aps.org/doi/10.1103/PhysRevResearch.4.043216.

[128] I. Stroescu, D. B. Hume, and M. K. Oberthaler. "Dissipative Double-Well Potential for Cold Atoms: Kramers Rate and Stochastic Resonance." In: *Phys. Rev. Lett.* 117.24 (2016). ISSN: 0031-9007, 1079-7114. DOI: 10.1103/PhysRevLett.117.243005.

[129] C. C. Gerry and P. Knight. *Introductory quantum optics*. Cambridge University Press, 2005.

[130] C. K. Hong, Z. Y. Ou, and L. Mandel. "Measurement of subpicosecond time intervals between two photons by interference." In: *Phys. Rev. Lett.* 59.18 (1987), pp. 2044–2046. DOI: 10.1103/PhysRevLett.59.2044.

[131] R. Lopes, A. Imanaliev, A. Aspect, M. Cheneau, D. Boiron, and C. I. Westbrook. "Atomic Hong-Ou-Mandel experiment." In: *Nature* 520.7545 (2015), pp. 66–68. ISSN: 0028-0836. DOI: 10.1038/nature14331.

[132] B. Canuel et al. "ELGAR - a European Laboratory for Gravitation and Atom-interferometric Research." In: *Class. Quant. Grav.* 37.22 (2020), p. 225017. DOI: 10.1088/1361-6382/aba80e.

DANKSAGUNG

Ich möchte mich ganz herzlich bei Carsten Klempt bedanken, der mir die Möglichkeit gegeben hat, sowohl meine Masterarbeit als auch meine Doktorarbeit in seiner Gruppe anzufertigen. Seine enorme Unterstützung und persönliche Betreuung haben mir während meiner Promotion sehr geholfen. Außerdem möchte ich mich bei Silke Ospelkaus und Augusto Smerzi für die Übernahme der Koreferate und bei Klemens Hammerer für die Übernahme des Prüfungsvorsitzes bedanken.

Bei Martin Quensen möchte ich mich für die wunderbare Zusammenarbeit, das Bauen von unzähligen Elektronikprojekten und das Ertragen meiner Launen und meines Musikgeschmacks im Labor bedanken. Ein besonderer Dank geht an Bernd Meyer-Hoppe für seine aufmunternden Gesten und unsere Diskussionen über sämtliche physikalische und nichtphysikalische Themen.

Ich danke Luca Pezzè für die erfolgreiche Zusammenarbeit und das Erstellen der theoretischen Analysen.

Außerdem möchte ich mich bei Andreas Hüper, Cebrail Pür, Jiao Geng, Lion Günster und Julian Lemburg für die schöne, gemeinsame Zeit und angenehme Zusammenarbeit am QAI-Experiment bedanken. Vielen Dank an die Klempt-Gruppe in ihrer momentanen Zusammensetzung, insbesondere an Janina Hamann, Simon Haase, Christophe Cassens, Kai Müller, Alexander Heidt, Christophe Cussens, Dr. Alexander Fieguth, Roman Schwarz und Jens Kruse, die durch ihre freundliche (und fiese) Art eine Atmosphäre schaffen, sodass ich mit Freude zur Arbeit komme (Feuerfalle?).

Bei Fabian Anders, Alexander Idel, Karsten Lange, Jan Peise und Ilka Kruse möchte ich mich für die freundliche Aufnahme in die Gruppe und für die Unterstützung in den Anfangszeiten meiner Promotion bedanken. Es war mir immer eine Freude, mit euch einen Kaffee im Café Kopi zu trinken.

Außerdem möchte ich mich bei allen herzlich bedanken, die das Institut für Quantenoptik zu dem besonderen Ort machen, der es ist. Mein Dank geht besonders an Ernst Rasel, Dennis Schlippert und an ihre Arbeitsgruppen, allen voran dem Painting-Team bestehend aus Henning Albers, Alexander Herbst, Sebastian Bode, Knut Stolzenberg und Dorothee Tell, die nicht nur fundamental zum Gelingen des all-optical BECs beigetragen haben, sondern mir auch stets mit Rat und Tat und zahlreichen Sprüchen zur Seite gestanden haben.

Ein großer Dank geht an Madeleine-Yasmin Miltsch, die mir bei jedem organisatorischen Problem geholfen hat, selbst wenn es gar nicht ihre Aufgabe gewesen ist. Ich möchte mich bei Brigitte Weskamp für die Hilfe bei der Organisation meiner Promotion bedanken. Vielen Dank an Stephanie Kaisik, Gunhild Faber, Elke Hünitzsch und Birgit Ohlendorf, ohne die alles im Chaos versinken würde.

Bei Kai-Martin Knaak möchte ich mich für die Hilfe bei sämtlichen Elektronikproblemen bedanken. Außerdem möchte ich mich auch beim Team der Mechanikwerkstatt um Alexander Vocino, Jonas Peter und Mathias Scholz bedanken, die stets bereit waren, meine kurzfristigen Anfragen so schnell wie möglich in die Tat umzusetzen.

Ich danke Torben für seine unersetzliche Hilfe und Unterstützung und für noch so viel mehr.

Meiner Familie danke ich für die Liebe, Geduld und Unterstützung, auf die ich mich immer verlassen kann.

Und ich danke dir, Julian, dass du mir das Gefühl gibst, dir alles erzählen zu können, für dein Verständnis und die peinlichen Geschichten.

Vielen Dank an euch alle!

LIST OF PUBLICATIONS

- A. Hüper, C. Pür, M. Hetzel, J. Geng, J. Peise, I. Kruse, M. Kristensen, W. Ertmer, J. Arlt, and C. Klempt.
  Number-resolved preparation of mesoscopic atomic ensembles
  New J. Phys. 23.11 (2021), p. 113046.
  DOI: 10.1088/1367-2630/abd058 [119]

- C. Pür, M. Hetzel, M. Quensen, A. Hüper, J. Geng, J. Kruse, W. Ertmer, and C. Klempt.
  Rapid generation and number-resolved detection of spinor rubidium Bose-Einstein condensates
  Phys. Rev. A 107 (2023), p. 033303.
  DOI: 10.1103/PhysRevA.107.033303 [121]

- M. Hetzel, L. Pezzè, C. Pür, M. Quensen, A. Hüper, J. Geng, J. Kruse, L. Santos, W. Ertmer, A. Smerzi, and C. Klempt.
  Tomography of a number-resolving detector by reconstruction of an atomic many-body quantum state
  arXiv:2207.01270
  DOI: 10.48550/ARXIV.2207.01270 [122]

CURRICULUM VITAE

PERSONAL DETAILS

Name	Mareike Hetzel
Date of birth	November 23, 1993
Place of birth	Herzberg am Harz

EDUCATION

since 06/2018	PhD studies, Physics Institut für Quantenoptik Leibniz Universität Hannover
10/2015-04/2018	Master of Science, Physics Leibniz Universität Hannover
04/2013-03/2016	Bachelor of Science, Physics Leibniz Universität Hannover
10/2012-03/2013	undergraduate studies, Meteorology Leibniz Universität Hannover
until 2012	Abitur Ernst-Moritz-Arndt Gymnasium Herzberg

SELBSTÄNDIGKEITSERKLÄRUNG

Hiermit versichere ich, die vorliegende Arbeit selbstständig verfasst und keine anderen als die angegebenen Quellen und Hilfsmittel verwendet zu haben. Alle Stellen der Arbeit, die wörtlich oder sinngemäß aus anderen Quellen übernommen wurden, sind als solche kenntlich gemacht. Die Arbeit hat in gleicher oder ähnlicher Form noch keiner Prüfungsbehörde vorgelegen.

Hannover, 2023

Mareike Hetzel